DEPARTAMENTO DE INVESTIGACIÓN Y DOCTORADO

ITBA Instituto Tecnológico de Buenos Aires

NUEVOS DESARROLLOS EN EL MODELADO MATEMÁTICO DEL PROCESO CONTINUO PARA LA PRODUCCIÓN EN MASA DE POLÍMEROS DE ESTIRENO EN PRESENCIA DE ELASTÓMEROS

AUTOR: Ing. Ma. Laura Laganá

DIRECTOR: Dra. Diana Estenoz
CO-DIRECTOR: Dr. Joge Stripeikis

TESIS PRESENTADA PARA OPTAR AL TÍTULO DE
DOCTOR EN INGENIERÍA

Jurado

Dra. Silvia Barbosa Dra. Silvina Andrea Regenhard Dr. César Gómez

CIUDAD AUTÓNOMA DE BUENOS AIRES
Julio 2022

Ing. Ma. Laura Laganá: NUEVOS DESARROLLOS EN EL MODELADO MATEMÁTICO DEL PROCESO CONTINUO PARA LA PRODUCCIÓN EN MASA DE POLÍMEROS DE ESTIRENO EN PRESENCIA DE ELASTÓMEROS. *Tesis presentada como requisito parcial para acceder al grado de* ***DOCTOR EN INGENIERÍA*** *del Instituto Tecnológico de Buenos Aires.*

DEPARTAMENTO DE INVESTIGACIÓN Y DOCTORADO

ITBA Instituto Tecnológico de Buenos Aires

NEW DEVELOPMENTS ON THE MATHEMATICAL MODELING OF THE CONTINUOUS BULK PROCESSES FOR THE PRODUCTION OF RUBBER-TOUGHENED STYRENE POLYMERS

AUTHOR: Ing. Ma. Laura Laganá

ADVISOR: Dra. Diana Estenoz
CO-ADVISOR: Dr. Joge Stripeikis

A THESIS SUBMITTED AS A REQUIREMENT FOR THE DEGREE OF
DOCTOR EN INGENIERÍA

Jurado

Dra. Silvia Barbosa Dra. Silvina Andrea Regenhard Dr. César Gómez

CIUDAD AUTÓNOMA DE BUENOS AIRES
July 2022

Ing. Ma. Laura Laganá: NEW DEVELOPMENTS ON THE MATHEMATICAL MODELING OF THE CONTINUOUS BULK PROCESSES FOR THE PRODUCTION OF RUBBER-TOUGHENED STYRENE POLYMERS. *A thesis submitted in partial fulfillment of the requirements for the degree of* ***DOCTOR EN INGENIERÍA*** *of Instituto Tecnológico de Buenos Aires.*

A Vito y Fidel

"La sabiduría no es un producto de la educación sino del intento de toda una vida para adquirirla"

Albert Einstein

Agradecimientos

Quiero expresar mi profundo agradecimiento a todos los que me acompañaron en el transcurso de esta tesis y que me ayudaron a hacer realidad este proyecto.

A mi directora, Diana, por la orientación y por brindarme siempre la palabra justa en mis peores momentos.

A mi co-director Jorge, por creer en mi y por su participación en mi formación como ingeniera.

A los departamentos de Ingeniería Química y Doctorado del ITBA por haberme dado el espacio para este trabajo.

A mis colegas y amigos Emilio y Juan por el apoyo que siempre me brindaron.

Al Laboratorio de Síntesis de Polímeros del CIQA por su apoyo y calidez humana.

Al ITBA, CONICET y CIQA, por el apoyo económico.

A mi marido y compañero de vida, Rodrigo por sus palabras de aliento para seguir adelante y por ser mi sostén en los momentos difíciles.

A mis hijos, Vito y Fidel que sin saberlo fueron mi gran motivación para avanzar en este proyecto.

A mis padres por su confianza y apoyo incondicional.

A todos ellos, Muchas gracias!

Resumen

El objetivo general de esta tesis es investigar aspectos aún no dilucidados en el área de la ingeniería del proceso de polimerización en masa de estireno (St) en presencia de elastómeros para la producción de Poliestireno de alto impacto (HIPS). La investigación se enfoca en el entendimiento y modelado matemático de los fenómenos fisicoquímicos involucrados, en el estudio y empleo de nuevas técnicas de modelado para la simulación de sistemas complejos, y en la optimización de los procesos. Se pretende lograr desarrollos que contribuyan a diseñar y operar los procesos industriales continuos con alto grado de comprensión, y optimizados desde el punto de vista de la productividad y de la calidad del producto final. Se incluyen estudios relacionados con el empleo de iniciadores mono- y multifuncionales y su efecto sobre la estructura molecular y morfológica. También se desarrolla un modelo matemático de la etapa de devolatilización (DV) incluyendo los fenómenos cinéticos, termodinámicos y de transporte. Además, se analizan las interrelaciones entre la estructura molecular y morfológica con las propiedades fínales (de procesamiento y de uso final).

En primer lugar se presenta un modelo que permite la simulación del tren de reactores para la polimerización continua en masa de St en presencia de polibutadieno (PB). Se estudia luego la etapa de DV correspondiente a los procesos de producción en masa para la obtención de poliestireno (PS), HIPS y acrilonitrilo butadieno estireno (ABS). Se desarrolla un modelo completo de dicha etapa para la producción continua en masa, capaz de simular cualquiera de los tres procesos mencionados. El modelo considera los mecanismos de transferencia de masa y las reacciones químicas involucradas y predice la composición de especies volátiles residuales y la estructura molecular del producto final.

Seguidamente se desarrolla el modelo matemático del proceso de producción industrial HIPS, el cual consta de tres submodelos: un modelo de polimerización para el tren del reactores, un modelo de DV y un modelo estructura-propiedades. El modelo completo permite la estimación de todas las variables globales a lo largo del proceso y las variables de calidad, como índice de hinchamiento (SI), índice de flujo de fusión (MFI), contenido de oligómeros y monómero residual.

Con el objetivo de ajustar y validar este modelo, se obtuvieron nuevos datos experimentales para la polimerización continua de St en presencia de PB utilizando diferentes iniciadores de peróxido en una planta piloto. Luego, este modelo es aplicado para estudiar teóricamente el uso de iniciadores multifuncionales y el efecto de las condiciones del proceso sobre las

propiedades finales del producto. La simulación de sistemas con iniciadores multifuncionales implican modelos multidimensionales, especialmente en los casos en que se quiere estimar la estructura molecular completa.

Finalmente, se investigó teórica y experimentalmente la copolimerización en masa de St y acrilonitrilo (AN) en presencia de diferentes elastómeros. Desarrollado sobre la base del modelo anterior de HIPS, se presenta un modelo matemático para la producción continua de ABS, el cual se ajusta y valida con datos experimentales obtenidos en la misma planta piloto.

Abstract

The general objective of this thesis is to investigate not yet elucidated aspects in the area of engineering of the mass polymerization process of styrene (St) in the presence of elastomers for the production of High Impact Polystyerne (HIPS). The research focuses on the understanding and mathematical modeling of the physicochemical phenomena involved, on the study and use of new modeling techniques for the simulation of complex systems, and on the optimization of processes. The aim is to achieve developments that contribute to designing and operating continuous industrial processes with a high degree of understanding, and optimized from the point of view of productivity and the quality of the final product. Studies related to the use of mono- and multifunctional initiators and their effect on molecular and morphological structures are included. A mathematical model of the devolatilization (DV) stage is also developed, including kinetic, thermodynamic and transport phenomena. In turn, the interrelationships between the molecular and morphological structures with the final properties (processing and end-use) are analyzed.

First, a model is presented that allows the simulation of the reactor train for the continuous mass polymerization of St in the presence of polybutadiene (PB). The DV stage corresponding to the mass production processes to obtain polystyrene (PS), HIPS and ABS is then studied. A complete model of this stage is developed for continuous mass production, capable of simulating any of the three mentioned processes. The model considers the mass transfer mechanisms and the chemical reactions involved and predicts the composition of residual volatile species and the molecular structure of the final product.

Next, the mathematical model of the HIPS industrial production process is developed, which consists of three sub-models: a polymerization model for the reactor train, a DV model and a structure-properties model. The complete model allows the estimation of all global variables throughout the process and quality variables, such as swelling index (SI), melt flow index (MFI), oligomer content and residual monomer.

In order to adjust and validate this model, new experimental data were obtained for the continuous polymerization of St in the presence of PB using different peroxide initiators in a pilot plant. The model is then used to theoretically study the use of multifunctional initiators and the effect of process conditions on the final properties of the product. The simulation of systems with multifunctional initiators involves multidimensional models, especially in cases where the complete molecular structure is to be estimated.

Finally, the mass copolymerization of St and acrylonitrile (AN) in the presence of different elastomers was theoretically and experimentally investigated. Developed on the basis of the previous HIPS model, a mathematical model for the continuous production of ABS is presented, which is adjusted and validated with experimental data obtained in the same pilot plant.

Contents

List of Figures

List of Tables

Chapter 1
Introduction

1.1 St Copolymers

The Styrene (St) market consists of sales of St and related services used for making synthetic rubbers, resins, and plastics and improving drying oils. The last years, the global St-petrochemical market has been expected to grow at a compound anual growth rate (CAGR) of 9-10% [13]. The increase is mainly due to the companies rearranging their operations and recovering from the COVID-19 impact, which had earlier led to restrictive containment measures involving social distancing, remote working, and the closure of commercial activities that resulted in operational challenges.

The high demand for St-polymers drives the growth of St market, however, the increasing health and environmental concerns due to the usage of St-polymers limits the demand for St. In order to increase the efficiency and popularity of St, companies are investing towards developing methods to recycle the polymers [13].

St is the precursor to polystyrene (PS) and several copolymers. The most produced St resins are crystal GPPS (General Purpose PS), expandable PS (EPS), High Impact PS (HIPS), and Acrilonitrile-Butadiene-Styrene (ABS). GPPS and EPS are homopolymeric materials, while HIPS and ABS are the two most important heterogeneous thermoplastics of St. St is typically obtained from the dehydrogenation of ethylbenzene, which is in turn obtained from benzene and ethylene, all derived from petroleum refining. The manufacture route using ethylbenzene consumes about half of the commercial benzene in the world [9]. Most of the St produced worldwide occurs in facilities that use licensed technologies, since the available patents are held by a small group of companies. The volume market share in 2019 is shown in Figure 1.1 [1].

Asia Pacific is likely to dominate the market and is expected to continue to lead the market during the next years. Increasing demand for electrical and electronic devices and packaging applications in the region is likely to drive the market growth. Increase in demand of innovative and attractive packaging materials by industries such as food and beverages, cosmetics, consumer goods is also the major factor that is driving the growth of the market in this region. In Asia Pacific region, China is dominating the market as it has one of the largest packaging industries worldwide [14]. Automotive industry uses St in the production of tires, interior and exterior parts of the vehicles. Europe is expected to share the largest

revenue growth due to the presence of numerous automotive manufacturers in the region [14].

With respect to the global plastic material and resin market, it is growing at a CAGR of 20%. The current growth is also mainly due to the COVID-19 effect. The market is expected to reach $48.96 billion in 2025 at a CAGR of 3% [15]. The PS market is significantly supported by the construction as well as the electronics industry and packaging. The demand for packaging products has increased recently, particularly in emerging economies such as China and India. As the size of the middle-class grew in these countries, the consumption of processed foods, poultry, meat and agricultural products increased too. The rise in per-capita income in these economies resulted in the emerging middle-class purchasing more packaged goods. The demand for packaged goods increased the consumption of PS for their packaging, driving the market [15]. The increasing application of expanded PS for insulation and construction purposes is propelling the PS market growth further. The construction industry is rapidly growing and is positively affecting the PS industry. The EPS market has been one of the fastest-growing St markets, due to high demand from the infrastructure and construction sector. The rising use of HIPS and GPPS in consumer electronic devices is supporting the growth of the industry. The HIPS and GPPS market are supported by the demand from the Asian market. The segment is also growing due to its extensive use for insulation purposes as it has to compete only with cotton wool in this segment. The consumer electronic sector has a consumption rate of around 20% of the material and is aided by the electric and electronic appliances market [16].

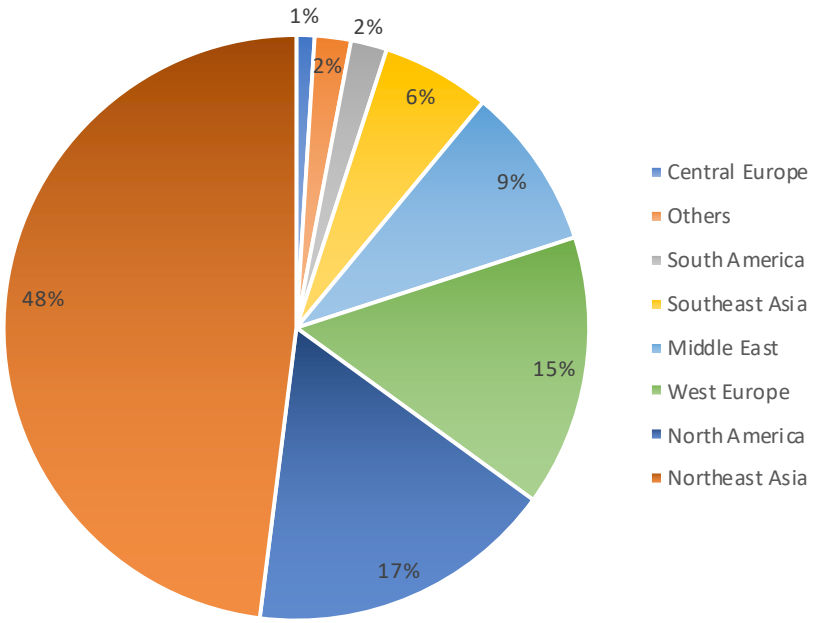

FIGURE 1.1: Distribution of St production capacity per region as in 2019 [1]

The volume market of St by product type is shown in Table 1.1, where the versatility

of the St polymers can be inferred. These polymers are easily extruded and molded, which makes it suitable for manufacturing a variety of products. PS, in all its forms, is the most important product of this vinyl monomer, as it is used in a large number of applications. St polymers include a broad range of types, from commodity plastics to engineering polymers. The characteristics of St copolymers allow a wide range of applications.

Table 1.1: Volume market of St by product type [9]

Product	**Demand (%)**
Polystyrene	64
Acrilonitrile-Butadien-Styrene	9
Styrene-Butadiene Latex	7
Unsaturated Polyester Resins	5
Syrene-Butadiene Rubbers	4
Others	11

GPPS is a versatile plastic used for the manufacturing of refrigerators, air conditioners, ovens, microwaves, and vacuum cleaners. The demand is also high in the automobile industry where it is used in manufacturing car knobs, instrument panels, trim, energy absorbing door panels and sound dampening foam.

St-Acrilonitrile (SAN) is a copolymer of St with between 20 and 30% of AN. It is basically used in GPPS applications when additional chemical resistance and slightly higher temperature resistance are needed. The following are among the main properties of SAN: high transparency, high rigidity, chemical resistance, glossy finish and high surface hardness. The additional scratch resistance makes it a suitable choice for point of sale displays and cosmetic items. Some common applications include: parts for refrigerators, shelf dividers, lightweight covers, cosmetic product packaging and cookware.

Both GPPS and SAN are highly versatile and have many applications due to its transparency, toughness, stability and easy processing. However, the low resistance to impact limits some of their applications. In this way, a small addition of an elastomer in the recipe considerably improves tenacity. Figure 1.2 qualitatively compares the stress-strain curves for GPPS, HIPS, SAN and ABS [2]. The toughness of HIPS, related to the area under the stress-strain curve, is greater than that of ABS because the latter material exhibits located flow at low speeds of extension, and fractures very close to the point of creep. In contrast, HIPS spreads evenly, fracturing at high percentages of deformation. ABS exhibits the same behaviour as HIPS when the test is carried out at high extension speeds, presenting higher tenacity.

Uses for these plastics are extensive. Packaging applications such as: disposable tumblers, television cabinets, meat and food trays and egg cartons, are among the largest area of use for St plastics. Rigid foam insulation in various forms is being used increasingly in the construction industry, and modified St plastics are replacing steel or aluminum parts in

automobiles; both applications result in energy savings beyond the initial investment in crude oil. The cost of achieving a given property, e.g., impact strength, is among the lowest for St plastics as compared to other competitive materials.

Table 1.2 compares the typical properties of GPPS, SAN, HIPS, and ABS [2–4, 10, 11]. HIPS and ABS are both a reinforced engineering thermoplastic with a rubbery disperse phase. The presence of an elastomer in the recipe confers the material an increased impact resistance (IR), without impairing the high tensile strength and ease of processing with respect to GPPS. The mechanical properties of both materials are mainly determined by the size, morphology, and volume fraction of the rubber particles [17].

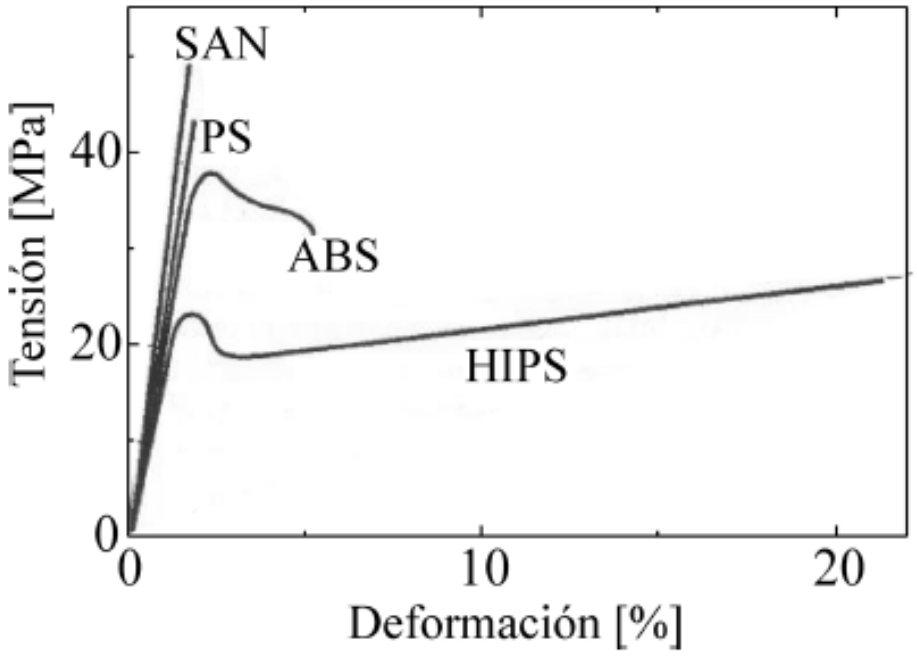

FIGURE 1.2: Stress-strain curves for some polymers of St [2]

.

Due to its low cost and easy processing, HIPS is used in various applications. Among the most important it can be mentioned the manufacture of packaging, disposable products, household appliances, toys, and products for construction. Some applications require special properties, such as low residual monomer content and transparency for packaging of food, high IR for interior of refrigerator doors, or low flammability for household appliances. In ABS, the presence of the AN polar group determines a high resistance to attack by waxes, solvents, mineral oils and vegetable, environment friendly, and a good surface finish. In general, the end-use properties of a material competes with the processing properties. An adequate balance of them, also considering cost and environmental impact, determine its choice for a specific application.

Both HIPS and ABS exhibit yellowing, hardening, and modification of their mechanical properties when exposed prolongedly to UV radiation. This behavior is mainly due to the

material degradation due to chain breakage and / or rubber crosslinking. For this reason, usually small amounts of UV stabilizers (benzotriazoles and benzophenones) and antioxidants (phenolic phosphites alkyl, esters, and thioesters) are added. Other common additives are: lubricants external (zinc stearate); internal lubricants and / or plasticizers (mineral oils); anti-static agents (ammonium compounds); and dyes [2, 18]. Dyes also often act as UV stabilizers due to that they absorb radiation and prevent the generation of free radicals that attack the polymer. Special additives, such as brominated organic compounds or oxides of antimony and aluminum, allow to obtain commercial grades of low flammability. These additives can be integrated into the polymer by means of mechanical mixers or static [3], although most of the time they are added in the reaction, as part of the recipe [3, 19].

TABLE 1.2: Typical properties of St polymers [2–4, 10, 11]

Property	**GPPS**	**HIPS**	**SAN**	**ABS**
Density (g/cm^3)	1.05	1.03-1.05	1.07-1.25	1.04-1.21
MFI (g/10 min)	1-30	2-20	1-40	1-45
Tensile Modulus (Mpa)	3000-3400	1400-2800	3400-3900	1800-3200
Yield Strength (Mpa)	35-60	20-45	42-82	29-65
Elongation at break (%)	1.5-3.0	25.0-70.0	1.0-7.0	2.0-110.0
Impact resistance (KJ/m^2)	1-2	5-13	1-2	16-28
Temp. Softening (°C)	78-102	75-97	107-111	91-108
Thermal conductivity (W/Km)	0.16-0.17	0.16-0.17	0.11-0.19	0.13-0.19
Thermal expansion coeff. (1/K)	$(6-8)x10^{-5}$	$(8-10)x10^{-5}$		$(7-11)x10^{-5}$
Dielectric Constant (10^6/MHz)	2.5	2.5-2.7	2.4-3.2	2.4-3.8
Dissipation Factor (10^2/MHz)	$(1-4)x10^{-4}$	$(2-8)x10^{-4}$	$(7-8)x10^{-3}$	$(5-19)x10^{-3}$
Transparency	Transp.	Opaque	Transp.	Opaque

1.2 Industrial Production of HIPS and ABS

ABS and HIPS represent the industrially most important thermoplastic two-phase systems. The principal reagents for HIPS production are St and the rubber, usually PB; and for ABS, AN monomer is also included in the recipe. The reaction recipe can also include polymerization initiators, chain-transfer agents (CTA), and other additives. Diluents are sometimes used to reduce the viscosity of monomers and polymer mixture to facilitate processing at high conversion. St was initially isolated by distillation of a natural occurring resin [20] and is currently typically obtained from dehydrogenation of ethylbenzene, which is in turn obtained from benzene and ethylene, all derived from petroleum refining. An inhibitor is added for its storage and transportation to avoid its thermal decomposition [21]. AN is obtained from the

catalytic reaction of propylene, oxygen and ammonia. PB is synthesized by the solution polymerization of butadiene (B) using Ziegler-Natta catalysts, or anionically using organometallic initiators.

HIPS, and ABS are commonly produced via free radical polymerizations (FRP). Such polymerization allows obtaining a wide range of commercially important products, combining high profitability and process control [11, 22].

Free-radical polymerization, like other chain growth mechanisms, involves the sequential addition of monomers to an active center, i.e. radical species. In general, a bulk St FRP reaction involves steps of initiation, propagation, transfer and termination. In the traditional kinetic approach, each of these steps consists of a series of elementary chemical reactions [23]. The active centers that can start the polymerization reaction as a result of the initiation step are initiating radicals.

In the case of HIPS production, St polymerizations can be initiated simply by applying heat [24–26]. In this case, the initiating radicals are derived from reactions involving only the monomer. Several mechanisms for spontaneous thermal St initiation have been proposed [25], with the Mayo and Flory mechanisms being the most widely accepted [26]. In the first mechanism, thermal initiation proceeds by a Diels-Alder dimerization of St, followed by assisted homolysis [25, 27] between the dimer and a third St molecule, generating two initiating monoradicals. For the second mechanism, Flory proposed that St dimerizes to form a diradical and a third St abstracts a hydrogen atom from the diradical to generate an initiating monoradical. Molecular modeling studies have found the Diels-Adler dimer to be the key intermediate for the reaction, thus favoring the mechanism proposed by Mayo [26]. Industrially, even though the controlled thermal polymerization would theoretically produce the highest molecular weights in a St FRP process, undesirable spontaneous polymerizations could clog production facilities [26]. In addition, as previously stated, if temperatures are low the polymerization rate would be too low for the process to be economically advantageous. In practice there must be a compromise between polymer productivity, mainly related to polymerization rate, and product quality, mainly related to molecular weight [28]. For these reasons, polymerization initiators are widely used in industrial polymerization processes [22, 27]. Removal of initiator residues from the finished product is not needed in most cases, avoiding possible purification steps [29].

At industrial scale the continuous bulk processes dominate the HIPS production, while two processes have been reported for laboratory scale manufacture, the first one based on melt blending a rubber with a PS resin [30], and the other one based on polymerizing a rubber/St solution firstly by bulk stirred stage to determine the morphology and a subsequent static (bulk-bulk) [31] or stirred (bulk-suspension) [32] stage, to complete the polymerization up to high St conversion [33]. The bulk process is also employed to produce ABS, however, emulsion polymerizations domain the actual market of ABS. This domain is due to the fact that emulsion polymerization allows to control particle size and is more versatile that bulk proceses in respect to the incorporation of high rubber content [4]. Bulk produced ABS typically has very good unpigmented color and is usually somewhat more translucent because

of the large rubber phase particle size and low rubber content. Increased translucency can reduce the concentration of colorants required. The extent of rubber incorporation is limited because of viscosity limitations in the process; however, the bulk-produced grafted rubber can be more efficient (on an equal percent rubber basis) at impact modification than emulsion-grafted rubber because of the presence of high occlusion levels in the rubber phase [34].

1.2.1 HIPS Synthesis

Industrial production of HIPS and GPPS is continuous and via bulk processes. The product should exhibit consistent quality, high purity, and a low residual monomer content (generally less than 500 ppm monomeric St)[3]. Generally, the key problems associated with manufacture of the polymer are removal of the heat of polymerization and pumping highly viscous solutions. Suspension processes are chiefly used for the production of EPS. PS molding materials may be produced by this process when the blowing agent is omitted.

The synthesis of HIPS requires careful control of the rubber particle size and morphology. Initially, the solution consists of PB dissolved in St and further additives such as diluents, CTA and initiators with the onset of polymerization, the PS forms a separate phase. St and optional diluents are the common solvents for the elastomer and the PS phase (oil-in-oil emulsion). The PS phase grows at the expense of the rubber phase with further conversion. The rubber phase initially is the continuous phase. In a stirred reactor, phase inversion (PI) occurs, largely depending on the phase volume ratios and viscosities of the two phases. The reaction conditions during PI determine the rubber morphology and particle size to a large extent [3, 35, 36].

The mechanical strength of HIPS is supported by PS molecules, which are grafted onto rubber molecules. Grafting occurs especially at low St conversions, when the volume of the PS phase is still small. Quantity and nature of these copolymers have big impact on the particle size and morphology of the HIPS rubber particles [37, 38]. Simple blending of PS and PB leads to a mechanically inferior product.

The shear field in the reactors is critical to control of particle size as well as to meet the minimum shear rate for PI, without which the product would consist of a continuous crosslinked rubber network with markedly inferior properties. After the particles are formed and sized, only gentle agitation is applied to aid heat transfer without disturbing the particle structure. Conditions that produce the desired PS-phase molecular weight are used [2].

The most difficult task in the bulk production of HIPS, from an industrial standpoint, is the control of the highly viscous melt and the removal of the heat of polymerization (71 kJ/mol). Solvents such as toluene or ethylbenzene are frequently present in small proportions (typically 5 – 15 %) to provide better control of the polymerization rate, the viscosity of the polymer melt, and the crosslinking of the rubber phase [3]. The solvent and the unreacted monomer must be removed by Devolatilization (DV). They are generally recovered, optionally purified and transferred back to the feed. In a running continuous operation, solvents are in essence introduced via St impurities (mostly ethylbenzene). The plant setup generally comprises a

polymerization section, a DV and solvent recovery section, and a pelletizing section [3].

HIPS plants generally consist of a series of three to five reactors, split into a prepolymerization and termination section. In the prepolymerization section PI takes place, and rubber morphology and particle size are largely adjusted. Various reactor designs have been proposed for this part of the plant. Common are one or two stirred-tank reactors, tower reactors, loop reactors with static mixers, or combinations of these. The prepolymerization stage is typically carried out at 100-150 °C to 15-30% conversion. The termination part commonly consists of several plug-flow type reactors to achieve high St conversions. Common temperatures are 140 – 190 °C in this part of the plant. Figure 1.3 shows several common reactor configurations [3].

In the continuous stirred-tank reactor, part of the heat is removed by means of reflux cooling. The heat of polymerization causes evaporation of a St part. The gaseous monomer is condensed in condensers with large surface areas and recycled back to the reactor. The prerequisite for this type of heat removal is effective mixing of the reactor contents. Anchor stirrers, impellers, or helical ribbon agitators are commonly used. The reaction temperature is the most important parameter affecting the molecular mass of PS and thus the properties of the product. It is controlled by varying the pressure and thus the boiling point of St in the stirred tank. The reactor feed can also be used to remove heat of polymerization. Reactors converting more than 40% of the St feed usually need additional cooling. The lower solid content of the HIPS prepolymerization reactors, on the other hand, requires preheating of the reactor feed.

The PS melt leaving the reactor section has a concentration of 60 – 80%. Prior to DV, the partial polymer is heated to 200 °C to crosslink the rubber chain in order to protect the rubber particles from the very high shear fields during processing [2]. Unreacted St monomer and solvent are commonly removed by flash DV. The polymer is fed into an evacuated, heated vessel where the volatile components evaporate and the melt is then pumped out. The St – solvent mixture formed is recycled to the first reactor. A small fraction must be discarded, however, to avoid increasing the concentration of St contaminants. A second flash tank or another degassing unit e.g., falling strand degassers, steam strippers, thin-film evaporators, degassing extruders) may be used to further decrease content of volatile compounds. Degassing of the PS melt is followed by pelletization [3].

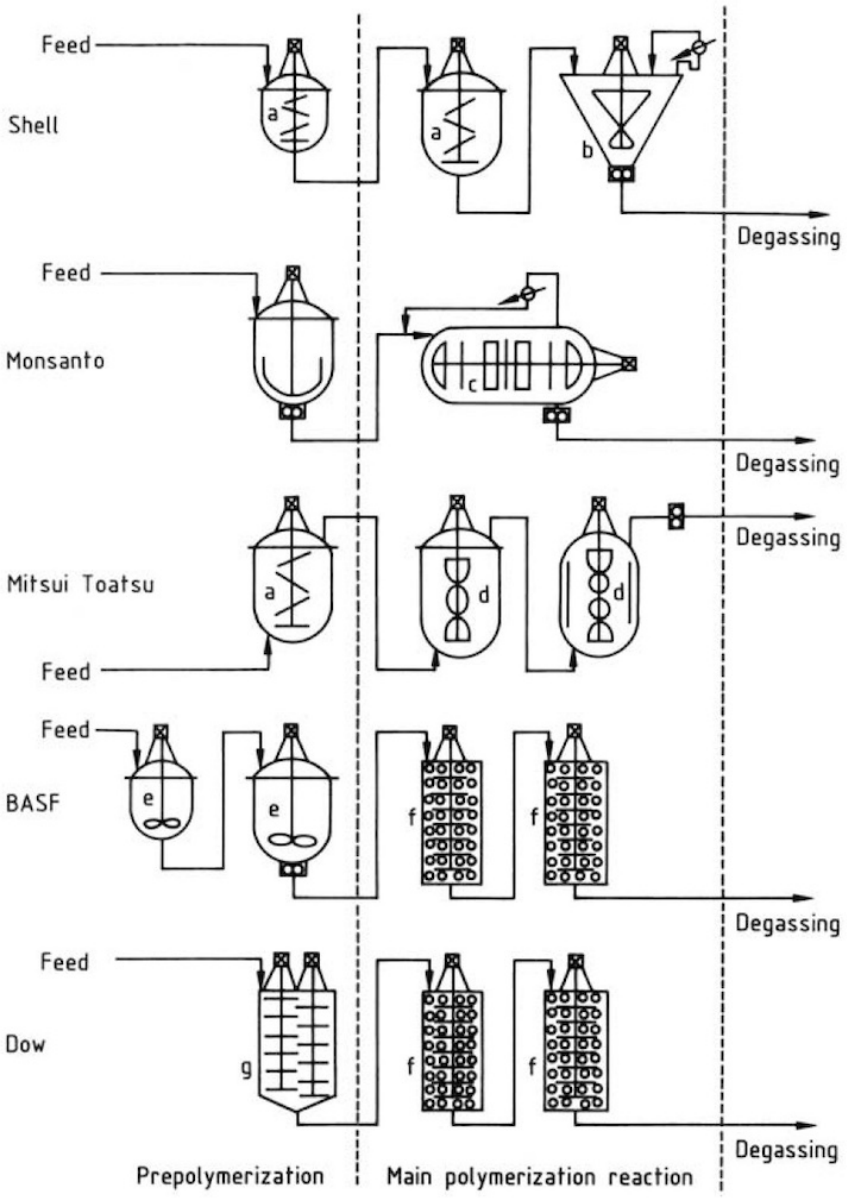

FIGURE 1.3: Reactor configurations for HIPS production a),b), d), e), g) Stirred-tank reactors; c) Horizontal plug-flow reactor, f) Tower reactors [3].

1.2.2 ABS Synthesis

The ABS polymers are based on three monomers: AN, B and St. The polymer components have different chemical compositions and coexist as two separate phases whose compatibility is controlled by their structure and chemical microstructure. In all classical ABS molding compounds the continuous phase (matrix) consists of copolymers of St and AN. An elastomer based on B forms the disperse phase that is distributed in the continuous phase and has a characteristic morphology. ABS is mainly produced via two major industrial processes: emulsion by compounding of emulsion-made rubbers into the SAN matrix; and solution via dissolving a rubber (commonly: B homopolymer) in St-AN and subsequent bulk polymerization, sim-

ilar to the HIPS bulk process [3]. The emulsion route allows wider variation of individual parameters such as morphology of the elastomer phase (average particle size, and degree of crosslinking [39]). The St and AN can also be copolymerized in different weight ratios [40], and the average molecular mass of the SAN copolymer modified as desired. The separate production of the grafted rubber and the SAN matrix has the advantage that the properties of each component can be controlled independently and different production processes can be used for the grafted rubber phase and the SAN matrix. The emulsion polymerization yields ABS graft rubbers with a rubber content of 5 – 85 wt % and consists on a separate production of the ABS graft rubber and SAN matrix with a subsequent mixing and compounding step. Bulk polymerization starts from a separately produced rubber base (BR or SBR solution rubbers). The compound is produced in a bulk process run continuously over several stages. Rubber content is limited to 20 wt % for viscosity reasons [3]. The bulk process has the advantage of an inherent degassing stage, so that products with very low residual monomer contents and thus high heat resistance can be obtained. However, yields and molecular masses are limited. The advantages of the bulk process lie in the fact that completely continuous processing is possible and that the grafted rubber particles are formed in situ, i.e., at the same time as SAN polymerization. The proportion of internal grafting is thus higher and products have a more favorable notched impact strength – hardness relationship than those produced by emulsion polymerization [41, 42]. The bulk ABS process includes a degassing step which means that unreacted monomers can be directly recycled.

Fig. 1.4 compares the ABS morphologies obtained through both processes [4] and Fig. 1.5 shows an overview of the ABS production processes. In the emulsion polymerization of ABS, it starts from a seeding of PB particles. For this reason, the morphology formation mechanism is very different from that of bulk processes, giving rise to core-shell type morphologies in which the nucleus is rubbery (See Fig. 1.4a). and which is outside of the scope this thesis.

Emulsion polymerizations dominate the current ABS market, with more than 85% of total production. This is due to the fact that emulsion polymerization allows to control the size of the particles, and is more versatile than the bulk processes in terms of incorporating high rubber contents [4]. The bulk polymerization process is considered to be more economical than the emulsion and bulk suspension processes because of lower investment costs [3]. Other St copolymers besides SAN can also be combined with the ABS graft rubber. a-Methylstyrene – AN (AMS – AN) copolymers or St – AN – N-phenylmaleimide terpolymers, for example, give products with a high heat resistance because of their high glass transition temperatures. Some copolymers are only accessible via the separate bulk polymerization route [3].

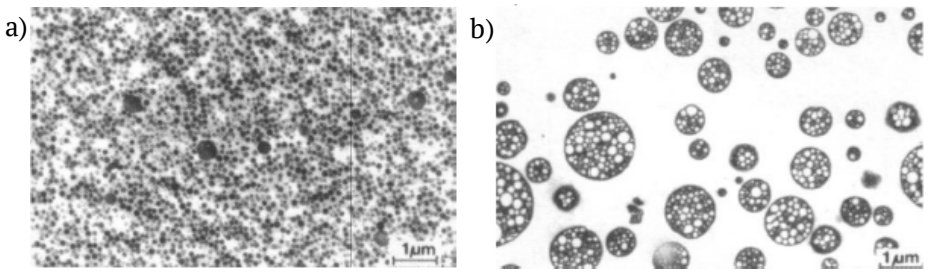

FIGURE 1.4: Morphologies of ABS according to the synthesis process [4]. a) Emulsion process; b) Bulk process.

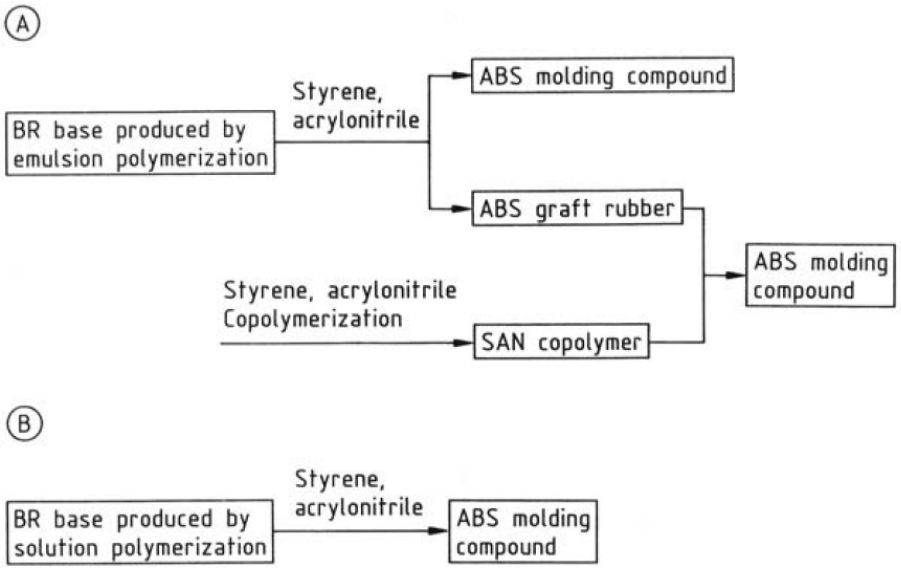

FIGURE 1.5: Overview of ABS production processes A) Emulsion polymerization; B) Bulk polymerization [3].

ABS Production by Emulsion Polymerization

The emulsion process is the standard ABS production process. The production of grafted rubbers with high rubber contents and their mixing with a separately produced SAN matrix is used worldwide.

The production of ABS grafted rubber consists of three stages:

1. Production of the graft base, i.e., a PB or B copolymer latex with defined particle size, particle size distribution, and gel content.

2. Grafting the St – AN monomer mixture onto the graft base.

3. Workup of the grafted rubber latex.

The particle size, particle size distribution, and crosslinking density of the graft base; the degree of grafting; the proportion and morphology of the rubber-phase volume; and the molecular mass of the grafted SAN chains largely determine the properties of the resulting

grafted rubber system. Bimodal ABS systems have optimal surface properties and toughness synergies. These systems are produced from a graft base with a bimodal particle size distribution, or from two grafted rubbers of differing particle size that are mixed at the latex stage and then worked up together. The particle size of ABS emulsion grafted rubbers lies in the range 50 – 600 nm, values of 100 – 400 nm being preferred [3].

The production of graft bases mostly takes place batch wise. The B monomer is polymerized at 5 – 75°C and 12 bar. In the case of B copolymers, the reactivities of the individual monomers must be taken into account. If compositions of the copolymers are chosen which lie outside the "azeotrope region" of the monomermixture, then high chemical nonuniformity is avoided by using a continuous process and carrying out the polymerization until a given monomer conversion is reached. Unreacted B is fed back into the first reactor of the reactor cascade. Monomer – water weight ratios of 1 : 0.6 to 1 : 2 are used. Anionic emulsifiers are added in quantities of 1 – 5 parts per 100 parts of monomer to disperse the monomers and stabilize the PB latex particles. The alkali salts of disproportionated abietic acid or fatty acids, C12 – C18 n-alkyl- and n alkylarylsulfonates are commonly used as emulsifiers. Polymerization is initiated with alkali peroxydisulfates or combinations of reducing agents with peroxydisulfates or organic hydroperoxides. The use of hydroperoxide systems allows a sufficiently high reaction rate at low temperature and modification of the PB microstructure [43].

The particle size can be controlled by varying the monomer – water ratio, by stepwise addition of emulsifier, and by adjusting the reaction temperature. The molecular mass and crosslinking density of the PB bases are adjusted by means of modifiers (e.g., n-alkylthiols). Increasing quantities of modifier decrease the average polymer chain length. Polymerization is usually terminated above 80% conversion to ensure sufficient crosslinking of the rubber (gel contents $>$ 60%, preferably $>$ 70 %). No shortstopping agents are used (apart from pure reducing agents) to prevent disruption of the subsequent grafting reaction. The latex product is devolatilized to remove residual monomers by using vacuum and/or steam in a batch reaction, or continuously in a bubble column [3].

For the grafted rubber production, a St – AN monomer mixture is polymerized in the presence of the graft base. An increase in the ratio of monomers to PB is accompanied by increases in the net reaction rate, in the molecular masses of the grafted chains and of the free SAN copolymer, and in the degree of grafting. Since the reaction is exothermic (DH 840 kJ/kg), a monomer-feed process or a completely continuous process is used. If the copolymer compositions lie outside the azeotrope region of St and AN, an increase in chemical nonuniformity is avoided by adding the more rapidly reacting monomer later (staggered dosing) [3]. The particle size, particle size distribution, and crosslinking density of the graft bases are directly related to the degree of grafting, graft density, rubber phase volume, and morphology of the grafted rubber. The proportion of internal grafting generally increases with increasing particle size and decreasing crosslinking density of the rubber base. At constant particle size and rubber crosslinking density, the degree of grafting and the graft density become the factors determining the properties of the ABS product [44].

If the weight ratio of monomers to graft base exceeds unity, molecular mass modifiers are usually added to the monomer mixture. They affect the graft reaction and the St – AN copolymerization, the molecular masses of the free and bound SAN chains, and the degree of grafting decrease. The emulsifier systems used in the grafting reaction are usually the same as those used in the production of the graft base. High latex stability during the polymerization and ready coagulation during the product workup are also desired.

After completion of polymerization, workup of the grafted rubber begins by reducing the excess hydroperoxide initiator with sodium hydroxymethanesulfinite. Stabilizers are added, generally in the form of a synergistically acting system, to protect the grafted rubber from oxidation during subsequent powder drying and compounding. To isolate the ABS graft rubber from the polymer latex, the emulsifier must be deactivated. Emulsifiers based on alkali carboxylates are coagulated and precipitated by adding dilute acid (acetic or mineral acid) to adjust the pH to below 3. Emulsifiers based on alkyl sulfonates are coagulated by adding dilute aqueous solutions of inorganic electrolytes. Strict control of the precipitation conditions is necessary to obtain a powder with a uniform particle structure and size distribution, from which all water-soluble polymerization and coagulation additives can be easily washed out. Coarse powder particles contain inclusions of precipitants which adversely effect drying and processing. Finely divided powders lead to filtration and wastewater problems. After coagulation the material is filtered with band, plane, or rotary filters and washed. The filter cake is then fed into a reslurry tank and mixed with fresh water. The slurry is processed in filter presses, extruders, or sieve centrifuges and the wastewater recycled to the process [3]. During the workup, measures are taken to lower the residual monomer content to comply with legal limits. Examples include latex degassing with a perforated plate column and countercurrent steam, the use of a precipitation – stripping process, and powder workup with a helical sieve followed by compacting and degassing in a twin-screw extruder [45, 46].

Figure 1.6 show the production process, where the first stage involves production of a PB latex with a defined particle size. An aqueous soap solution is formed in the polymerization reactor (a) at ca. 65 °C and the molecular mass modifier is added. After flushing with nitrogen, B is pumped in and the polymerization is initiated with potassium peroxydisulfate solution. The reaction rate is determined by the heat removal capacity of the reactor. The maximum conversion rate is ca. 10 %/h. At conversions of a. 80 – 90% the reaction rate decreases; the monomer is then extensively consumed and crosslinking reactions begin. Polymerization is terminated by lowering the temperature to below 50 °C. Unconverted B is vented and stirred out under vacuum. In the second stage (the ABS graft rubber production process), the PB latex, an aqueous potassium persulfate solution, and part of the emulsifier solution are charged to the grafting reactor (d). The temperature is increased to ca. 60 °C and a St – AN monomer mixture and the remainder of the emulsifier solution are charged to the reactor at a constant rate over 5 h. The reaction temperature is then increased to ca. 65 °C to complete polymerization (conversion 96%, cycle time ca. 8 h, average reactor size is ca. 40 m^3). After running through the stabilization tank (h), the latex is coagulated. Washing and drying yield a powder which is subjected to a compounding step. After the addition of

lubricants, dyes, and other additives, the polymer is pelletized (p).

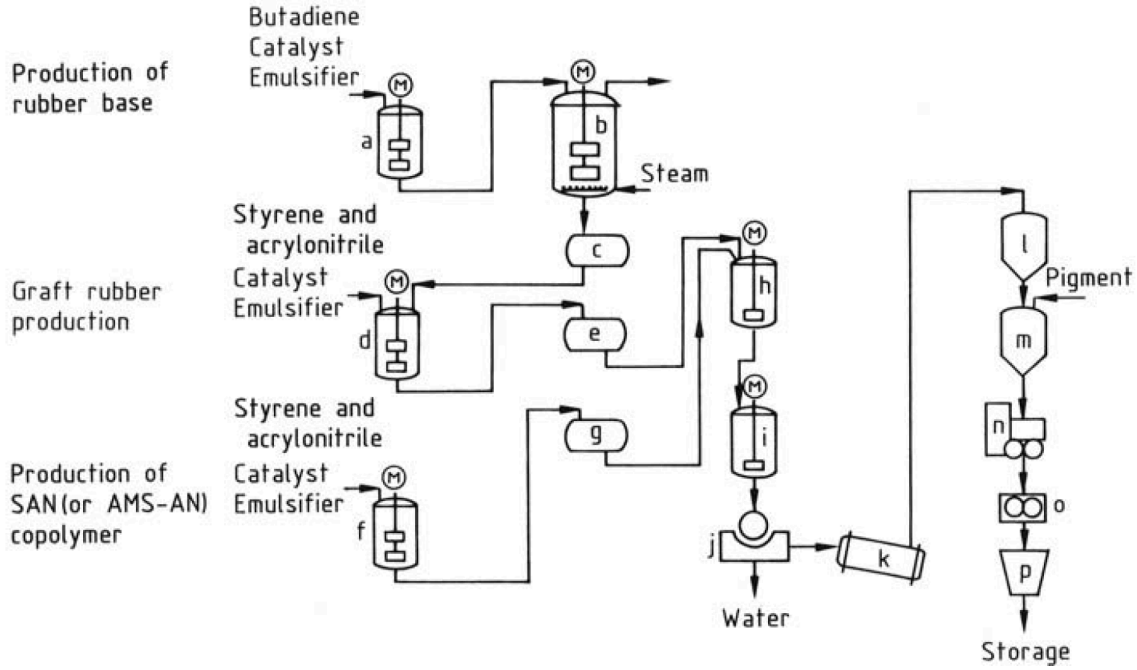

FIGURE 1.6: Production of ABS graft rubber and ABS by emulsion polymerization a) Polybutadiene reactor; b) Degassing reactor; c) Polybutadiene latex tank; d) Grafting reactor; e) Graft latex tank; f) SAN reactor; g) SAN latex tank; h) Latex mixing and stabilization tank; i) Coagulation reactor; j) Filter; k) Dryer; l) Powder silo; m) Premixer; n) Internal kneader; o) Rollers; p) Granulator [3].

ABS Production by Bulk Polymerization

ABS production by bulk polymerization (Fig. 1.5B) is based on the polymerization of St – AN mixtures in the presence of a rubber substrate dissolved in this monomer phase. The process can be divided into three steps:

1. The rubber substrate is dissolved in the monomer mixture,
2. The rubber – monomer mixture is prepolymerized with continuous mixing (conversion 15 – 30 wt %) and
3. The polymer – monomer mixture is polymerized further by bulk suspension polymerization or by continuous bulk polymerization in a high-viscosity reactor cascade.

Unlike the emulsion process, no preformed rubber particles are present at the beginning of the grafting reaction. In emulsion polymerization the particle size distribution is determined by the particle size of the grafting base, in bulk polymerization it is mainly determined by

the choice of the rubber base and the reaction conditions during prepolymerization and PI. B rubbers with a glass transition temperature of $\leq -80°C$ are usually used as the grafting base. B rubbers containing ca. 40% of units with a 1,4-cis configuration are preferred because they do not crystallize and the resulting ABS blend has a good low-temperature toughness. The molecular mass and degree of branching are very important for adjusting the particle size and the rubber phase volume in the prepolymerization stage. Long-chain branched B rubbers with an average molecular mass of 180 000 – 260 000 are commonly used [3]. High glass grades are made from star-branched B rubbers with low solution viscosity. The rubber content is limited to ca. 20wt% in ABS bulk processes for viscosity reasons.

The rubber is chopped to pieces and charged to a dissolving vessel. Dissolution in the monomer mixture and optionally a solvent (ethylbenzene; usually 5 – 15 %) may take up to 10h. AN acts as a precipitation agent for the B rubber; with increasing AN content of the solution less rubber can be dissolved and additional solvents are necessary. The rubber solution is transferred to a feed tank and continuously fed to the reactor cascade. The prepolymerization stage is performed with continuous stirring. Phase separation and PI begin during prepolymerization and largely determine the size, structure, and particle size distribution of the rubber phase in the resin matrix and thus the properties of the products. In the radical-initiated prepolymerization step, an oil-in-oil emulsion is formed at conversions of ca. 2% [47, 48]. Monomer charged SAN droplets are emulsified in the rubber solution by graft SAN polymer chains which are simultaneously formed on the rubber. With increasing SAN formation the phase volume ratio changes [49]. When the phase volume ratio reaches approximately unity, PI begins and the rubber phase is then dispersed in the SAN phase [50], i.e., the SAN – St – AN monomer phase becomes the continuous phase [51]. SAN is enclosed in the newly formed PB particles in the form of occlusions. The PI process, is terminated at conversions of ca. 12 – 15%, depending on the rubber content of the starting solution. The rubber particle size is determined by three main parameters:

1. The shear forces applied during stirring [52],
2. The viscosity ratio of the two phases [53] and
3. The interfacial tension between the two phases [54].

PI can be detected by viscosity measurements. After PI polymerization is continued to a conversion of ca. 25 – 30%. The viscosity of the polymerizing mass is then already so high that the PI becomes irreversible.

Another important factor affecting ABS production by bulk polymerization is the degree of grafting [55]. Grafting occurs as a result of hydrogen abstraction in the allyl position. The degree of grafting depends on the nature of the initiators and modifiers, as well as the different solubilities of St and AN in the rubber and matrix phases [56]. This difference in solubility lowers the degree of grafting and leads to differing AN contents in the grafted rubber and the matrix resin. The molecular mass and molecular mass distribution are principally determined

by process parameters (temperature, initiator concentration, solvent, and CTA). Thiols are especially effective as molecular mass modifiers in the initial phase of polymerization, CTA (e.g., terpinols) are only effective at higher conversions because of their smaller transfer constants. Another important parameter is the establishment of defined rubber crosslinking densities. Since the crosslinking density is thermally controlled, this parameter is mainly determined in the degassing stage of the continuous bulk ABS process by variation of the temperature and the residence time [3].

In the continuous bulk solution process, polymerization is carried out in a cascade of two or more reactors [57, 58]. Solvents or mineral oils are often added to lower the viscosity and improve heat transfer. Prepolymerization is performed in tower or stirred-tank reactors. Prepolymerization is followed by polymerization in a high-viscosity reactor or a tower reactor cascade [3]. The average residence times are ca. 10 – 15 h, and the reaction temperatures 170 – 270 °C [3]. Final conversions of 80 – 85% are established. Various processes are used to separate the polymer and residual monomer at the end of the bulk polymerization stage: strand degassers, degassing extruders, thin-film evaporators, and spray evaporators. Common are two-stage processes involving a flash tank and a second facility. The SAN matrix of ABS polymers usually has molecular masses in the range 50 000 – 170 000, the molecular nonuniformity Mw/Mn is ca. 1.5 – 3.0. To achieve maximum toughening, an average rubber particle size of ca. 2.5 mm is aimed at. The particles generally have a cellular structure but other structures (e.g., capsules or lamellae) can be obtained by using PB or B – St block copolymer bases or special phase and reaction conditions in the prepolymerization stage [59–61].

1.2.3 Grafting Reaction

The radical-initiated grafting of vinyl monomers (e.g., St, AN, or methyl methacrylate) only produces satisfactory graft yields with a few rubbers. Industrially, B polymers are used almost exclusively as the rubber (graft) base, PB being the most common because of its low glass transition temperature. Grafting of vinyl monomers (e.g., St) on PB can take place by two mechanisms [3]:

1. **Addition to the double bond**

$$-CH_2-CH=CH-CH_2- + R^{\bullet} \longrightarrow -CH_2-\underset{\displaystyle R}{\underset{|}{CH}}-\overset{\displaystyle \bullet}{CH}-CH_2- \quad (1)$$

2. **Abstraction of hydrogen**

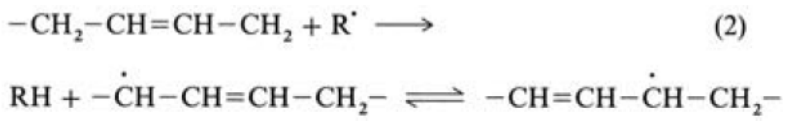

where $R\cdot$ is a polymer or initiator radical. The PB radicals formed according to Equation (1) or (2) react further with monomeric St to give the graft copolymer (3):

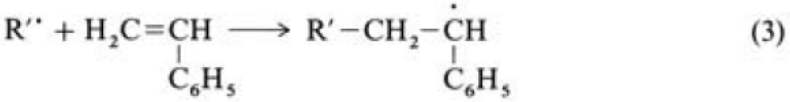

The allyl radical (2) is not very reactive because of its high resonance stabilization. Its resonance energy is comparable with that of a St radical [62, 63]. Common PB rubbers are composed of 1,4-cis, 1,4-trans and 1,2-vinyl units. Grafting occurs mostly via abstraction of the allylic hydrogen atom of the 1,2-vinyl group. A copolymerization mechanism has also been proposed for the grafting reaction [64, 65]. The kinetics of the radical grafting reaction largely correspond to the normal kinetics of radical polymerization. At low rubber concentrations deviations occur because of crosslinking reactions. In the thermally initiated grafting of St onto PB the graft yield increases with increasing temperature and with the 1,2-vinyl group content of the graft base [3].

1.2.4 Polymerization Initiators in Bulk Polymerization Processes

Polymerization initiators are chemical species that contain thermally labile radical-generating functional groups. They are added to the recipe in a small proportion, usually $< 1\%$ by weight based on the monomer [66]. The use of chemical initiators has been found to increase the polymerization rates, while keeping molecular weights at acceptable levels. The decomposition of a labile group in a polymerization initiator generates a primary radical, which adds to the monomer C-C double bond to form an initiating radical. This decomposition can be characterized by the rate of decomposition k_d or its half-life time, given by

$$t_{1/2} = \frac{\ln 2}{k_d} \tag{1.1}$$

Most conventional polymerization processes require values of k_d in the range of $10^{-6} - 10^{-4} s^{-1}$, i.e half-life times in the order of $1 - 100$ h. Initiators typically have acceptable half-life times only within a relatively narrow temperature range, around 20-30 °C [27]. The dependance with pressure is very weak and should only be considered for very high pressure systems [67]. Given their technological value, polymerization initiators are the object of a number of patents and patent applications [68, 69].

The two most important types of polymerization initiators contain azo or peroxide groups as labile groups. Due to their very limited use in industrial process, other types of polymer-

ization initiators, such as carbon-carbon and photochemical initiators, will not be considered in this thesis.

Dialkyldiazenes and dialkyl hyponitrites are the main classes of azo initiators. Dialkyldiazenes, of general formula $R-N=N-R$ are sources of alkyl primary radicals. Most dialkyldiazenes employed as polymerization initiators are symmetrical, and their substituents are usually tertiary, which gives the generated radical greater stability. The most common compounds of this category include 2,2'-azobis(isobutyronitrile) (AIBN), 1,1'-azobis(cyclohexanecarbonitrile) (ACBN), 2,2'-azobis(2-methylbutanenitrile) and 4,4'- azobis(4-cyanovaleric acid), as shown in Figure 1.7.

Peroxides, of general formula $R-O-O-R$, are widely used as polymerization initiators. Among the most used peroxide types are: diacyl peroxides, peroxycarbonates, peroxyesters, dialkyl peroxides, hydroperoxides and inorganic peroxides (e.g persulfate) [27]. Dibenzoyl peroxide (BPO) and dilauroyl peroxide (LPO) are among the most common diacyl peroxide initiators, which are sources of primary alkyl radicals (see Figure 1.8).

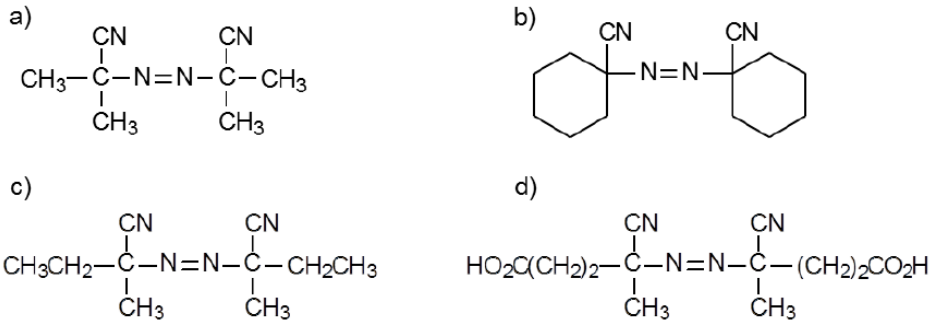

FIGURE 1.7: Symmetrical dialkyldiazene initiators a) AIBN, b) ACBN, c) 2,2'-azobis(2-methylbutanenitrile) and d) 4,4'-azobis(4-cyanovaleric acid).

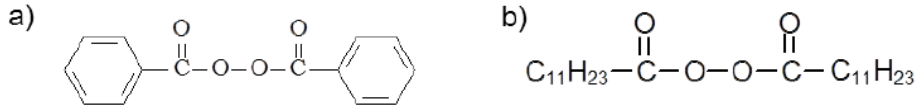

FIGURE 1.8: Peroxide initiators a) BPO, b) LPO.

The relative ease of synthesis of peroxide type initiators compared to azo compounds makes their industrial use advantageous [29]. The leading producers of organic peroxide initiators are Arkema (with trade names such as Luperco, Luperox, Lupersol), Akzo (Trigonox, Perkadox) and Solvay. The worldwide market of peroxide initiators is about 10 times larger than the market for azo initiators [70].

As in various industrial free radical polymerization processes, the use of monofunctional initiators is limited due to the difficulty of achieving a good balance between process productivity and product properties [72, 73]. The use of multifunctional initiators has been increased in the recent decades, since they allow obtaining high polymerization rates and polymers with

high average molecular weights, as a consequence of the sequential decomposition of the initiator [72, 74, 75].

Multifunctional initiators are chemical species with more than one radical-generating group. This category includes polyperoxides, polyazo compounds and azoperoxidic compounds. Multifunctional initiators may suffer two types of decomposition reactions. Total decomposition can occur in initiators where radical generating labile groups are in appropriate proximity, such as in peroxyoxalate esters and hydroperoxy diazenes [27]. It may also occur in cyclic multifunctional peroxide initiators [74, 76], depending on reaction temperature. In this decomposition mechanism, all labile groups decompose simultaneously. Sequential decomposition occurs when labile groups are suffciently remote from each other and generate radical species that may contain undecomposed labile groups [27]. The labile groups decompose, generating new primary radicals and re-initiating the polymerization reaction. Some cyclic compounds can be too sterically hindered for sequential decomposition to be possible, and thus fail to initiate the reaction [74]. St polymerization was successfully achieved with certain cyclic peroxides [74, 76, 77] and it was found that the thermolysis of peroxide bonds in cyclic polyperoxide initiators involves diradical species [74]. The polymerization mechanism may cause the polymer species to contain these undecomposed labile groups, either at the chain end or within the polymer chain [72, 78]. The subsequent decomposition in the sequential mechanism may form long chain radicals.

Bifunctional initiators in HIPS production processes have been studied [22, 79–83]. It was observed that said initiators allow both high productivity and high-molecular weights. Initiators with higher functionalities (tri- and tetra-functional) have been studied in the case of PS homopolymerization [74, 84], as well as for HIPS production [85, 86]. It was observed that the sequential decomposition of the initiators leads to significant increases in the rate of polymerization and high molecular weights. Depending on the initiator molecular structure, it may also introduce branching in the chains, leading to improvements in rheological and processing properties [19, 87]. Some of the most used multifunctional initiators in the production of PS-resins are shown in Fig. 1.9

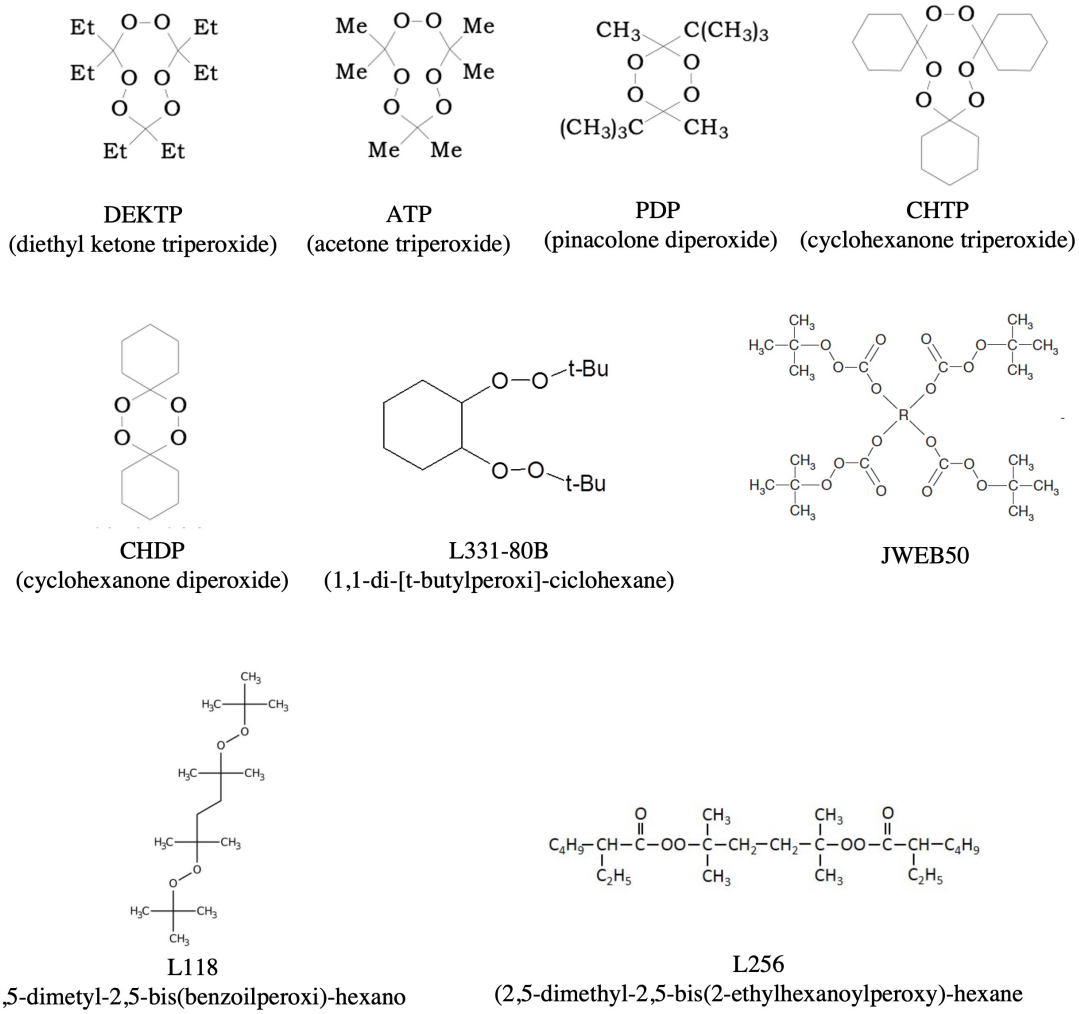

FIGURE 1.9: Multifunctional initiators used in the PS industry.

1.2.5 Devolatilization Stage in Bulk Polymerization Processes

The chain polymerization of monomers rarely proceeds to completion and there is inevitably a level of unreacted monomer remaining in the polymer. The presence of residual monomer is undesirable, particularly when the monomers are toxic, which is the case of St and AN. Contamination with monomers is a problem particularly when the polymer is used for food packaging, as well as in biomedical applications and in interior paints. Moreover, polymers may contain small amounts of nonpolymerizable compounds that result from impurities in the raw material or by-products formed from side reactions during the polymerizaton process. This results in an increase in the level of the residual volatile organic compounds (VOCs) in the polymer and can adversely affect its final properties [67]. The increasingly strict environmental regulations and the higher market sensitivity to environmental and health issues are pushing the polymer manufacturing industry to reduce the amount of monomoers and VOCs in polymers.

In a bulk process, polymerization at high conversions is complicated by the effect of

viscosity on initiator efficiency, monomer diffusion, and heat transfer. The efficiency of the initiator radicals can be dramatically lowered due to the cage effect resulting from the low mobility of the radicals, leading to a decrease in the polymerization rate. On the other hand, in polymerizations taking place at temperatures below the glass transition temperature of the polymer, the mobility of the monomer molecules is restricted, causing a severe decrease in the polymerization rate (glass effect). The use of higher temperatures would reduce the viscosity of the system, thus avoiding some of the drawbacks associated with high viscosities. However, high temperatures have deleterious effects on the properties of the polymer, such as a decrease in the molecular weight and degradation of the polymer.

The understanding of the origin of residual monomers and VOCs will help to design strategies to polymerize up to very high monomer conversions (the higher the monomer conversion, the less residual monomer) while simultaneously avoiding the formation of new VOCs by side reactions. However, post-treatments are always necessary in order to fulfill the legislation and market requirements.

In particular, in the processes for obtaining polystyrenes (GPPS, HIPS and ABS), the final stage is DV, which is carried out at high temperatures and under vacuum to remove low molecular weight components such as monomers, oligomers and other species from the polymeric melt [88–90]. Chemical reactions and transport of low molar mass species during DV have an important effect on the quality of the final product during this part of the process [91]. Also, high-temperature reactions, such as crosslinking, oligomer formation, and degradation that affect the material final properties, occur at this stage. Furthermore, particle breakdown can cause changes in morphology. The volatile species content affects the Melt Flow Index (MFI) which is the main processing property. The degree of crosslinking is measured indirectly through the Swelling Index (SI) and is also clearly affected.

1.3 Characterization and final properties of rubber-toughened St polymers (HIPS and ABS)

The choice of a material for a given application is determined, in part, by its final properties. Final properties also depend on the composition, molecular structure, and morphology. In the case of HIPS and ABS, the composition considers the fraction of free PS/SAN, unreacted PB, GC, the content of residual monomer(s), additives, and gel content in the final polymer. In addition to the final composition of the polymer, industries require intermediate compositional measurements throughout the polymerization, such as conversion or solids content (i.e.: ratio of the mass of polymerized monomers to the mass of total monomers) and grafting efficiency (GE) or insoluble content (i.e.: ratio of grafted monomers mass to polymerized monomers mass). The molecular properties of interest are the molecular weight distributions (MWDs) of the PS, SAN, PB and GC, and the branching degree and chemical composition distributions of the GC. Morphological properties include the distribution of particle sizes and occlusions, and the type of morphology (i.e., salami, core-shell, etc.). The quality properties for HIPS

and ABS are: a) the processing properties (i.e., viscosity, MFI, etc.); b) the mechanical properties of the solid (i.e., tensile, compression and flexural behavior, dynamic-mechanical behavior, IR, etc.); c) optical properties (i.e., transparency, gloss, surface finish, etc.); d) thermal properties (i.e., glass transition temperature, melting temperature, heat capacity, etc.); and e) the general physico-chemical properties (i.e .: density, solubility, resistance to attack of certain solvents, resistance to the environment, etc.). Next, the most commonly used methods and techniques to characterize some of the properties described above will be considered. In addition, some standardized procedures for characterizing the final properties of greatest interest will be discussed. For simplicity, the following is described for HIPS, but it should be noted that these methods are esencially equivalent for ABS.

1.3.1 Characterization of the Composition

The compositional properties that are measured throughout the HIPS synthesis process are: a) conversion; b) solid content; c) grafting efficiency; and d) the content of insolubles. Most of these properties are evaluated by gravimetric methods and solvent extraction techniques [6, 17, 19, 81, 92, 93]. While the conversion basically depends on the monomer consumption in the reactor, the solid content includes the presence of other species such as rubber, mineral oils, antioxidants, and other non-volatile additives. To characterize the composition of HIPS throughout the prepolymerization and termination, the technique consists of dissolving the polymers in toluene, precipitating them in methanol, and drying under vacuum until volatile species are removed (i.e .: monomer and solvents). The conversion is calculated as the ratio between the mass of precipitated polymer (free of rubber and non-volatile additives), and the total St mass. In the case of continuous processes, the definition is valid only in steady state, since the estimation of the rubber fraction and non-volatile additives is referred to the input conditions. Solvent extraction techniques are used to separate the polymers that make up HIPS. The free PS is extracted from the PB and from the GC by dissolving a sample of non-volatiles in a mixture of 50% by volume methyl ethyl ketone (MEK) and dimethylformamide (DMF). The MEK / DMF insoluble sample fraction (i.e., graft copolymer + residual PB) is separated by centrifugation. After several redissolutions and extractions, the free PS present in the supernatant fractions is precipitated in methanol and dried to constant weight. For the subsequent characterization of the rubber, the insoluble precipitate is dried under vacuum, at room temperature, to avoid crosslinking reactions [6, 19, 81, 92–95]. For samples where the rubber crosslinking is low enough, and the unreacted PB and GC are still soluble, treating the insoluble precipitate with petroleum ether allows separating the PB from the GC [92]. After several centrifugation and re-dissolution steps, the PB remains dissolved in the supernatant liquid and is separated by precipitation with methanol. Despite their extensive use, the extraction techniques described above have some limitations, such as the impossibility of completely extracting the free PS fraction present in the occlusions of the gummy particles [6, 19, 94–96]; neglecting some solubility of the oligomers in the solvents; and using relatively low masses [92, 93]. Once the free PS has been separated, the content of

insolubles is estimated as the ratio between the mass of insolubles in MEK / DMF and the mass of the initial sample. Grafting efficiency is calculated in the same way, but subtracting the initial rubber mass [6, 19, 81, 92–95]. Since it is practically impossible to completely extract the free PS fraction that is part of the occlusions within the rubber particles, this technique provides values in excess for grafting efficiency [6, 19, 94–96].

1.3.2 Characterization of the Molecular Structure

The St homopolymer is usually characterized using tetrahydrofuran (THF) as a solvent because it exhibits a very different refractive index than that of the polymer. For calibration, anionically synthesized monodisperse PS standards are used [97]. A detailed description of PS chromatographic analysis is found in ASTM D5296. Molecular characterization of HIPS and St heterogeneous polymers presents difficulties with respect to St homopolymer because: a) it contains mixtures of various polymer components, which usually must be separated after chromatographic analysis; and b) contains chromatographically complex polymeric species (i.e., presence of co- and terpolymers, branching, etc.). In HIPS, free PS is extracted from PB and GC using the same technique described for determining grafting efficiency [6, 19, 81, 92–95]. So far, the chromatographic analysis of complex polymers has not been completely resolved [97–99]. For linear and block copolymers, calibrations obtained by interpolating those corresponding to homopolymer standards are usually used, with contributions given by the global and / or instantaneous average chemical composition of each fraction [97, 98, 100–102]. For the GC generated in the HIPS synthesis, Estenoz et al. [92] degraded the PB by ozonolysis and used SEC with simple detection (refractive index) to determine the MWD of the PS branches. Huang et. al. [95] used the software for the separation of the peaks, and measured the distribution of molecular weights and the frequency of grafts for a mixture of cis-PB, PS, and GC, by means of SEC with dual detection (refractive index). and UV-visible). In the first part of a series of publications, Estenoz et al. [103] compared the estimates of molecular weight, branching degree, and chemical composition distributions of the GC provided by a mathematical model of HIPS polymerization with the distributions obtained after applying an ideal SEC model. They found that the molecular weight and branching degree distributions were almost completely overlapping, while the chemical composition distribution estimated by SEC was much narrower than that obtained from the polymerization model, because the wide instantaneous distributions presented very similar average values. In the second part of the series, Vega et al. [104] compared the results of the mathematical model of the polymerization with experimental values of branching parameters determined with an in-line viscometer, and adjusted the branching exponent of the GC in THF to a value of 2. From a completely experimental point of view, there are little history of graft copolymer analysis. Mrkvičková [105] determined the DPM and the chemical composition distribution of a polydimethylsiloxane-grafted polymethylmethacrylate copolymer. For this purpose, they used SEC with dual detection (refractive index and low angle light scattering), using toluene and THF as solvents. Polydimethylsiloxane was isorefractive (invisible) in THF, while poly-

methylmethacrylate was in toluene.

1.3.3 Characterization of the Morphology

The methods used to characterize the morphology of HIPS are: a) the selective dissolution of the PS matrix, followed by the characterization of the insoluble phase; and b) the global characterization of the material by light or electron microscopy [106]. Regarding the application of the selective matrix dissolution technique, [107] considered a mixture of toluene / MEK (57% by volume), while Craig et al. [108, 109] used DMF, and Hall et al. [110] MEK. The dried particles were examined by light microscopy, or by SEM, and particle size distribution (PSD) was determined. Another commonly applied method of analysis is to resuspend the particles in a suitable medium and analyze them by light scattering [6, 110], or by using electric field sensors [108, 109] . The main problem with this type of technique lies in the choice of solvent, and in the severe physical-chemical manipulations to which the sample must be subjected, prior to and during microscopic characterization. An alternative to selective dissolution techniques is observation of the entire sample by microscopy. Given the difference between the different refractive indices of the PS matrix and the rubber particles, phase contrast microscopy allows images with light and dark areas without the need to use a dye [107, 111–114]. However, the low magnification of light microscopy, added to the impossibility of detecting intraparticle structures, has determined that Transmission Electronic Microscopy (TEM) is the preferred technique for the morphological characterization of HIPS and ABS. The technique involves cutting a sample of the material into extremely thin sections (50-60 nm), cryogenically or at room temperature. The film of material is then stained with osmium or ruthenium oxides and irradiated with an electron beam. The electron density distribution transmitted through the sample is recorded to generate a photomicrograph of the cut. The main advantage of this technique is the direct observation of the particles. However, it has disadvantages regarding the determination of PSDs, since a high number of micrographs is required for the sampling to be representative.

1.3.4 Characterization of the Final Properties

Although there are numerous final properties that define the quality of HIPS, the most important from an industrial point of view are MFI and IR. Nevertheless, the thermal, optical, and electrical properties are also used to decide possible applications of the material [42]. A list of methods for sample preparation and characterization of the final properties of HIPS can be found in ISO 2897. The following is a summary description of the mechanical and processing properties most commonly used to characterize HIPS. Among the mechanical properties, those associated with hardness (elastic modulus), toughness (IR), creep (stress and elongation), and fracture (stress and elongation at break) are considered. Traditionally, determinations are made through static, dynamic, fatigue, and / or impact tests [115]. The static stress test is carried out by deforming a standardized specimen unidirectionally and at a constant strain rate (ASTM D638). From the point of view of the mechanical description of the material,

the torsion and compression tests are complementary to the stress test (ASTM D790, ASTM D695). From the stress test, it is common to determine the following HIPS properties: a) the elastic modulus, which represents the intrinsic capacity of a material to resist a certain load without permanently deforming, and corresponds to the relationship between the applied stress and the deformation suffered; b) toughness, given by the area under the stress-strain curve, indicates the ability of the polymer to absorb energy by impact without fracturing; c) the yield point, given by the transition between the elastic deformation and the plastic deformation, is associated with a change in the molecular configuration, and experimentally coincides with the formation of a neck in the specimen and a maximum in the stress curve-deformation; and d) the breaking point, given by the fracture of the material.

IR is evaluated in terms of the energy absorbed during the impact process, and the methods used to measure are: Izod (ASTM D256), Charpy (ISO R179), Gardner (ASTM D3029), and Tensile Impact (ASTM D1822). Unlike toughness, impact tests are high in intensity, with Izod and Charpy IR being the most popular methods, which involve triaxial stress. Less used are the Gardner and Tensile Impact tests, because they involve biaxial and uniaxial stresses, respectively. The Izod and Charpy tests are consistent in hitting a standardized probe with a pendulum at speeds between 300-400 cm/s. The presence of a notch in the probe promotes stress concentration in this area, and results in lower IR measurements than those obtained in the analogous test with specimens without a notch.The behavior of HIPS during processing is linked to its rheological properties in the molten state. Although the flow curve (viscosity as a function of strain rate) provides more complete information, the MFI is the quality variable mostly used to characterize the material from a rheological point of view [116].

MFI is a measure of the flow (in g/10 min) of molten polymer that passes through a plastometer when it is forced by a piston under constant load (ASTM D1238). Polymer accumulates inside a heated cylinder attached to a capillary through an abrupt contraction or inlet zone. The test is carried out between 160-200 °C, conditions similar to those of extrusion of the material. The more viscous the material, the slower it flows. In this way, a lower MFI will result in greater processing difficulty.

1.4 Final Properties-Structure Relationships

In general, the final properties of HIPS and St heterogeneous plastics are determined by composition, molecular structure, and morphological structure. Heterogeneous St polymers are designed for applications where good impact properties are required, either at room temperature or below. As a general rule, the reinforcement of the rubber is considered to be acceptable when it exhibits: a) a low elastic modulus with respect to the matrix; b) adequate crosslinking and good adhesion with the matrix; c) an optimal distribution and average particle size; and d) a low glass transition temperature [115].

Fig. 1.10 presents a qualitative diagram of the variation of certain HIPS properties with the structural variables and / or the recipe. This scheme shows conflicting structural variables in relation to the improvement of final properties. For example, an increase in the molecular

weight of the PS or the rubber content determines an improvement in the toughness of the material, but simultaneously, a reduction in the MFI (and more expensive processing). An increase in the plasticizer content increases the value of the MFI, but simultaneously reduces the mechanical and thermal resistance of the material. An increase in crosslinking density improves tensile strength but worsens toughness, because the rubber loses elasticity. The above examples show the complex interrelationship between the structural variables and the final properties of HIPS.

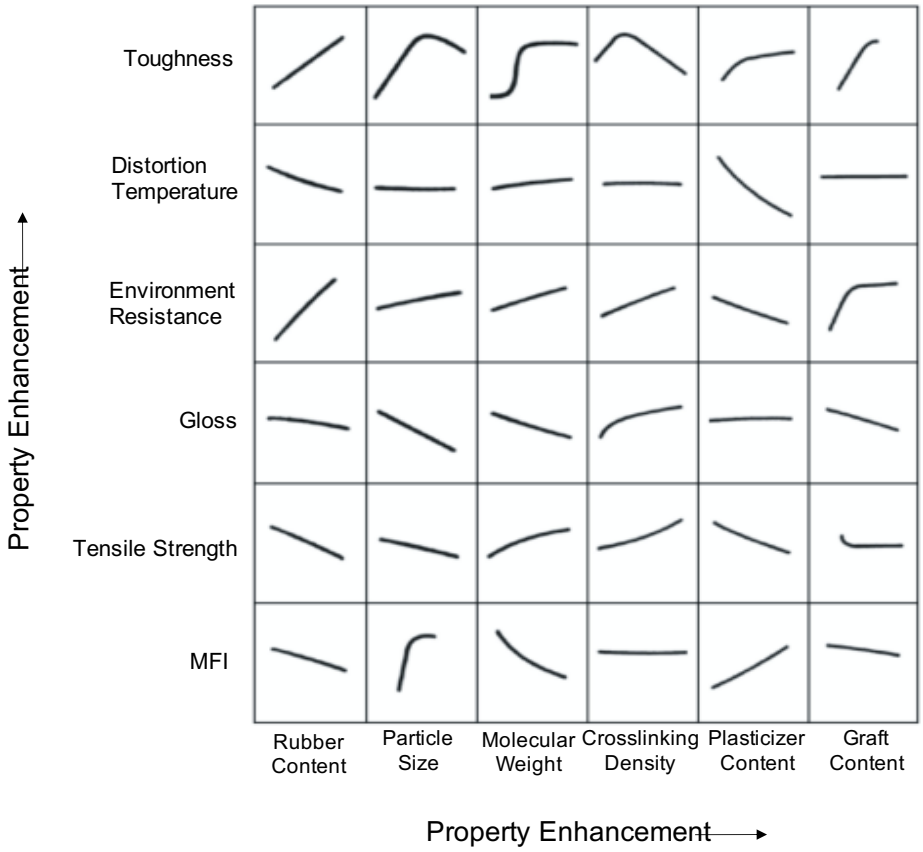

FIGURE 1.10: Relationships between structure/recipe and final properties

1.5 Mathematical Modeling of Radical Polymerization Processes Using Multifunctional Initiators - Optimization and Control

The environmental problem, added to the global financial situation, puts St polymer manufacturing industries in search of alternatives to increase their productivity and profitability, and reduce the environmental impact of their products and processes. Thus, there is a growing technological interest in improving the quality of St resins and enhancing the process efficiency through its design and optimization.

The final properties depend not only on the recipe and the operating conditions, but also

on the technology used [117]. Figure 1.11 shows the complex and highly multivariable nature of the quality control problem [5]. The manipulative input data for the recipe, equipment choice and design are listed. The quality variables are divided into "chemical" and "physical" variables. The former are vitally important to understanding, modeling, and controlling bulk polymerization. The main "physical" variables are the thermo-mechanical characteristics of the final material and also include other properties such as gloss, color, transparency and environmental resistance. The latter are the ones included in the commercial specifications as they directly impact processing. In addition, the need to devolatilize on a cost-efficient basis together with the increasing number of restrictions on the acceptable volatile contents in polymers has led to increased attention towards understanding and optimizing this stage of the process [88].

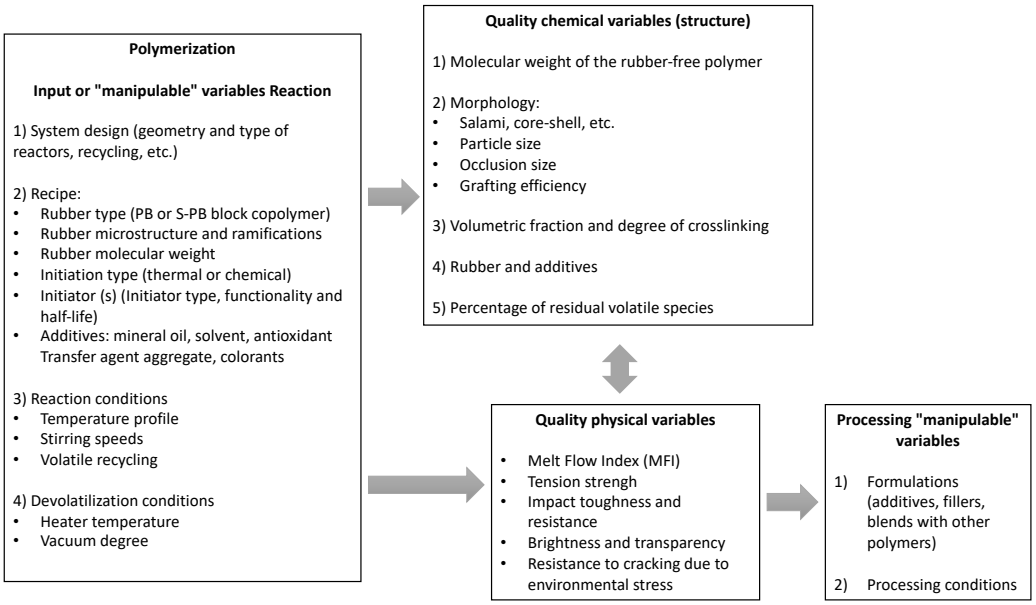

FIGURE 1.11: Variables involved in quality control for the continuous mass process of HIPS[5].

As in most polymerizations of industrial interest, the control of the production process of these materials is extremely complex. Figure 1.12 illustrates the various feedback loops that operate in a HIPS production plant [5]. Strictly, the system features 4 control loops. A first internal loop that considers the measurable and controllable variables of the system, such as temperature, pressure, flow, and level of the reactors. Usually, this loop is closed by feedback drivers. More externally, there is a link that considers those properties measured off-line, which specify the quality of the material (i.e., IR, MFI, elongation at break, molecular weights, etc.). This tie is closed by the process engineer. The two external loops include the properties of the final material and are usually outside the polymerization plant. The inner loop is closed by the main customers of the plants, who process the material and define its desired properties, while the outer loop considers the material in its final application and is

closed by global demand, usually through the adjacent inner loop.

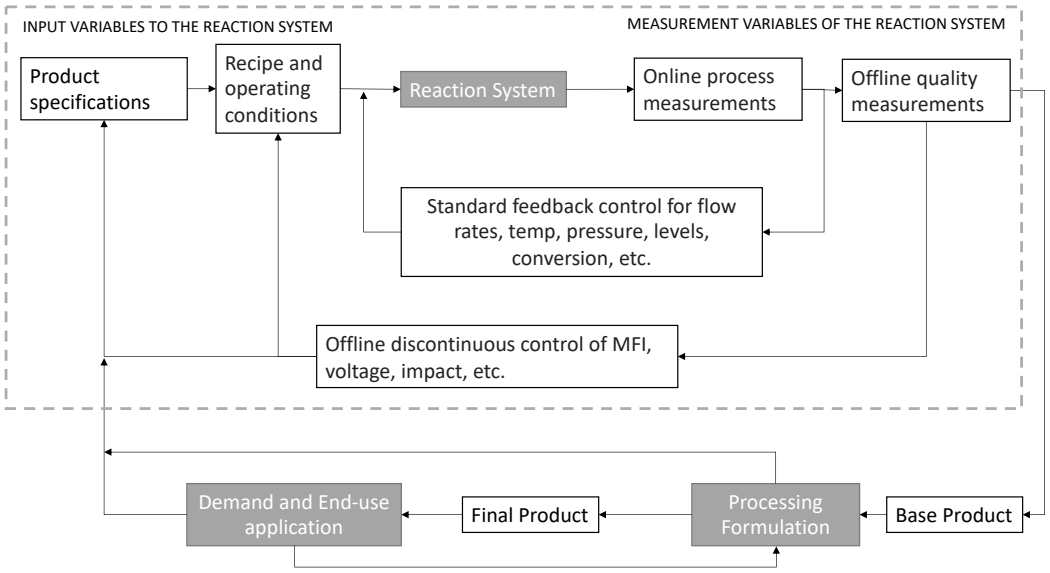

FIGURE 1.12: Control Scheme for a continuous plant of HIPS bulk production [5]

Although the basic technological process is well known, there are still many aspects to be elucidated related to the quantitative interrelationships between the process variables, the molecular and/or morphological characteristics, and the final properties. On the other hand, there is a growing technological interest in improving the quality of the material and increasing the efficiency of the processes by designing and optimizing them. The objective of the industry is to be able to study the effect on the final properties of possible changes in the recipe and the conditions of synthesis, and thus develop "made to measure" polymers.

On the other hand, polymerization reactors are often used to make various "grades" of the same polymer types. In a continuous plant, the “grade transition” is carried out with the application of a set of heuristic rules, based mainly on the experience of the plant. The problem in using heuristic rules is that it leads to a high amount of non-homogeneous products. Therefore, and given the strong market pressures, there is a clear need to systematize grade transition procedures in order to minimize the production of out-of-specification materials. These processes can be optimized to improve the quality of the final product and / or also the productivity of the system. Dynamic optimizations aim to improve start-up, reducing out-of-specification products generated during grade changes and eliminating long-term deviations due to fouling or volatile build-up from recycle streams.

As a consequence of the complexity of these chemical processes, modeling has become a necessary and useful tool for their understanding and design.

The mathematical models developed for the bulk HIPS process have mostly assumed the reaction system to be homogeneous and allowed: i) to estimate the global molecular structure; [19, 81, 94] ii) to simulate steady states in continuous industrial plants; [19, 81] iii) to

optimize transitions between steady states; [118–120] and iv) to improve the estimations of the GC molecular structure and of the grafting efficiency using size exclusion chromatography (SEC) combining these models with fractionation models. [103, 104, 121].The hypothesis of homogeneity in the models was justified by the fact that the monomer and initiator partition coefficients between the phases are both close to unity[122, 123]. The heterogeneous models published for the discontinuous synthesis of HIPS allowed: i) predicting the molecular structure of HIPS in each phase present; [93] and ii) estimating grafting efficiency using SEC in combination with extended fractionation models of polymerization models [93].

Very few mathematical models are reported in the literature regarding the use of multifunctional initiators, and most of them consider batch reactors [73, 81, 83, 84, 124]. In Estenoz et al. [81] monofunctional, bifunctional and initiator mixtures were studied in a batch reactor. In Berkenwald et al. [84], the performance of three multifunctional peroxide initiators in a bulk HIPS batch process was experimentally and theoretically investigated. A series of batch reactions was carried out using multifunctional initiators with varying functionality and structure. The theoretical work consisted of a mathematical model for bulk HIPS polymerization using multifunctional initiators that predicts the evolution of the main polymerization variables as well as the detailed molecular structure of the polymeric species and the melt flow index (MFI) of the obtained HIPS. Except in Estenoz et al. (1996b) [81] and in Berkenwald et al. [84], in all the aforementioned models the initiation kinetics were modeled with monofunctional initiators. No models have yet been published that consider the use of multifunctional initiators in continuous HIPS production systems. Neither have the thermal degradation, oligomer formation or crosslinking mechanisms present at high temperatures been considered. These mechanisms occur at temperatures above approximately 180 °C and were studied theoretically and experimentally for the polymerization of St in various works [125–129]. Despite the importance of these chemical processes in the rheological, processing and final solid properties, they have not been included in the mathematical models that represent the synthesis of HIPS. From a technological point of view, these processes present at high temperatures are of importance during the DV stage. Although there is bibliographic material referring to the study of polymer DV, there are few works specifically referring to PS or HIPS [12, 130–132]. In particular, there are no references for the study of the modification of molecular structure (degree of crosslinking and MWDs) and the morphology of the material during the DV process, variables that in turn have importance on the final properties such as "swelling index" (SI), MFI, and others. On the other hand, attempts to model an industrial process are few or have been made through simulations using commercial software [90].

Attempts at modeling complex reactions, such as scission or multiradical formation for other materials using either deterministic or stochastic models, such as Monte Carlo (MC) can also be found in the literature [76, 133]. The election of the method to be used depends basically on a personal choice. MC method is very useful in such cases, but can be more time consuming because it depends on the sample size and may disadvantageously present fluctuations and noisiness due to stochastic variation [134].

Moreover, purely stochastic models can be challenging to incorporate into optimization

routines, therefore limiting their simulation capabilities. In the present work, a deterministic model was used to solve the mass balances for each species. For the reinitiation step, a probabilistic method based on random number generation was employed.

Chapter 2
Mathematical Model of a Continuous Bulk Process for the Production of High-Impact Polystyrene Using Multifunctional Initiators

2.1 Introduction

In this chapter, the continuous bulk production of HIPS and the use of multifunctional initiators in the process is experimentally and theoretically investigated. A mathematical model that allows the simulation of the HIPS process using multifunctional initiators is developed. The modeled process comprises a polymerization train of stirred tank reactors (CSTRs) and a devolatilizer, where no chemical reactions occur and perfect separation of components is assumed. The model is based on a kinetic mechanism that includes thermal initiation, chemical initiation by sequential decomposition of a multifunctional initiator, propagation, transfer to monomer, transfer to rubber, termination by combination and re-initiation. The present model is comprehensive from a kinetic perspective, since it can be used to simulate a HIPS or GPPS process using initiators of any functionality and structure. The model is adjusted and validated using novel experimental data for bulk continuous HIPS polymerization in a pilot-scale plant. The pilot plant comprised the main stages of an industrial HIPS process: pre-polymerization, finishing and DV. The experimental work includes a series of polymerizations using three different multifunctional initiators: (1) luperox-331 M80 (L331), (2) pinacolone diperoxide (PDP), and (3) diethyl ketone triperoxide (DEKTP). Theoretical results for the reaction train show a very good agreement with the experimental measurements.

2.2 HIPS Production Process

In the industrial production process of HIPS, St is polymerized in bulk in the presence of about 6% in weight of dissolved polybutadiene (PB). This heterogeneous product consists of a PS matrix containing dispersed rubber particles, which in turn contain PS occlusions typically exhibiting "salami" or "core-shell" morphologies as shown in Figure 2.1 [6]. The graft copolymer (GC), generated during the process, is accumulated at the interface stabilizing the

heterogeneous system and promoting development of the morphology [35, 36, 135, 136].

The industrial continuous bulk process for HIPS production comprises four main stages: Dissolution, Prepolymerization, Finishing, and DV [19]. In the first stage, 5-10% w/w of previously grated rubber is dissolved in the monomer at relatively low temperatures (50-70 °C), in cycles of 4 to 8 h. A rubber content less than 5% w/w generates low or medium impact resistance (IR) polymers. Contents greater than 10% w/w involves solubility problems of the rubber in the monomer, and also an increase in the viscosity throughout prepolymerization. At an industrial scale, St is not purified since it contains inhibitors that prevent unwanted polymerization reactions in this stage [19]. Typically, small amounts of solvent (i.e. ethylbenzene or toluene), antioxidants (i.e. octadecyl-3,5-di-tert-butyl-4-hydroxyhydrocinnamate), lubricants such as mineral oils, and CTA (i.g. tert-dodecyl mercaptan) are loaded together with the monomer in the discontinuous dissolver, which is coupled to the rest of the continuous plant by means of a feed tank (see Fig 2.2).

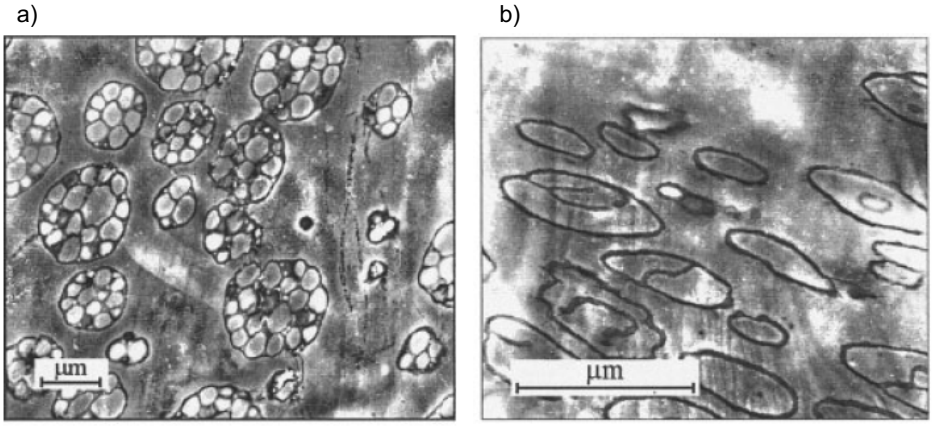

FIGURE 2.1: Typical HIPS morphologies [6]

Prepolymerization begins with the addition of a chemical initiator and an increase in temperature to 90-120°C, until 30-40% conversion. During this stage, the morphology of the material is developed. Unlike simple St/PS/PB mixtures, in the polymerization reaction of HIPS a fourth species is generated, namely GC. This species is generated from the beginning of the Prepolymerization as a consequence of the attack of polystyryl radicals to the rubber [62, 136]. Initially, the mixture of St and PB is homogeneous, but at relatively low conversions ($x \geq 2\%$) the phase separation is produced as consequence of thermodynamic incompatibility between preexisting chains of PB and produced PS chains [123, 137–139].

Events taking place during this polymerization can be monitored with the ternary phase diagram shown in Figure 2.3 [2]. For example, for a feed mixture made up of 8 wt% rubber in styrene (point A) on an increment of conversion to PS (to D), phase separation occurs. Small droplets of PS, which are stabilized by the GC, are dispersed in the St–PB solution. The composition of the two phases is given by points B and C for the PS-rich phase and PB-rich phase, respectively. The phase–volume ratio (i.e. rubber phase/PS phase) is given by the ratio DB/DC. As the reaction proceeds along the line AE, the phase composition

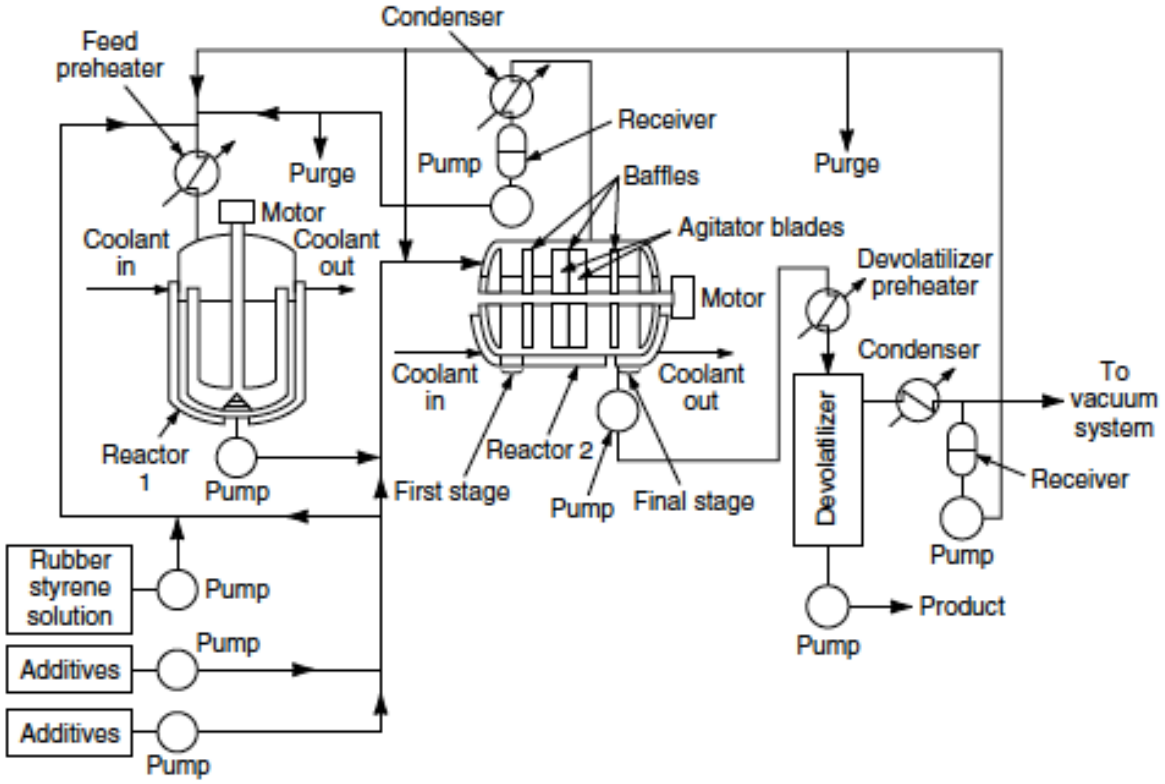

FIGURE 2.2: Typical staged CSTR process for HIPS.[2].

and phase–volume ratio can be read from the tie lines. Larger droplets of PS solution form and the small, original ones remain. When the phase–volume ratio is about unity (point F), provided that there is sufficient shearing agitation, the larger PS-containing droplets, which have mostly coalesced into large pools, become the continuous phase and PB-containing droplets are dispersed therein [140]. However, the latter contain the small, original PS particles as occlusions.

The particle size and size distribution are largely controlled by the applied shear rate during and after PI, the viscosity of the continuous phase, the viscosity ratio of the two phases, and the interfacial tension between the phases [140]. The viscosity parameters depend on phase compositions, polymer molecular weights, and temperatures; the interfacial tension is largely controlled by the amount and structure of the graft copolymer available at the particle surface. If shearing agitation is insufficient, then PI does not occur and the product obtained is a network of cross-linked rubber with PS and its properties are much inferior. The morphology of the dispersed rubber phase remains much as formed after PI. Rubber-phase volume, including the occlusions, largely controls performance. The PI period is crucial for the development of HIPS morphology [2].

Once the desired particle size and morphology with sufficient GC to provide adequate adhesion between the rubber particles and the PS phase have been achieved, the integrity of the particle must be protected against deformation or destruction during fabrication by crosslinking of the PB chains. If peroxide initiators are used, about one half of the rubber

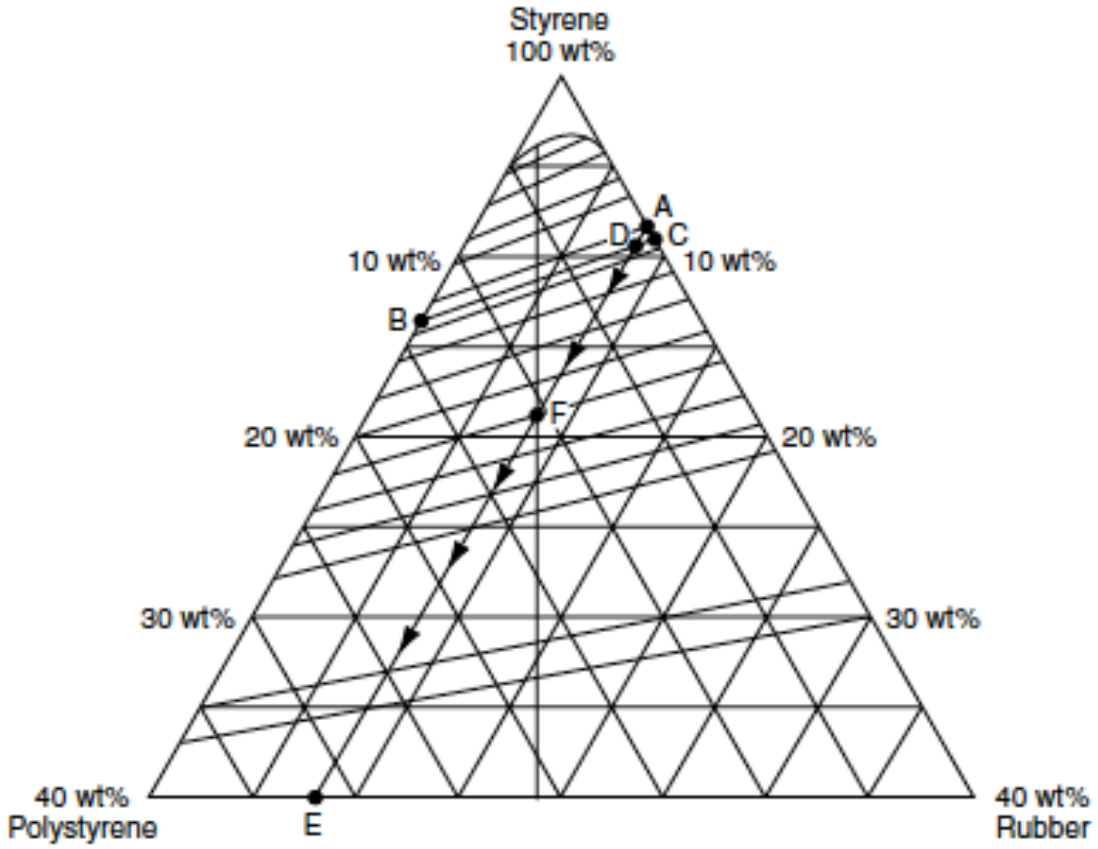

FIGURE 2.3: Ternary-phase diagram for the system St–PS–PB rubber[2].

is grafted by the time PI occurs; less is grafted in the absence of peroxides [62]. Hydrogen abstraction by alkoxy radicals at any of the allylic sites yields a site for St polymerization, resulting in a graft [62]. The double bonds in PB are much less reactive than those in styrene but as conversion exceeds approximately 80% and temperature approaches or exceeds 200 °C, copolymerization through the PB (1,2 units) chain seems to occur and leads to crosslinking and hence gel formation [8].

The Termination stage is carried out at elevated temperatures (120-150 °C) and in the absence of agitation. During this stage, the initiator has been almost completely consumed, and the rise in temperature promotes both thermal initiation of the monomer and reduction of the viscosity of the system. The agitation is reduced (or eventually eliminated) to preserve the morphology developed during the PI. In this way, the Termination is conducted without major changes in the type of morphology [6]. Freeguard [141] and Fischer and Hellmann [135] indicated that in case of continuing with the agitation after the PI, important changes in the morphology would be observed, and the developed morphology could eventually be destroyed during Prepolymerization.

Finally, in the DV, the polymer is separated from the nonreacted monomer by applying vacuum and high temperature (∼250 °C). These high temperatures promote crosslinking of the rubber that preserves morphology during further processing of the material and oligomer

formation. However, the residence time of the polymer in the devolatilizer equipment should be minimized to avoid its degradation [142].

The use of multifunctional initiators has been increased in the recent decades, since they allow obtaining high polymerization rates and polymers with high average molecular weights, as a consequence of the sequential decomposition of the initiator [72, 74, 75]. The use of bifunctional initiators has been widely investigated in relation to St homopolymerization. It was shown that operating at high temperatures, it is possible to obtain high reaction rates and molecular weights, with relatively narrow molecular weight distributions [143–145]. Bifunctional initiators in HIPS production processes have also been studied [22, 79–83] and it was observed that said initiators allow both high productivity and high-molecular weights. Initiators with higher functionalities (tri- and tetra-functional) have been investigated in the case of PS homopolymerization [74, 84], as well as for HIPS production [85, 86]. It was observed that the sequential decomposition of the initiators leads to significant increases in the rate of polymerization and high molecular weights. Depending on the initiator molecular structure, it may also introduce branching in the chains, leading to improvements in rheological and processing properties [19, 87].

Very few mathematical models are reported in the literature regarding the use of multifunctional initiators, and most of them consider batch reactors [73, 81, 83, 84, 124]. In Estenoz et al. [81] monofunctional, bifunctional and initiator mixtures were studied in a batch reactor. In Berkenwald et al. [84], the performance of three multifunctional peroxide initiators in a bulk HIPS batch process was experimentally and theoretically investigated. A series of batch reactions was carried out using multifunctional initiators with varying functionality and structure. The theoretical work consisted of a mathematical model for bulk HIPS polymerization using multifunctional initiators that predicts the evolution of the main polymerization variables as well as the detailed molecular structure of the polymeric species and the melt flow index (MFI) of the obtained HIPS. The continuous process of HIPS production using multifunctional initiators has not been investigated either theoretically or experimentally.

2.3 Experimental Work

The experimental work consisted on a series of continuous bulk St polymerizations in the presence of dissolved PB, using the multifunctional initiators DEKTP, PDP and L331 (Fig. 2.4) at 0.016% in weight. The polymerizations were carried out in a pilot plant as the one shown in the diagram of Figure 2.7. A 6% in weight of an alkyl lithium polymerized PB of medium cis –Diene 40AC10- was dissolved into the monomer. The polymerization recipe also included mineral oil to lower the viscosity of the solution and antioxidant to prevent rubber degradation. Variations in the temperature of the Finishing Reactor were studied in order to obtain different average molecular weights at the DV inlet. Conditions in the Prepolymerization Reactor were not altered and selected to achieve a proper steadying of the system and to ensure that PI is achieved at this stage.

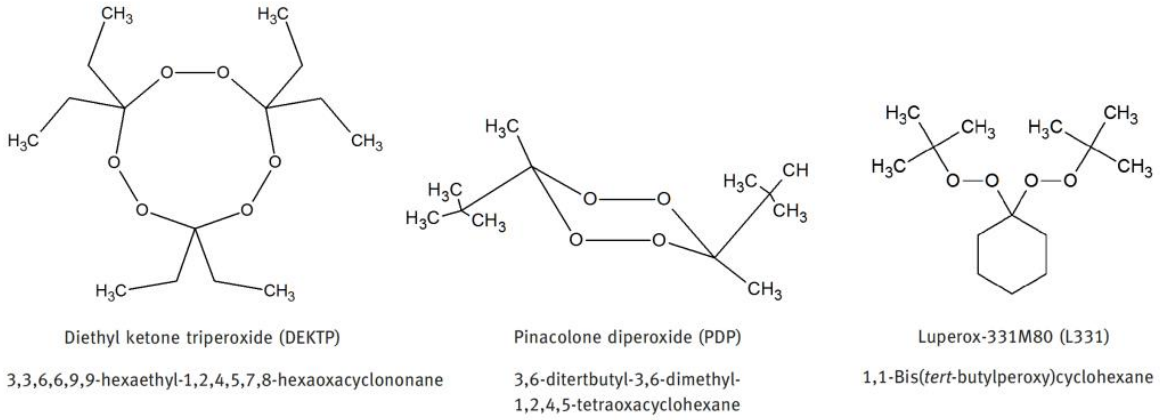

FIGURE 2.4: Initiators molecular structures with their commercial and IUPAC names.

2.3.1 Initiator Synthesis

The molecular structures of the initiators are shown in Fig. 2.4. L331 is a linear bifunctional initiator supplied by Sigma-Aldrich and was used as received. PDP and DEKTP are a cyclic bifunctional and a cyclic trifunctional initiator, respectively.

Synthesis of PDP

PDP was prepared according to methods previously described in the literature [76]. 50 mmol of 3,3-dimethyl-2-butanone were dripped into a stirred mixture of H_2O_2 (56 mmol) and HSO4 (195 mmol) at -15 to -20 °C. After 3 hours of reaction, the mixture was extracted with petroleum ether (3x25 mL). The organic layer was freed of H_2O_2 by washing with a saturated solution of NH_4Cl (3x10 mL) and with water (3x10 mL). The organic layer was dried over Na_2SO_4 for 24 hours. The solution was filtered and the product was isolated by solvent evaporation. The obtained white solid was recrystallized twice from methanol. The purity was confirmed by nuclear magnetic resonance (NMR) analysis as is shown in Fig. 2.5.

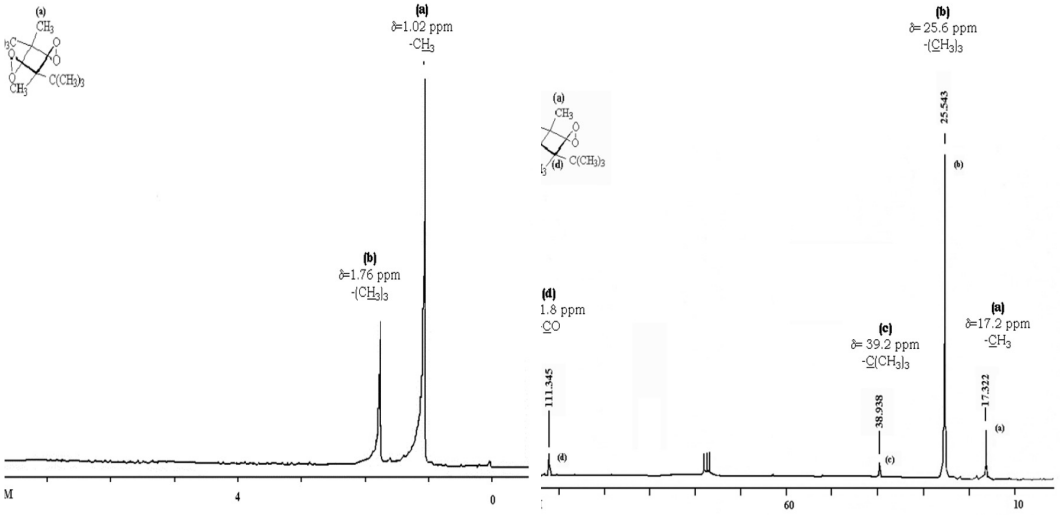

(a) (b)

FIGURE 2.5: (a) ^{1} H NMR spectrum of PDP and (b) ^{13} C NMR spectrum of PDP.

Synthesis of DEKTP

DEKTP initiator was synthesized according to the following procedure [74]: in a 250 mL Erlenmeyer ask 4.6 mL of hydrogen peroxide and 7.3 mL of sulfuric acid (70% v/v) were added and the temperature was kept at -10 °C. Then, 5.6 mL of diethyl ketone was added into the reaction medium and the reaction remained under agitation for 3h. Thereafter, the organic phase was extracted with petroleum ether and dried with sodium sulfate for 12 hours. The petroleum ether was removed under distillation and the product was crystallized from methanol, yielding a white powder. The purity was confirmed by NMR analysis as is shown in Fig. 2.6.

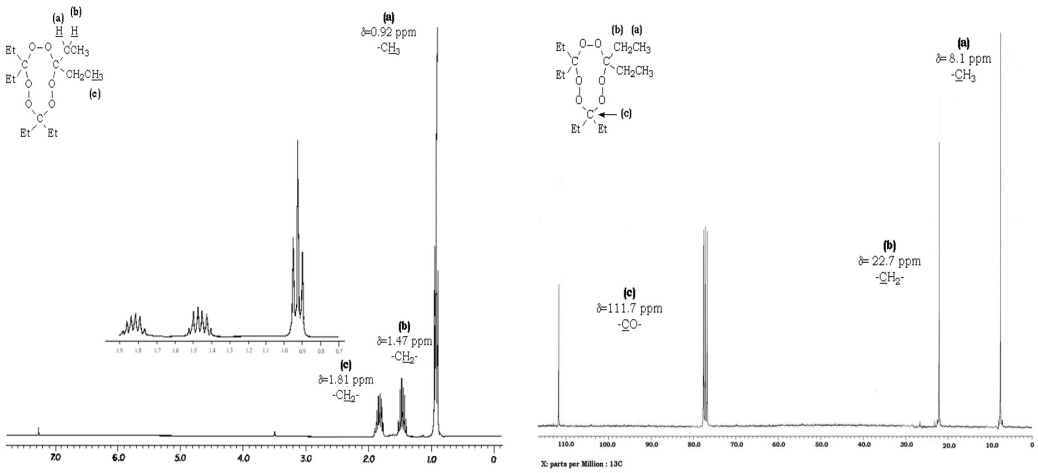

(a) (b)

FIGURE 2.6: (a) ^{1} H NMR spectrum of DEKTP and (b) ^{1}3 C NMR spectrum of DEKTP.

2.3.2 Synthesis and Characterization of HIPS by a Bulk Process Using Multifunctional Initiators

Reagents

The medium cis-PB was provided by Dynastol Elatomeros S.A de C.V., Mexico. The rubber was analyzed by size exclusion chromatography (SEC), and the average molecular weights resulted were: $Mn = 208,600$ g/mol and $Mw = 464,238$ g/mol. Monomer (St, 99.6%) was provided by Plastiformas (Monterrey, Mexico) verified by spectrophotometry according to ASTM D4590 and was used as received. Toluene, Methanol (99.8%) and tetrahydrofuran (THF, ≥99%, HPLC grade) were supplied by Sigma-Aldrich and were used without further purification. The mineral oil was supplied by Productos Químicos de Saltillo. The antioxidant was Irganox 1076 from BASF.

Pilot plant scale process

Figure 2.7 illustrates the pilot plant that was used for all experiments. The prepolymerization stage is carried out in the first CSTR, reaching approximately 30% conversion. The operating temperature is typically not higher than 115 °C. Termination takes place in a second CSTR, at higher temperatures. The selected polymerization temperatures are such that initiator decomposition is mostly sequential [146]. Finally, the DV stage takes place in a Falling Strand Devolatilizer (FSD) for the separation of low-molecular weight components under vacuum conditions and at elevated temperatures (i.e. 200-220 °C). The plant also includes a Zapper Unit (ZU), the purpose of which is to lower the viscosity of the DV inlet stream. Upstream the train reactor, the rubber is dissolved at room temperature into the monomer in a semi-batch Dissolver Tank (DT) with the addition of a small amount of mineral oil. After 8 hours of dissolution, its content is discharged into the Feed Tank (FT) and the chemical initiator and antirust are added. Table 2.1 summarizes the range of operating conditions for each stage.

Table 2.1: Equipment operating conditions and reaction volumes.

Equipment	Volume (L)	T (°C)	P (mmHg)
Disolver	24.1	21	760
Feed Tank	2	21	760
R1	1.85	115	760
R2	1.1	125-135	760
Zapper Unit	0.06	180-185	760
Devolatilizer	0.85-1.4	200-220	14-18

The operating conditions selected for each experiment in the reactor train are presented in Table 2.2. In all experiments, DV was carried out at 220 °C, 14-18 mmHg and with a pool level in the Devolatilizer of 90 mm. Two of the experiments were carried out using L331 as

initiator. In experiments 1-a and 2-a, two different temperatures were considered for R2. Two further reactions were completed; one with PDP and another with DEKTP as initiators. The molecular structure of the initiators were presented in Fig 2.4. Samples were taken at points S1-S4 as shown in Fig. 2.7.

TABLE 2.2: Equipment operating conditions adopted in the experiments for the study of HIPS production with three different multifunctional initiators

Experiment	Initiator	TR1 (°C)	TR2 (°C)
1-a	L-331	115	125
2-a	L-331	115	135
3	PDP	115	135
4	DEKTP	115	120/130 [1]

Characterization

Conversion (X), Grafting Efficiency (GE) and MWDs of free PS were measured for samples S1-S4 in all experiments. For samples S3 and S4, Monomer Content (%St) and Morphology were also determined. In addition, final product properties (i.e. MFI, SI, IR and Elongation at Break) were analyzed in all the experiments.

Conversion was determined by gravimetric analysis and the physical-chemical parameters (GE and SI) of different samples were measured directly from the pellets according to references [146, 147] .

Free PS MWD and the Free PS Average Molecular Weights ($M_{n,PS}$ and $M_{w,PS}$) were measured by SEC. A Hewlett-Packard instrument equipped with a series of three ultrastyrogel columns at porosities of 10^3, 10^4 and 10^5 Å was used. Calibration was carried out with PS standards (162-7,800,000 g/mol) and THF (HPLC grade) was used as mobile phase at a flow rate of 1 mL/min at 40 °C.

The different morphological structures in the synthetized HIPS were observed by Transmission Electron Microscopy (TEM). The samples were first cut to a thickness less than 100 nm with a diamond knife in a cryogenic ultra microtome provided by Leica at a chamber temperature of -130 °C, and -180 °C. The obtained cuts were placed in a closed container and osmium tetroxide was added in order to stain and contrast the insoluble phase. Samples were left to stain for a period of 2 hours. The Average Particle Diameters (PD) were estimated from the micrographs using a public domain digital image processing program (ImageJ).

The MFI of the final product was determined following ASTM D-1238-13. An extrusion plastometer Dynisco Ph 800-332-224 was operated at 200 °C, and weighted with a 5 kg load.

The SI was determined by gravimetric analysis of 0.3 g of swelled sample. The gel of the material removed from the Devolatilizer, was solvated and swollen in toluene. IR was determined by Izod Impact Testing. First, the samples were processed to obtain test specimens

[1] Two different temperatures are reported since the reaction was not stable during all the experiment duration.

by compression molding. The test specimens were conditioned according to specifications required by standard ASTM D-256 (test specimens dimensions: 64 x 12.7 x 3.2 mm) and were subjected to an IZOD impact strength measurement. All measurements were made using a CSI equipment model 137 according to ASTM D-256 standard. Finally, Elongation at Break (E) was determined according to ASTM-D 638-10. The test speed was 0.2 in/min and the separation between jaws was 4.5 in.

Experimental Results

Fig. 2.8 shows the evolution of X, $M_{n,PS}$, $M_{w,PS}$ and GE along the pilot plant for experiments 1-a, 2-a and 3, and the final product quality variables carried out with similar DV conditions are presented in Table 2.3 and Fig. 2.9. For exp. 4, that uses DEKTP as initiator, only final properties were determined.

In all cases, an increase in GE along the process is observed because of the temperature profile and the addition of initiator. $M_{n,PS}$ and $M_{w,PS}$ are almost constant due to the opposite effects of the increase in temperature and the "gel effect". As expected, for experiments 1-a and 2-a, the increase in R2 temperature results in higher X, higher GE and lower $M_{n,PS}$ and $M_{w,PS}$ (Figs. 2.8.a)-.f)). When comparing the experimental results of L331 and PDP at the same conditions (Figs. 2.8.d)-6.i)), the higher X for L331 can be attributed to a higher decomposition rate of the peroxide, as well as a higher initiator efficiency [74]. Further, the higher GE for L331 is associated to the higher rate of H-abstraction reactions by initiator radicals. As regards the molecular weights, it is observed that in the case of exp. 3 that uses the cyclic initiator PDP, $M_{n,PS}$ and $M_{w,PS}$ are higher than in the case of the linear initiator L331, in accordance with a higher decomposition rate of the peroxide groups in L331 and the cyclic structure of the initiator, which generates di-radicals upon decomposition. These outcomes are consistent with what was found in previous publications [84, 148].

In respect to the results presented in Table 2.3, as expected, higher residual monomer content is found for reactions where lower conversions are obtained. As for the oligomer generation reactions, they are affected both by monomer content and temperature. Thus, comparing reactions 1-a with 2-a, the lower oligomer content observed for the former is due to a lower oligomer generation rate, compensating the higher residual monomer content. In contrast, oligomer content for experiment 2-a, carried out at the same temperature than experiment 3, is lower due to the lower monomer concentration. MFI measurements corresponding to experiments 1-a, 2-a and 3 show higher values due to higher residual monomer content in spite of the slightly higher $M_{n,PS}$ and $M_{w,PS}$. Similarly, higher IR is obtained for experiments with higher monomer content, which acts as a plasticizer, enhancing mechanical properties [149]. Even though the same DV conditions were used, in experiments where monomer contents are higher at this stage, materials with higher SI are obtained. This is due to crosslinking reactions that compete with propagation reactions, as it has been reported in the literature [150].

Fig. 2.9 shows the morphologies for the final materials, where larger number of particles

with smaller PD are observed for experiments with the linear initiator L331, in agreement with the higher measured GE. However, it should be noted that this variable is expected to have a large uncertainty as a consequence of the experimental technique [81]. Results for experiment 4 are not discussed in this section since no intermediate data could be determined due to the difficult control of the reactor temperature. DEKTP final results are presented for comparison with the final results obtained using DEKTP in a batch reactor.

Finally, Fig. 2.10 presents the morphologies of HIPS materials synthetized in a single batch reactor, using the initiators employed in the present work [148]. As the prepolimerization stage-where morphology is developed—has been held at similar conditions in both processes, it can be observed that products with smaller PD are obtained with linear initiator L331 as compared with the cyclic initiators PDP and DEKTP for the batch reactor as well. Moreover, the morphology of materials obtained in a batch process present less dispersion, probably as a result of a better control of the morphology development.

TABLE 2.3: Final product quality variables for experiments with constant DV conditions (T=220 °C and P=16 mmHg).

Exp.	$M_{w,PS}$	GE	Residual St	Oligomer content	SI	MFI	IR	E	PD
	(g/mol)	(%)	(%)	(%)		(g/10min)	(J/m)	(%)	(mm)
1-a	288358	19.71	3.97	1.38	15.85	6.5	264	13.7	1056
2-a	268338	19.47	2.04	1.43	10.53	4.1	191	32.0	955
3	274163	17.15	2.95	1.70	12.42	5.5	196	33.2	1123
4	263464	16.35	1.10	1.44	9.21	5.5	149	26.9	1196

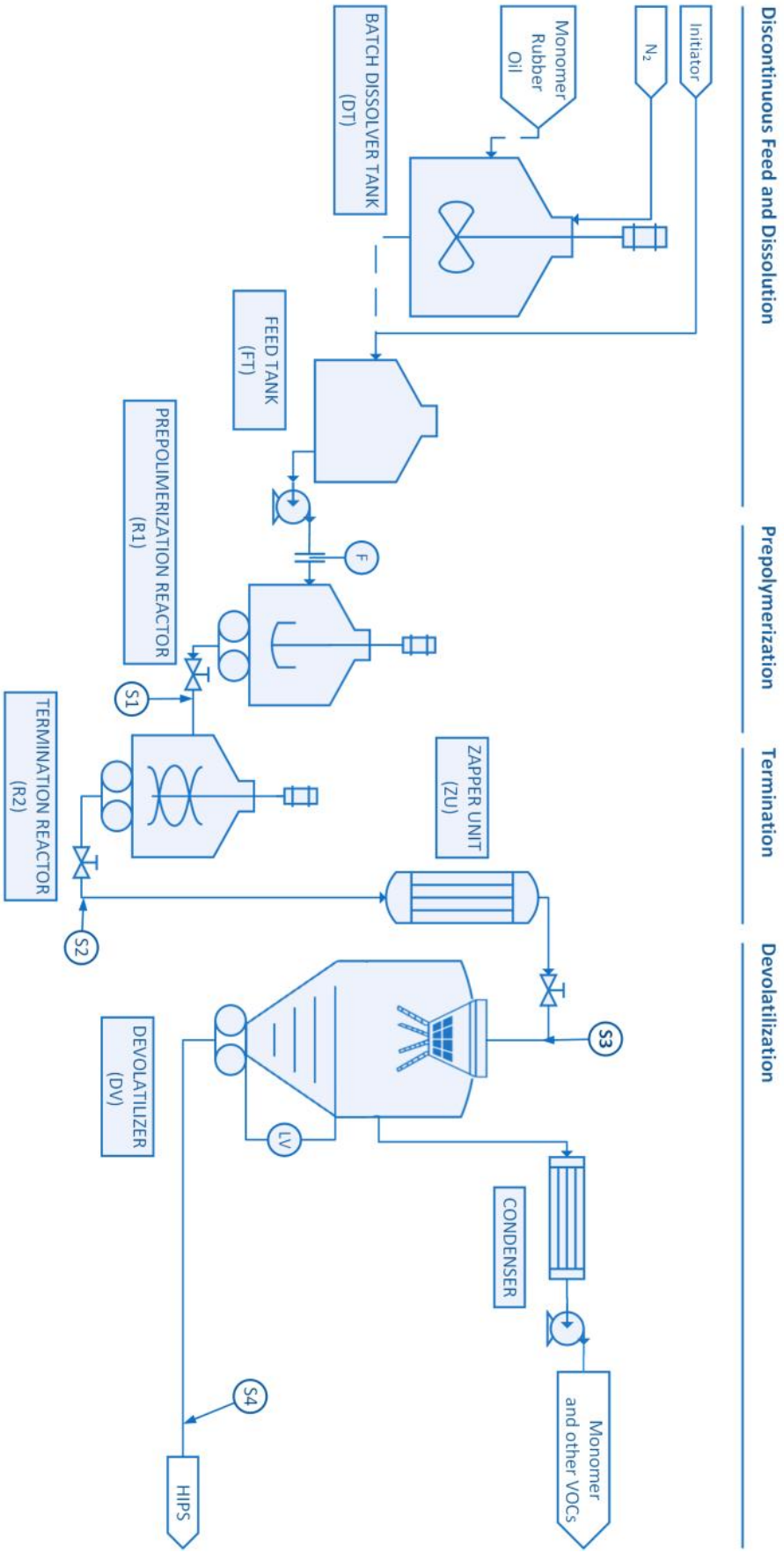

FIGURE 2.7: Continuous bulk process for the production of HIPS. Pilot plant process flow diagram.

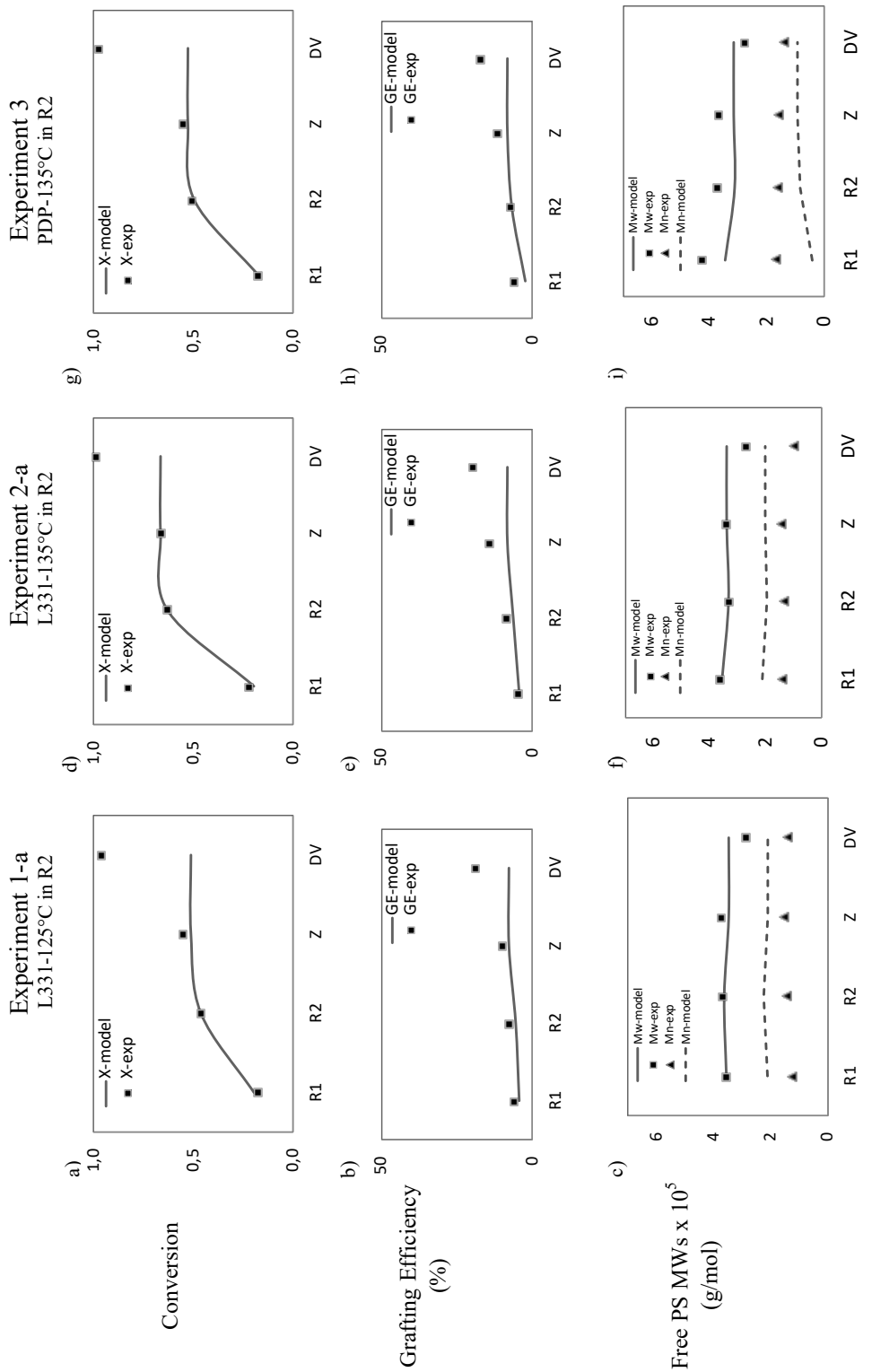

FIGURE 2.8: Experimental results for polymerizations with L331 and PDP at different temperatures in R2.

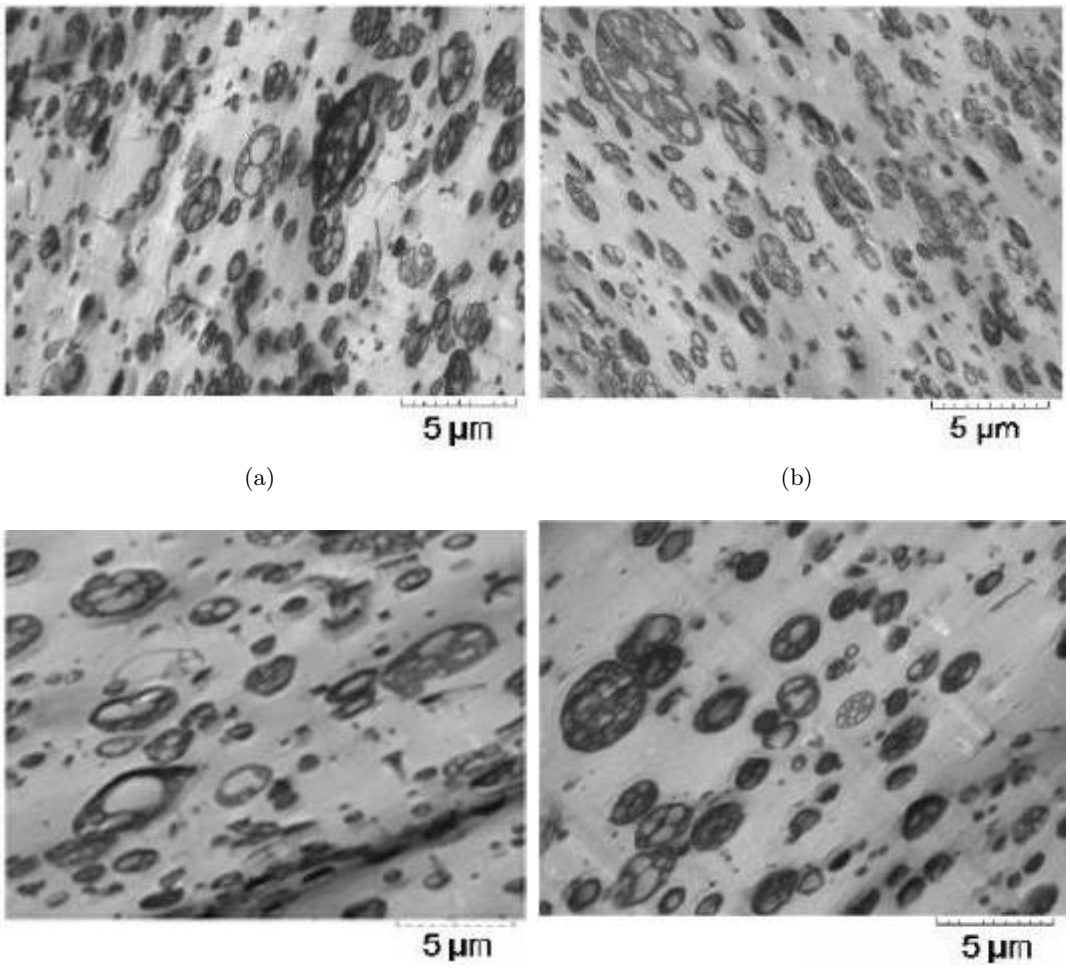

(a) (b)

(c) (d)

FIGURE 2.9: Final product morphologies observed by TEM for polymerizations 1-a (a), 2-a (b), 3 (c), and 4(d).

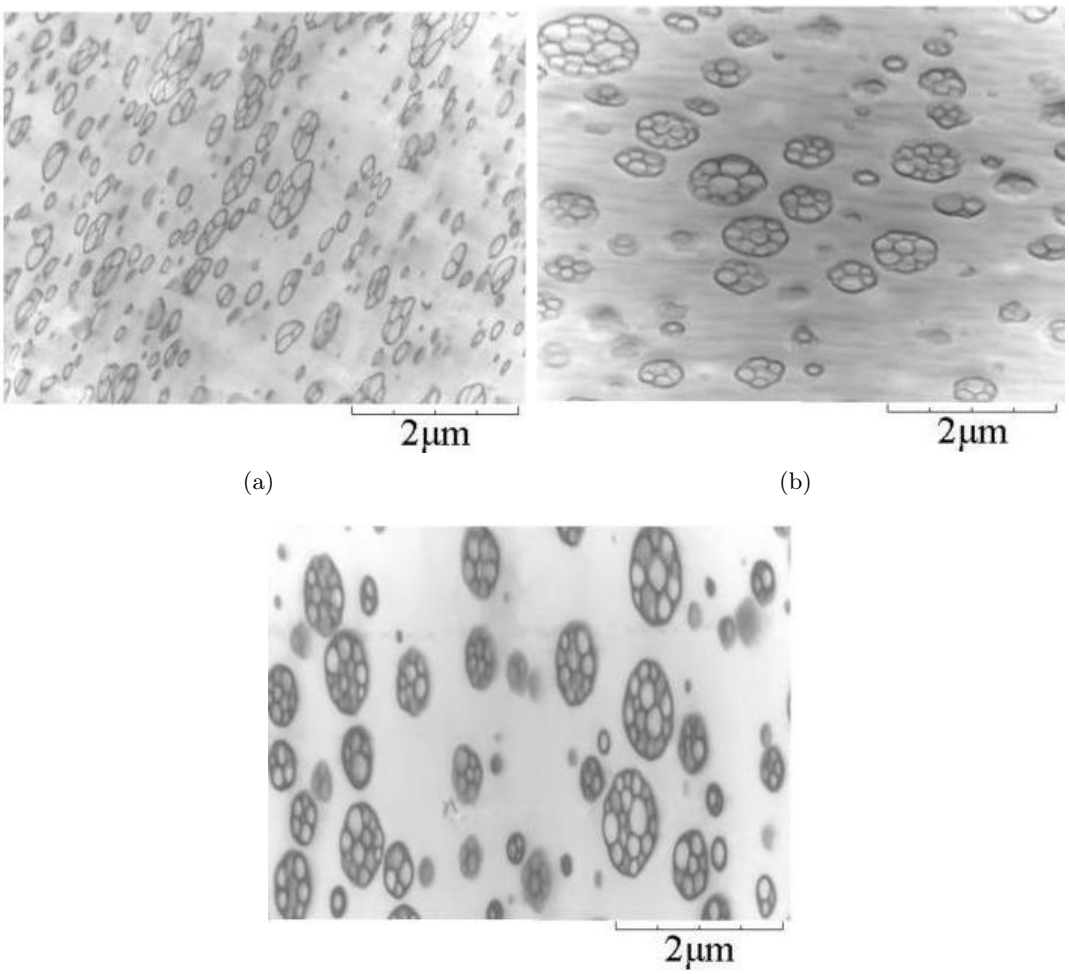

(a) (b)

(c)

FIGURE 2.10: Morphologies as observed by TEM for HIPS synthesized in a batch reactor with (a) L331, $PD = 290$nm , (b) PDP , $PD = 510$nm, and (c) DEKTP. , $PD = 870$nm

2.4 Mathematical Model for the Continuous HIPS Process

A reactor model of a generic CSTR based on the kinetic mechanism presented in Table 2.4 was developed. The kinetic mechanism includes initiation via a multifunctional initiator, thermal initiation, propagation, transfer to the monomer, transfer to the rubber, combination termination and re-initiation. The model is an extension of our previous work for a batch reactor [148]. The following is considered: i) at the temperatures employed, the initiators decompositions are due exclusively to sequential decomposition [72, 74, 76], ii) intra-molecular termination is negligible [19], iii) disproportion termination is negligible [134], iv) all peroxide groups in the initiator and the accumulated homo- and copolymers exhibit the same thermal stability [151], v) because of the short lifetime of radicals, decomposition of undecomposed peroxide groups does not occur in radical molecules [19], vi) propagation and transfer reactions are unaffected by chain length or conversion [19] and vii) degradation reactions are negligible [24].

TABLE 2.4: HIPS polymerization using multifunctional initiators - Proposed kinetic mechanism.

Initiation ($\phi = 1, 2, 3; i < \phi; j = 0, 1, ...$)

Thermal Initiation

$3\mathrm{St} \xrightarrow{k_{i0}} 2S_1.^{(0)}$

Chemical Initiation

$I^{(\phi)} \xrightarrow{\phi k_{d1}} .I.^{(\phi-1)}$

$\bar{I}^{(\phi)} \xrightarrow{\phi k_{d1}} I.^{(i)}$

$.I.^{(i)} + \mathrm{St} \xrightarrow{2k_{i1}} .S_1.^{(i)}$

$I.^{(i)} + \mathrm{St} \xrightarrow{k_{i1}} S_1.^{(i)}$

$.I.^{(i)} + P^{(j)} \xrightarrow{2k_{i2}} P_0.^{(j)} + I.^{(i)}$

$I.^{(i)} + P^{(j)} \xrightarrow{k_{i2}} P_0.^{(j)} + \bar{I}^{(i)}$

Propagation ($n = 1, 2, 3...; i = 0, 1, 2...$)

$S_n.^{(i)} + \mathrm{St} \xrightarrow{k_p} S_{n+1}.^{(i)}$

$.S_n.^{(i)} + \mathrm{St} \xrightarrow{2k_p} S_{n+1}.^{(i)}$

$P_0.^{(i)} + \mathrm{St} \xrightarrow{k_p} P_1.^{(i)}$

$P_n.^{(i)} + \mathrm{St} \xrightarrow{k_p} P_{n+1}.^{(i)}$

Transfer to monomer ($n = 1, 2, 3...; i = 0, 1, 2...$)

$S_n.^{(i)} + \mathrm{St} \xrightarrow{k_{fM}} S_n^{(i)} + S_1.^{(0)}$

$.S_n.^{(i)} + \mathrm{St} \xrightarrow{2k_{fM}} S_n.^{(i)} + S_1.^{(0)}$

$P_0.^{(i)} + \mathrm{St} \xrightarrow{k'_{fM}} P^{(i)} + S_1.^{(0)}$

$P_n.^{(i)} + \mathrm{St} \xrightarrow{k_{fM}} P^{(i)} + S_1.^{(0)}$

Transfer to rubber ($n = 1, 2, 3...; i, j = 0, 1, 2...$)

$S_n.^{(i)} + P^{(j)} \xrightarrow{k_{fG}} S_n^{(i)} + P_0.^{(j)}$

$\cdot S_n.^{(i)} + P^{(j)} \xrightarrow{2k_{fG}} S_n.^{(i)} + P_0.^{(j)}$

$P_0.^{(i)} + P^{(j)} \xrightarrow{k_{fG}} P^{(i)} + P_0.^{(j)}$

$P_n.^{(i)} + P^{(j)} \xrightarrow{k_{fG}} P^{(i)} + P_0.^{(j)}$

Re-initiation $(n = 2, 3, ...; m = 1, 2, ..., n-1; i = 1, 2...; j = 0, 1, ..., i-1)$

$S_n^{(i)} \xrightarrow{ik_{dp}} S_{n-m}.^{(i-j)} + S_m^{(j-1)}.$

$P^{(i)} \xrightarrow{ik_{dp}} P_{n-m}.^{(i-j)} + S_m^{(j-1)}.$

Combination termination $(n, m = 1, 2, 3...; i, j = 0, 1, 2...)$

$\cdot S_n.^{(i)} + \cdot S_m.^{(j)} \xrightarrow{4k_{tc}} \cdot S_{n+m}.^{(i+j)}$

$\cdot S_n.^{(i)} + S_m.^{(j)} \xrightarrow{2k_{tc}} S_{n+m}.^{(i+j)}$

$S_n.^{(i)} + S_m.^{(j)} \xrightarrow{k_{tc}} S_{n+m}^{(i+j)}$

$P_0.^{(i)} + P_0.^{(j)} \xrightarrow{k'_{tc}} P^{(i+j)}$

$P_0.^{(i)} + P_m.^{(j)} \xrightarrow{k'_{tc}} P^{(i+j)}$

$P_n.^{(i)} + P_m.^{(j)} \xrightarrow{k'_{tc}} P^{(i+j)}$

$P_0.^{(i)} + \cdot S_m.^{(j)} \xrightarrow{2k''_{tc}} P_m.^{(i+j)}$

$P_n.^{(i)} + \cdot S_m.^{(j)} \xrightarrow{2k''_{tc}} P_{n+m}.^{(i+j)}$

$P_0.^{(i)} + S_m.^{(j)} \xrightarrow{k''_{tc}} P^{(i+j)}$

$P_n.^{(i)} + S_m.^{(j)} \xrightarrow{k''_{tc}} P^{(i+j)}$

Nomenclature:

$I^{(\phi)}$	Cyclic multifunctional initiator with ϕ undecomposed peroxide groups
$\bar{I}^{(\phi)}$	Linear multifunctional initiator with ϕ undecomposed peroxide groups
$\cdot I.^{(i)}$	Initiator diradical with i undecomposed peroxide groups
$I.^{(i)}$	Initiator monoradical with i undecomposed peroxide groups
$\cdot S_1.^{(i)}$	Monomer diradical with i undecomposed peroxide groups
$S_1.^{(i)}$	Monomer monoradical with i undecomposed peroxide groups
$S_n^{(i)}$	Polymer with n repetitive units of St and i undecomposed peroxide gropus
$\cdot S_n.^{(i)}$	PS diradical of chain length n and i undecomposed peroxide gropus
$S_n.^{(i)}$	PS monoradical of chain length n and i undecomposed peroxide gropus
$P^{(i)}$	Copolymer with i undecomposed peroxide gropus in the grafted chain
$P_0.^{(i)}$	Primary radical produced by attack to a butadiene repetitive unite (B) present in the residual PB or the $P^{(i)}$
$P_n.^{(i)}$	Copolymer radical with i undecomposed peroxide gropus and n repetitive units of St in the active branch

A mathematical model for a generic CSTR was developed assuming a pseudo-homogeneous bulk polymerization [19]. The proposed model does not include an energy balance. However, temperature variations can be simulated through the use of standard or modified Arrhenius

expressions for the kinetic parameters [19, 24]. The mathematical model consists of two modules:

I. The Basic module allows the prediction of global chemical species (monomer, initiators, total radical species, unreacted butadiene units, undecomposed peroxide groups). To this effect, the subset of Eqs. eqs. (2.1) to (2.4), (2.6), (2.8), (2.9), (2.19) and (2.23) to (2.30) must be solved.

II. The Distributions module, which allows the estimation of all chemical species concentrations, characterized by their chain length and number of undecomposed peroxide groups. The subset of Eqs.eqs. (2.31) to (2.36) and eqs. (2.39) to (2.42) estimate the complete MWD of each radical and polymer species, including free PS and residual PB. In order to consider the effect of re-initiation reactions in the MWDs, PS chains were assumed to have uniformly distributed peroxide groups. A random-chain scission is simulated with a uniformly distributed random variable. The uniform peroxide group distribution hypothesis is expected to be valid for cyclic initiators and for linear initiators with functionalities greater than two [84]. From the MWDs, the corresponding averages can be calculated using Eqs. eq. (2.38).

2.4.1 Basic Module

The mathematical model is based on the kinetic mechanism of Table 2.4 and considers the mass balances for the chemical species in the reaction system.

Balances for non-polymeric reagents and products

Multifunctional initiators ($\phi = 1, 2, 3$)

$$\frac{d}{dt}\left([I^{(\phi)}]V\right) = -\phi k_{d1}[I^{(\phi)}]V + q_{in}[I^{(\phi)}]_{in} - q[I^{(\phi)}] \tag{2.1}$$

$$\frac{d}{dt}\left([\bar{I}^{(\phi)}]V\right) = -\phi k_{d1}[\bar{I}^{(\phi)}]V + q_{in}[\bar{I}^{(\phi)}]_{in} - q[\bar{I}^{(\phi)}] \tag{2.2}$$

Secondary initiator species ($\phi > i = 1, 2$)

$$\frac{d}{dt}\left([\bar{I}^{(i)}]V\right) = -ik_{d1}[\bar{I}^{(i)}]V + (1-f_1)\sum_{j=i+1}^{\phi} jk_{d1}\left([I^{(j)}] + [\bar{I}^{(j)}]\right)V + q_{in}[\bar{I}^{(i)}]_{in} - q[\bar{I}^{(i)}] \tag{2.3}$$

Monomer (St)

Assuming the long chain hypothesis, by which propagation is the only monomer-consuming reaction:

$$\frac{d}{dt}\left([\mathrm{St}]V\right) = -R_pV = -k_p[\mathrm{St}]\left([R\cdot] + 2[\cdot R\cdot]\right)V + q_{in}[\mathrm{St}]_{\mathrm{in}} - q[\mathrm{St}] \tag{2.4}$$

where R_p is the global St polymerization rate, and

$$[R\cdot] = [S\cdot] + [P\cdot] = \sum_{i=0}^{\infty}\sum_{n=1}^{\infty}[S_n{\cdot}^{(i)}] + \sum_{i=0}^{\infty}\sum_{n=1}^{\infty}[P_n{\cdot}^{(i)}] \tag{2.5a}$$

$$[\cdot R\cdot] = \sum_{i=0}^{\infty}\sum_{n=1}^{\infty}[\cdot S_n{\cdot}^{(i)}] \tag{2.5b}$$

represent the total concentrations of mono- and diradicals respectively. In Equation 2.5, an S species is a PS homoradical and a P species is a PB or copolymer radical.

Unreacted B units

Let us represent with $B*$ an unreacted B unit in the copolymer or in the initial (or purely crosslinked) PB. When a P molecule is attacked, a $B*$ unit is consumed, and a $B*$ unit is generated in transfer reactions of a $P_0\cdot$ radical. Therefore,

$$\frac{d}{dt}([B*]V) = -\left\{k_{i2}\left(2\sum_{j=0}^{\phi-1}[\cdot I{\cdot}^{(j)}] + \sum_{j=0}^{\phi-1}[I{\cdot}^{(j)}]\right) + k_{fG}\left([R\cdot] + 2[\cdot R\cdot]\right)\right\}[B*]V + k_{fM}[\mathrm{St}][P_0\cdot]V + q_{in}[B*]_{in} - q[B*] \tag{2.6}$$

with

$$[P_0\cdot] = \sum_{i=0}^{\infty}[P_0{\cdot}^{(i)}] \tag{2.7}$$

Radical species ($i = 0, 1, ...; n = 2, 3, ...$)

Consider the mass balances of all free radicals appearing in the global kinetics. Such balances provide:

$$\frac{d}{dt}\left([\cdot I{\cdot}^{(i)}]V\right) = f_1(i+1)k_{d1}[I^{(i+1)}]V - 2\left(k_{i1}[\mathrm{St}] + k_{i2}[B*]\right)[\cdot I{\cdot}^{(i)}]V + q_{in}[\cdot I{\cdot}^{(i)}]_{in} - q[\cdot I{\cdot}^{(i)}] \tag{2.8}$$

$$\frac{d}{dt}\left([I{\cdot}^{(i)}]V\right) = \sum_{j=i+1}^{\phi} p_j(i)f_1 j k_{d1}[\bar{I}^{(j)}]V + 2k_{i2}[B*][\cdot I{\cdot}^{(j)}]V - \left(k_{i1}[\mathrm{St}] + k_{i2}[B*]\right)[I{\cdot}^{(i)}]V + q_{in}[I{\cdot}^{(i)}]_{in} - q[I{\cdot}^{(i)}] \tag{2.9}$$

Where $p_i(j)$ is the probability that the decomposition of the initiator of functionality j generates a monoradical with i undecomposed peroxide groups.

For PS homoradicals,

$$\frac{d}{dt}\left([\cdot S_1{}^{\cdot(i)}]V\right) = 2k_{i1}[\cdot I^{\cdot(i)}][\mathrm{St}]V - 2\left(k_p[\mathrm{St}] + k_{fM}[\mathrm{St}] + k_{fG}[B*] + k_{tc}\left([R\cdot] + 2[\cdot R\cdot]\right) + k''_{tc}[P_0\cdot]\right)[\cdot S_1{}^{\cdot(i)}]V + q_{in}[\cdot S_1{}^{\cdot(i)}]_{in} - q[\cdot S_1{}^{\cdot(i)}] \quad (2.10)$$

$$\frac{d}{dt}\left([S_1{}^{\cdot(i)}]V\right) = \left\{k_{i1}[I^{\cdot(i)}][\mathrm{St}] + \right\}V + \delta_{i0}\left(2k_{i0}[\mathrm{St}]^3 + k_{fM}\left([R\cdot] + 2[\cdot R\cdot]\right)[\mathrm{St}]\right)V - \left(k_p[\mathrm{St}] + k_{fM}[\mathrm{St}] + k_{fG}[B*] + k_{tc}\left([R\cdot] + 2[\cdot R\cdot]\right) + k''_{tc}[P_0\cdot]\right)[S_1{}^{\cdot(i)}]V + q_{in}[S_1{}^{\cdot(i)}]_{in} - q[S_1{}^{\cdot(i)}] \quad (2.11)$$

where δ_{i0} is the Kronecker Delta ($\delta_{i0} = 1$ if $i = 0$ and $\delta_{i0} = 0$ otherwise).

$$\frac{d}{dt}\left([\cdot S_n{}^{\cdot(i)}]V\right) = 2k_p[\mathrm{St}]\left([\cdot S_{n-1}{}^{\cdot(i)}] - [\cdot S_n{}^{\cdot(i)}]\right)V - 2\left(k_{fM}[\mathrm{St}] + k_{fG}[B*] + k_{tc}\left([R\cdot] + 2[\cdot R\cdot]\right) + k''_{tc}[P_0\cdot]\right)[\cdot S_n{}^{\cdot(i)}]V + 2k_{tc}\sum_{j=0}^{i}\sum_{m=1}^{n-1}[\cdot S_{n-m}{}^{\cdot(i-j)}][\cdot S_m{}^{\cdot(j)}]V + q_{in}[\cdot S_n{}^{\cdot(i)}]_{in} - q[\cdot S_n{}^{\cdot(i)}] \quad (2.12)$$

$$\frac{d}{dt}\left([S_n{}^{\cdot(i)}]V\right) = \left(k_p\left([S_{n-1}{}^{\cdot(i)}] - [S_n{}^{\cdot(i)}]\right) + 2k_{fM}[\cdot S_n{}^{\cdot(i)}]\right)[\mathrm{St}]V + 2k_{fG}[\cdot S_n{}^{\cdot(i)}][B*]V - \left(k_{fM}[\mathrm{St}] + k_{fG}[B*] + k_{tc}\left([R\cdot] + 2[\cdot R\cdot]\right) + k''_{tc}[P_0\cdot]\right)[S_n{}^{\cdot(i)}]V + 2k_{tc}\sum_{j=0}^{i}\sum_{m=1}^{n-1}[\cdot S_{n-m}{}^{\cdot(i-j)}][S_m{}^{\cdot(j)}]V + f_2k_{d2}\sum_{j=i+1}^{\infty}\sum_{m=n+1}^{\infty}\left(p_{mj}(n,i)j[S_m^{(j)}] + p'_{mj}(n,i)j[P_m^{(j)}]\right)V + q_{in}[S_n{}^{\cdot(i)}]_{in} - q[S_n{}^{\cdot(i)}] \quad (2.13)$$

In Equation 2.13, $p_{mj}(n,i)$ is the probability that a scission of a chain of temporarily dead free PS of length m and j peroxide groups yields a growing monoradical of chain length n with i peroxide groups and $p'_{mj}(n,i)$ is the probability that a scission of a temporarily dead PS chain in the GC of length m and j peroxide groups yields a growing monoradical of chain length n with i peroxide groups.

Adding this probability over all ns and is, the following can be proven:

$$\sum_{i=1}^{\infty}\sum_{n=1}^{\infty}\sum_{j=i+1}^{\infty}\sum_{m=n+1}^{\infty}\left(p_{mj}(n,i)j[S_m^{(j)}] + p'_{mj}(n,i)j[P_m{}^{(j)}]\right) = \sum_{i=1}^{\infty}\sum_{n=1}^{\infty}\left(2i[S_n^{(i)}] + i[P_n^{(i)}]\right) = 2[\mathrm{Pe_{PS}}] + [\mathrm{Pe_C}] \quad (2.14)$$

where $[\mathsf{Pe_{PS}}]$ is the concentration of peroxide groups in the free PS chains and $[\mathsf{Pe_C}]$ is the concentration of peroxides groups in the GC. Note that the scission of any free PS chain with peroxide groups produces 2 PS homoradicals, whereas the scission of a chain within the copolymer generates only one PS homoradical and one copolymer radical.

For PB radicals and copolymer radicals,

$$\begin{aligned}\frac{d}{dt}\left([P_0{\cdot}^{(i)}]V\right) = &\left(k_{i2}\sum_{j=0}^{\phi-1}\left(2[\cdot I{\cdot}^{(j)}] + [I{\cdot}^{(j)}]\right) + k_{fG}\left([R\cdot] + 2[\cdot R\cdot]\right)\right)[B*^{(i)}]V \\ &- \left(k_{p1}[\mathrm{St}] + k'_{fM}[\mathrm{St}] + k'_{tc}[P_0\cdot] + k_{tc}\left([R\cdot] + 2[\cdot R\cdot]\right)\right)[P_0{\cdot}^{(i)}]V \\ &+ q_{in}[P_0{\cdot}^{(i)}]_{in} - q[P_0{\cdot}^{(i)}]\end{aligned} \tag{2.15}$$

$$\begin{aligned}\frac{d}{dt}\left([P_1{\cdot}^{(i)}]V\right) = &\, k_{i1}[\mathrm{St}][P_0{\cdot}^{(i)}]V + 2k_{tc}\sum_{j=0}^{i}[P_0{\cdot}^{(i-j)}][\cdot S_1{}^{(j)}\cdot]V \\ &- \left(k_p[\mathrm{St}] + k_{fM}[\mathrm{St}] + k_{fG}[B*] + k''_{tc}[P_0\cdot] + k_{tc}\left([R\cdot] + 2[\cdot R\cdot]\right)\right)[P_1{\cdot}^{(i)}]V \\ &+ q_{in}[P_1{\cdot}^{(i)}]_{in} - q[P_1{\cdot}^{(i)}]\end{aligned} \tag{2.16}$$

$$\begin{aligned}\frac{d}{dt}\left([P_n{\cdot}^{(i)}]V\right) = &\, k_p[\mathrm{St}][P_{n-1}{\cdot}^{(i)}]V \\ &+ f_2k_{d2}\sum_{j=i+1}^{\infty}\sum_{m=n+1}^{\infty}p'_{mj}(n,i)j[P_m^{(j)}]V + 2k_{tc}\sum_{j=0}^{i}\sum_{m=1}^{n-1}[P_{n-m}{\cdot}^{(i-j)}][\cdot S_m{\cdot}^{(j)}]V \\ &- \left(k_p[\mathrm{St}] + k_{fM}[\mathrm{St}] + k_{fG}[B*] + k''_{tc}[P_0\cdot] + k_{tc}\left([R\cdot] + 2[\cdot R\cdot]\right)\right)[P_n{\cdot}^{(i)}]V \\ &+ q_{in}[P_n{\cdot}^{(i)}]_{in} - q[P_n{\cdot}^{(i)}]\end{aligned} \tag{2.17}$$

where $[B*^{(i)}]$ is the molar concentration of total B units in PB or copolymer molecules with i undecomposed peroxide groups and

$$[B*] = \sum_{i=0}^{\infty}[B*^{(i)}] \tag{2.18}$$

Note that $i = 0$ for PB.

Summing Equation 2.15 all over is,

$$\begin{aligned}\frac{d}{dt}\left([P_0\cdot]V\right) = &\left(k_{i2}\sum_{j=0}^{\phi-1}\left(2[\cdot I^{\cdot(j)}] + [I^{\cdot(j)}]\right) + k_{fG}\left([R\cdot] + 2[\cdot R\cdot]\right)\right)[B*]V \\ &- \left(k_{i1}[\mathrm{St}] + k'_{fM}[\mathrm{St}] + k'_{tc}[P_0\cdot] + k_{tc}\left([R\cdot] + 2[\cdot R\cdot]\right)\right)[P_0\cdot]V \\ &+ q_{in}[P_0\cdot]_{in} - q[P_0\cdot]\end{aligned} \tag{2.19}$$

From Equations 2.16 and 2.17, summing all over ns and is, the total concentration of PB and copolymer radicals may be obtained:

$$\begin{aligned}\frac{d}{dt}\left([P\cdot]V\right) = &\, k_{i1}[\mathrm{St}][P_0\cdot]V + k_{fG}\left([S\cdot] + 2[\cdot R\cdot]\right)[B*]V \\ &+ k_{d2}[\mathrm{Pe_C}]V - \left(k_{fM}[\mathrm{St}] + k''_{tc}[P_0\cdot] + k_{tc}\left([S\cdot] + [P\cdot]\right)\right)[P\cdot]V \\ &+ q_{in}[P\cdot]_{in} - q[P\cdot]\end{aligned} \tag{2.20}$$

From Equations 2.10 and 2.12, the total concentration of diradicals (which are only PS homoradicals) may be obtained:

$$\begin{aligned}\frac{d}{dt}\left([\cdot R\cdot]V\right) = &\, k_{i2}\sum_{j=0}^{\phi-1} 2[\cdot I^{\cdot(j)}][\mathrm{St}]V + 2k_{tc}[\cdot R\cdot]^2V \\ &- 2\left(k_{fM}[\mathrm{St}] + k_{fG}[B*] + k_{tc}\left([R\cdot] + 2[\cdot R\cdot]\right) + k''_{tc}[P_0\cdot]\right)[\cdot R\cdot]V + q_{in}[\cdot R\cdot]_{in} - q[\cdot R\cdot]\end{aligned} \tag{2.21}$$

From Equation 2.11 and 2.13 and considering Equation 2.14, the total concentration of PS monoradicals may be obtained:

$$\begin{aligned}\frac{d}{dt}\left([S\cdot]V\right) = &\left(k_{i2}\sum_{j=0}^{\phi-1}[I^{\cdot(j)}] + k_{fM}\left([P\cdot] + 4[\cdot R\cdot]\right)\right)[\mathrm{St}]V + 2k_i[\mathrm{St}]^3V + 2k_{fG}[B*][\cdot R\cdot]V \\ &- \left(k_{tc}\left([S\cdot] + [P\cdot] + 2[\cdot R\cdot]\right) + k_{fG}[B*] + k''_{tc}[P_0\cdot]\right)[S\cdot]V + f_2k_{d2}\left(2[\mathrm{Pe_{PS}}] + [\mathrm{Pe_C}]\right)V \\ &+ q_{in}[S\cdot]_{in} - q[S\cdot]\end{aligned} \tag{2.22}$$

The total radicals are calculated as $[R\cdot] + 2[\cdot R\cdot] = [S\cdot] + [P\cdot] + 2[\cdot R\cdot]$. Using Equations 2.20

trough 2.22,

$$\frac{d}{dt}\left(\left([R\cdot]+2[\cdot R\cdot]\right)V\right)=k_{i1}\sum_{j=0}^{\phi-1}\left(4[\cdot I^{\cdot(j)}]+[I^{\cdot(j)}]\right)[\mathrm{St}]V+2k_i[\mathrm{St}]^3V+k_{i1}[\mathrm{St}][P_0\cdot]V$$
$$+2f_2k_{d2}\left([\mathrm{Pe_{PS}}]+[\mathrm{Pe_C}]\right)V-k_{tc}([R\cdot]+2[\cdot R\cdot])^2V-k''_{tc}\left([R\cdot]+2[\cdot R\cdot]\right)[P_0\cdot]V$$
$$+q_{in}([R\cdot]+2[\cdot R\cdot])_{in}-q\left([R\cdot]+2[\cdot R\cdot]\right) \tag{2.23}$$

Peroxide groups

Neglecting the concentration of peroxide groups in the radicals, the total concentration of peroxide groups is

$$[\mathrm{Pe}]=\sum_{j=1}^{\phi}j\left([I^{(j)}]+[\bar{\mathrm{I}}^{(j)}]\right)+[\mathrm{Pe_{PS}}]+[\mathrm{Pe_C}] \tag{2.24}$$

with

$$[\mathrm{Pe_{PS}}]=\sum_{i=0}^{\infty}\sum_{n=1}^{\infty}i[S_n{}^{(i)}] \tag{2.25a}$$

$$[\mathrm{Pe_C}]=\sum_{i=0}^{\infty}i[\mathrm{P}^{(i)}] \tag{2.25b}$$

Peroxide groups are consumed only by decomposition reactions. Therefore:

$$\frac{d}{dt}\left([\mathrm{Pe}]V\right)=-\sum_{i=1}^{\phi}jk_{d1}\left([I^{(i)}]+[\bar{\mathrm{I}}^{(i)}]\right)V-k_{d2}\left([\mathrm{Pe_{PS}}]+[\mathrm{Pe_C}]\right)V+q_{in}[\mathrm{Pe}]_{in}-q[\mathrm{Pe}] \tag{2.26}$$

Using this result and Equation 2.24, the molar concentration of peroxide groups accumulated in the free PS and the GC can be calculated from the following difference

$$\frac{d}{dt}\left(\{[\mathrm{Pe_{PS}}]+[\mathrm{Pe_C}]\}V\right)=\frac{d}{dt}\left([\mathrm{Pe}]V\right)-\sum_{j=1}^{\phi}j\frac{d}{dt}\left(\left([I^{(j)}]+[\bar{\mathrm{I}}^{(j)}]\right)V\right)+q_{in}([\mathrm{Pe_{PS}}]+[\mathrm{Pe_C}])_{in}-q([\mathrm{Pe_{PS}}]+[\mathrm{Pe_C}]) \tag{2.27}$$

Conversion and volumetric flow rate

The monomer conversion can be calculated from

$$X=\frac{[\mathrm{St}]_{in}q_{in}-[\mathrm{St}]q}{[\mathrm{St}]_{in}q_{in}} \tag{2.28}$$

where the subscript "in" indicates inlet conditions. The reaction volumetric flow rate q is obtained from

$$q=q_{in}^{\mathrm{St}}\left(1-\varepsilon X\right)+q_{in}^{\mathrm{PB}} \tag{2.29}$$

with

$$\varepsilon = \frac{q_{in}^{St} - q_f^S}{q_{in}^{St}} \tag{2.30}$$

Where ε is the St volume contraction factor, q_{in}^{St} and q_{in}^{PB} are the inlet St and PB volumetric flow rates respectively and q_f^S is the final volumetric flow rate of free and grafted St at full conversion.

With derivatives equal to zero, equations 2.1 to 2.6, 2.8, 2.9, 2.19, 2.23, and 2.24 to 2.29 are solved to find the concentration at the reactor outlet of species $[I^{(i)}]$,$[\bar{I}^{(i)}]$, $[St]$, $[B*]$, $[\cdot I \cdot^{(i)}]$, $[I \cdot^{(i)}]$, $[P_0\cdot]$, $([R\cdot] + 2[\cdot R\cdot])$, $([Pe_{PS}] + [Pe_C])$, x and q.

The Basic module is solved using a Newton-Raphson method programmed in Matlab V. 8.3. To account for the non-ideality of the reactors, each reactor is considered as a series of "n" CSTRs, where "n" is an adjustment parameter.

2.4.2 Distributions Module

Polystyrene species ($i = 0, 1, ...$; $n = 2, 3, ...$)
The mass balances for the PS species provide

$$\frac{d}{dt}\left([S_n{}^{(i)}]V\right) = k_{fM}[St][S_n\cdot^{(i)}]V + \frac{k_{tc}}{2}\sum_{j=0}^{i}\sum_{m=1}^{n-1}[S_{n-m}\cdot^{(i-j)}][S_m\cdot^{(j)}]V - i[S_n{}^{(i)}]V$$
$$+ (1 - f_2)\, k_{d2}\sum_{j=i+1}^{\infty}\sum_{m=n+1}^{\infty}\left(p_{mj}(n,i)j[S_m^{(j)}] + p'_{mj}(n,i)j[P_m^{(j)}]\right)V$$
$$+ q_{in}[S_n{}^{(i)}]_{in} - q[S_n{}^{(i)}] \tag{2.31}$$

In order to account for the generation of monoradicals from random scission of the free PS or graft copolymer chains by sequential decomposition of peroxide groups within the chains, consider a PS chain with length n and i peroxide groups, all of which have the same thermal stability. Let m be a uniformly distributed random variable whose value ranges 1 from 1 to $n-1$. The polymer chain may form 2 monoradicals, one with length m, and the other one with length $n-m$. These chains will have $i-j$ and $j-1$ undecomposed peroxide groups respectively. If the peroxide groups are assumed to be uniformly distributed within the polymer chains in the course of polymerization, the following relation must hold:

$$\frac{j-1}{n-m} = \frac{i-j}{m}$$

Therefore,

$$j = \left[\frac{i(n-m)+m}{n}\right]$$

where the brackets indicate the integer part of the expression.

The scission has then generated two monoradicals, one with length m and $i-j$ peroxide

groups, the other one with length $n - m$ and $j - 1$ peroxide groups.

Note that this chain scission algorithm can be modified for specific cases. For example, in the case of a linear bifunctional initiator, since all peroxide groups are located at a chain end, $m = 1$ for every scission.

The Number Chain Length Distribution (NCLD) for the free PS species is

$$N_{\mathrm{PS}}^{(i)}(n) = [{S_n}^{(i)}]q \tag{2.32}$$

The concentration of the total PS species characterized by the number of undecomposed peroxide groups can be calculated with

$$[P^{(i)}] = \sum_{n=1}^{\infty} [{S_n}^{(i)}] \tag{2.33}$$

The NCLD for the total polymer can be calculated using

$$P_n = \sum_{i=0}^{\infty} [{S_n}^{(i)}]q \tag{2.34}$$

The total moles of PS are

$$N_{\mathrm{PS}} = \sum_{i=0}^{\infty} \sum_{n=1}^{\infty} N_{\mathrm{PS}}^{(i)}(n) \tag{2.35}$$

To obtain the corresponding Weight Chain Length Distribution (WCLD), multiply the NCLD by sM_{St} and replace n by s to obtain

$$G_{\mathrm{PS}}^{(i)}(s) = sM_{\mathrm{St}}[{S_s}^{(i)}]q \tag{2.36}$$

The mass of free PS can then be calculated as

$$G_{\mathrm{PS}} = \sum_{i=0}^{\infty} \sum_{s=1}^{\infty} G_{\mathrm{PS}}^{(i)}(s) \tag{2.37}$$

The average molecular weights can then be calculated from

$$\bar{M}_{n,\mathrm{PS}} = \frac{G_{\mathrm{PS}}}{N_{\mathrm{PS}}} = \frac{\sum_{i=0}^{\infty} \sum_{s=1}^{\infty} G_{\mathrm{PS}}^{(i)}(s)}{\sum_{i=0}^{\infty} \sum_{n=1}^{\infty} [{S_n}^{(i)}]q} \tag{2.38a}$$

$$\bar{M}_{w,\mathrm{PS}} = \frac{\sum_{i=0}^{\infty} \sum_{s=1}^{\infty} sG_{\mathrm{PS}}^{(i)}(s)}{G_{\mathrm{PS}}} = \frac{\sum_{i=0}^{\infty} \sum_{s=1}^{\infty} sG_{\mathrm{PS}}^{(i)}(s)}{\sum_{i=0}^{\infty} \sum_{s=1}^{\infty} G_{\mathrm{PS}}^{(i)}(s)} \tag{2.38b}$$

Residual PB

Let $[n_{\mathrm{PB}}(b)]$ denote the molar concentration of unreacted PB with b units of B ($b \geq 1$).

Assuming that the number of attacked $B*$ is proportional to the $B*$ contents of each chain length class, the fraction of $P_0\cdot$ radicals that are primary PB radicals of chain length b is therefore $b[n_{\mathrm{PB}}(b)]/[B*]$. Then, from the kinetic mechanism,

$$\frac{d}{dt}[n_{\mathrm{PB}}(b)]V = -\left(k_{i2}\sum_{j=0}^{\phi-1}\left(2[\cdot I^{\cdot(j)}] + [I^{\cdot(j)}]\right) + k_{fG}\left([R\cdot] + 2[\cdot R\cdot]\right)\right) b[n_{\mathrm{PB}}(b)]V + k'_{fM}[\mathrm{St}][P_0\cdot]\frac{b[n_{\mathrm{PB}}(b)]}{[B*]} + q_{in}[n_{\mathrm{PB}}(b)]_{in} - q[n_{\mathrm{PB}}(b)] \quad (2.39)$$

where $N_{\mathrm{PB}}(b)$ at $t = 0$ is *a priori* known from experimental data. The corresponding WCLD for the residual PB can be obtained from

$$G_{\mathrm{PB}}(b) = bM_B q[n_{\mathrm{PB}}(b)] \quad (2.40)$$

The total moles and mass of residual PB are

$$N_{\mathrm{PB}} = \sum_{b=1}^{\infty} N_{\mathrm{PB}}(b) \quad (2.41)$$

$$G_{\mathrm{PB}} = \sum_{b=1}^{\infty} G_{\mathrm{PB}}(b) \quad (2.42)$$

Grafting efficiency

The grafted St mass can be calculated from

$$G_{\mathrm{GS}} = M_{\mathrm{St}}[\mathrm{St}]_{in}q_{in}X - G_{\mathrm{PS}} \quad (2.43)$$

The St grafting efficiency is calculated from

$$E_{\mathrm{GS}} = \frac{G_{\mathrm{GS}}}{G_{\mathrm{PS}} + G_{\mathrm{GS}}} \quad (2.44)$$

Phase volumetric flow rates

The volumetric flow rates of the individual phases, considered completely immiscible, is obtained from

$$q_{\mathrm{I}} = \frac{G_{PB} + G_{GS}}{\rho_{PB}} \quad (2.45a)$$

$$q_{\mathrm{II}} = \frac{M_{\mathrm{St}}[\mathrm{St}]\mathrm{q_{II}}\rho_{\mathrm{St}} + \mathrm{G_{PS}}}{\rho_{PS}} \quad (2.45b)$$

where ρ_k is the density of chemical species k.

The Distributions module is solved using the results from the Basic module. In the Distributions module, a large number of equations (more than 500,000) must be simultaneously solved for the calculation of MWDs. Given the large number of species considered and the

re-initiation reactions involved, these mass balances are solved using an iteration algorithm, also programmed in Matlab V. 8.6.

2.5 Model Simulation and Adjustment

The simulation of the reactor train model involved the sequential resolution of each CSTR reactor of the pilot plant. Note that the Prepolymerization Reactor (R1), the Termination Reactor (R2), the Zapper Unit (ZU) are considered CSTR reactors. With respect to the DV, it was considered as a flash tank with perfect separation where no chemical reaction occur.

The model was adjusted using the experimental data in Fig. 2.8 and the parameters are presented in Table. 2.5

Parameter adjustment was sequential, using least-squares optimization algorithms. First, k_{d1}, k_{dp}, f_1 and f_2 for each initiator were adjusted with conversion and grafting effciency. Since all peroxide groups are assumed to have thermal stability, $k_{dp} = k_{d1}$ and it was assumed that $f1 = f2 = 1$. Subsequently, k_{i2}, k_{fM} and k_{fG} were simultaneously adjusted with the average molecular weights and grafting efficiency data. The values for initiator decomposition, transfer to monomer and transfer to rubber constants are within the range reported in the literature [81]. All other kinetic parameters were taken from the literature [24].

It was found in our previous publications [84, 148] that $f_1 * k_{d1}$ (L331)> $f_1 * k_{d1}$ (DEKTP) and that k_{i2} (L331) > k_{i2}(DEKTP), by which the bifunctional linear initiator generates a higher number of grafting points at a given temperature. This results are in agreement with the lower grafting efficiencies observed for DEKTP compared to L331 and with the different morphologies observed in the final products.

Simulation results for the reactor train are compared to experimental results in Fig. 2.8 and a very good agreement between experimental and predicted values is observed.

Other simulation results using the model are presented in Fig. 2.11. Fig. 2.11.a) shows how the GE can be affected by polymerization conditions and Fig. 2.11.b) shows how the concentration of the initiator L331 at the reactors outlet decreases with temperature in R1. It should be noticed that temperature in R1 can be increased considering the temperature range where the initiator decomposes sequentially. During the model adjustment, it was observed that in all the experiments, the initiator was not totally consumed during polymerization. Around 50% is consumed at the termination reactor (R2) outlet, in all cases. This indicates that unreacted peroxides are entering into the Devolatilizer, which results in non desirable side reactions such as branching, excess of crosslinking and also lower MWs. As can be observed in Fig. 2.11.b), a total consumption of the initiator is not posible, therefore, a lower inlet initiator concentration should be considered to counteract unreacted peroxides in the Devolatilizer. It should also be noticed that, since the initiator decomposition is considered as a first order reaction, the inlet concentration will not affect the half-life time of the initiator.

[2] $C_1 = 2.75 - 0.00505T, C_2 = -9.56 - 0.0176T, C_3 = 3.03 + 0.00785T$

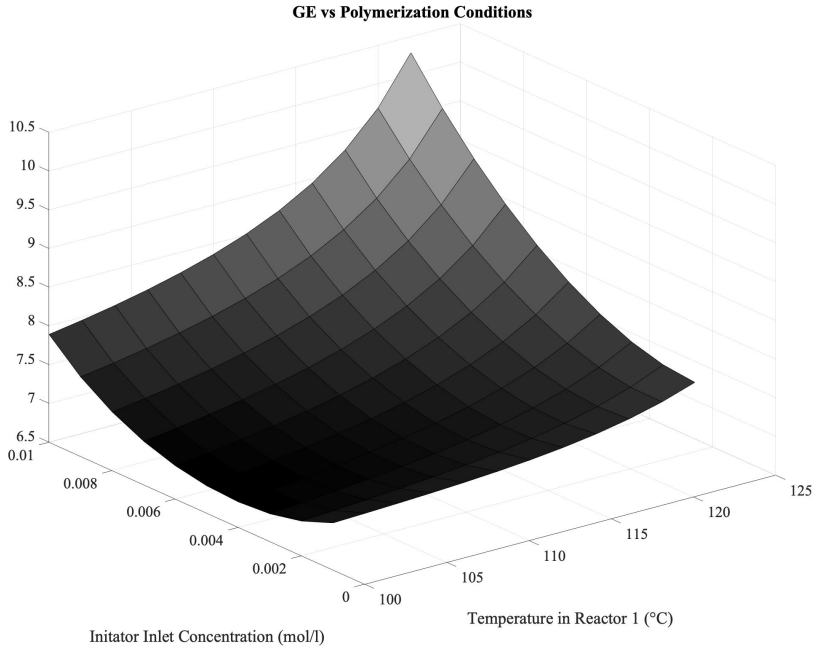

(a)

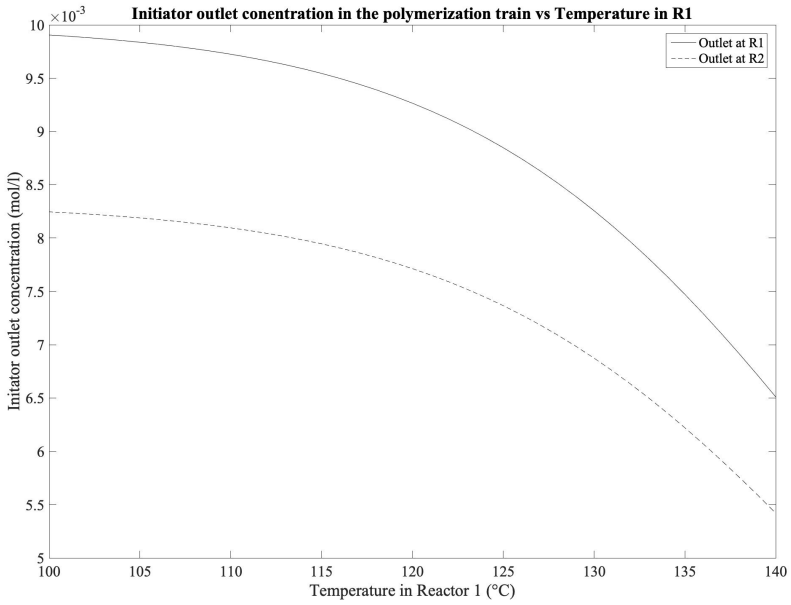

(b)

FIGURE 2.11: Theoretical simulations for HIPS polymerization using the multifunctional initiator L331 in a polymerization train of a continuous plant

TABLE 2.5: Polymerization model parameters.

Parameter	Units	Expression or value	Reference
k_{d1}, k_{dp} (L331)	s^-1	$8.06x10^{11}e^{-30800.9/RT}$	Adjusted in this work
k_{d1}, k_{dp} (PDP)	s^-1	$1.22x10^{10}e^{-28006.7/RT}$	Adjusted in this work
f_1, f_2 (L331)	-	1	Adjusted in this work
f_1, f_2 (PDP)	-	1	Adjusted in this work
k_{i0}	L^2/mol^2s	$1.1x10^5e^{-13810/T}$	[93]
k_{i1}, k_p	L/mol s	$1.051x10^7e^{-7067/RT}$	[81]
$k_{i2}(L331)$	L/mol s	$2.13x10^3e^{-5867.6/RT}$	Adjusted in this work
$k_{i2}(PDP)$	L/mol s	$3.05x10^4e^{-24062.4/RT}$	Adjusted in this work
k_{fM}	L/mol s	$7.28x10^4e^{-10080.3/RT}$	Adjusted in this work
k_{fG}	L/mol s	$6.03x10^8e^{-17311/RT}$	Adjusted in this work
k_{tc}	L/mol s	$1.686x10^9e^{-844/T-2(C_1X+C_2X^2-C_3X^3)2}$	[93]

2.6 Conclusions

A mathematical model for the HIPS continuous polymerization process using multifunctional initiators was developed. The experimental work was carried out in a continuous pilot plant to study the effects of operating conditions on final properties and structure– properties relationships. This is a comprehensive model, meaning it can be used with any mono- or multifunctional initiator, either linear or cyclic. The model was adjusted and validated using new experimental data and thus can be used to simulate the polymerizaton of HIPS in a CSTR train. The model provides a full insight into the molecular structure of the different polymer species (free PS, residual PB and graft copolymer). The presented model could also be extended to other St polymers, such as SAN and ABS, or polymers from other monomers such as PMMA. The model could also be complemented with a mathematical model of a falling strand devolatilizer (FSD) as it is exposed in Chapter 4.

Chapter 3
Mathematical Model of a Continuous Devolatilizer for the Production of Styrene Polymers

3.1 Introduction

In the processes for obtaining polystyrenes (GPPS, HIPS and ABS), DV is carried out at high temperatures and under vacuum to remove low molecular weight components such as monomers, oligomers and other species from the polymeric melt [88–90]. Chemical reactions and transport of low molar mass species during DV have an important effect on the quality of the final product during this part of the process [91]. Also, high-temperature reactions, such as crosslinking, oligomer formation, and degradation that affect the material final properties, occur at this stage. Furthermore, particle breakdown can cause changes in morphology. The volatile species content affects the MFI which is the main processing property. The degree of crosslinking is measured indirectly through the Swelling Index (SI) and is also clearly affected.

Despite the industrial relevance of the DV stage on the final product properties, it has not yet been included in mathematical models for the synthesis of HIPS. As regards DV models, transport phenomena mechanisms have been considered in several works, but no reactions kinetics have been included. Thermal degradation, oligomer formation and crosslinking mechanisms have not been considered [12, 130–132]. These mechanisms occur at temperatures higher than 180°C and have been theoretically and experimentally studied for St polymerization [128, 152, 153]. From a technological standpoint, these high temperature reactions are of great importance during the DV stage. While bibliographic material based on the study of DV in polymers is available, only a limited number of studies relate specifically to PS [12, 130].

In this chapter, the DV stage corresponding to the bulk production process for obtaining PS is studied. The model considers the mechanisms of mass transfer and the chemical reactions involved and predicts the composition of residual volatile species and the molecular structure of the final product. The model consists of a system of differential equations that represents the material balances derived from a kinetic scheme and considers the mechanisms of mass transfer between phases and it was adjusted with experimental data from the literature for a continuous process of PS, obtaining a very good degree of agreement. Finally, it

was used to study the effect of process conditions on the characteristics of the final product.

This DV model can be coupled to a reactors train model to simulate the complete industrial process and also can be easily adapted for the HIPS or ABS production processes. It can then be coupled to structure-properties modules that calculate the MFI and SI of HIPS and ABS, so it can be used to assess the impact of the operating conditions on the quality of the final product.

3.2 Fundamentals of the Mass Transfer Phenomena during DV

Polymer DV is a separation process in which residual VOCs are removed from the polymer matrix by application of a reduced pressure (lower than the equilibrium partial pressure of the volatile component), and/or heat. Stripping agents are also commonly used. It is a complex process that involves the transport of volatiles to a polymer-vapor interface, the evaporation of the volatiles at the interface and their subsequent removal by a vacuum system. DV progresses through a foaming mechanism: bubbles containing the volatiles to be removed are formed within the polymer melt. These bubbles may grow, coalesce and finally rupture at the polymer-vapor interface, releasing their volatile contents in the vapor phase. The crucial factors that determine the extent and rate of DV are the thermodynamics of the polymer-volatile system, the diffusion of the volatile through the polymer, and the nucleation and growth of vapor bubbles in the polymer melt [88, 90].

In a first aspect, DV of molten polymers generally involves first the transport by diffusion of volatile species to a polymer/vapor interface and then the transport of volatiles compounds to a gas stream through the boundary layer. The rate of removal of the volatile species through the interface can be expressed by

$$\frac{dVOC}{dt} = -N_{VOC}AN_{VOC} = -D\nabla c \tag{3.1}$$

where A is the interfacial area and N_{VOC} is the flux of VOC through the interface. The concentration profile of the VOC in the polymer melt is required, which can be calculated from the material balance in the polymer melt.

The diffusion coefficient D of the volatile in the polymer melt depends on both the temperature of the system and the concentration of volatiles, and can be estimated through the Vrentas-Duda free-volume theory [154, 155]. Then, assuming the convective flux is negligible,

$$\frac{\partial c}{\partial t} = \nabla \dot{D} \nabla c \tag{3.2}$$

and the following boundary conditions representing the diffusion process:

$$t = 0, c = c_0 \tag{3.3}$$

$$t > 0, c_{interface} = c_e \tag{3.4}$$

where c_0 is the initial interface volatile concentration and c_e is the concentration at the interface, as will be detailed below.

In the DV of polymer melts, the diffusion of the volatiles through the polymer is usually the rate-controlling part of the process [156].Therefore, the volatile concentration at the interface, c_e, is in equilibrium with the concentration of the volatile in the gas phase.

The equilibrium concentration is related to the partial pressure of the volatile in the gas phase, P_1 ,by means of Henry's law.

$$c_e = \frac{P_1}{H} \tag{3.5}$$

where H, the Henry's law constant which depends on the temperature, pressure, and nature of the volatile.

The interfacial area between the polymer and the gas phase is one of the key parameters in the DV processes, because the rate of VOC removal is proportional to it. The devolatilizers are designed to maximize this interfacial area.

For free-bubble DV, the area of the polymer film that is exposed to DV can be calculated taking into account the geometry of the equipment. However, bubbles are produced in most of the DV processes and can be formed when the polymer melt is exposed to a pressure lower than the partial pressure of the monomer or the solvent in equilibrium with the polymeric solution. Those bubbles are composed of monomer and solvent. After formation, the bubbles grow by diffusion of monomer or solvent from the polymeric melt, and ultimately they separate, releasing the monomer and solvent.

Bubbles can also be formed when stripping agents are introduced into the polymer melt under pressure. If the vapor pressure of the stripping agent is higher than the equilibrium partial pressure of the volatile, gas bubbles composed mainly of the stripping agent will be produced. In this case, DV involves diffusion of the volatiles to the surface of these bubbles. The area of the bubbles is determined by the interplay between bubble nucleation, growth, coalescence, and rupture. Under these circumstances, the determination of the interface area is not straightforward. Bubble nucleation during DV of polymer melts has been explained by homogeneous nucleation [157], heterogeneous nucleation [158–160], and a mixed-mode nucleation [161, 162] considered as a secondary nucleation. Models that account for the growth of the bubbles, assume either a single spherical bubble growing in an infinite sea of liquid [163] or many spherical bubbles growing together with a thin shell of liquid surrounding them [164], have been developed.

The foregoing equations show that DV may be accelerated by acting on the diffusion coefficient, the thermodynamic equilibrium, or the interfacial area. The diffusion coefficient depends on the temperature of the system and on the concentration of volatiles. An increase in the temperature results in an increase in diffusivity and a decrease in viscosity, both beneficial to DV. However, many polymers are thermally sensitive, so there may be a practical upper limit for the temperature to which the polymer may be exposed, as higher temperatures may degrade the polymer.

On the other hand, the diffusion coefficient through the polymer strongly decreases as the concentration of the volatile approaches zero.This drawback can be overcome by introducing an inert substance (usually water), which increases the free volume of the polymer, enhancing the molecular diffusion of the volatile to be removed [165, 166]. Furthermore, the inert substance reduces the partial pressure of the volatile in the gas phase, increasing the driving force for DV. Adding an immiscible liquid as the inert substance presents the additional advantage that the total vapor pressure of the system increases, and therefore the temperature and volatile concentration needed to produce bubbles in the polymer melt is lowered.

3.2.1 DV Equipment

There exists a wide variety of DV equipment. Conforming to Bieseberger [156], the processes can be classified according to the equipment employed: non-rotating or still equipment, and rotating equipment, in which DV is enhanced by mechanical agitation. Non-rotating equipment, such as the falling-strand [88, 161] (Figure 3.1) and falling-film [88] devolatilizers, include mainly flash evaporators and other equipment with specific configurations of the flash chamber, aimed at increasing the exposed interfacial area between the gas and the polymeric phase. In these equipment, the polymer melt/solution is preheated before entering the flash chamber, where the pressure and temperature conditions are such that the volatiles boil. Vaporization of volatiles is prompted by continuous removal of their vapor through the vacuum outlet port of the flash tank.

In those processes, three different regimes can be distinguished [156]. Each of them has a different rate-limiting mechanism, which depends mainly on the difference between the equilibrium partial pressure of the volatile in equilibrium with the melt (P_1) and the total pressure within the vacuum chamber (P).This difference ($P_1 - P$) is often called the "degree of superheat" (SH).

The first regime, termed “free boiling", occurs when SH is large and the liquid viscosity is low. This usually happens under volatile-rich conditions. Vapor bubbles initiate and grow very fast, causing convective mixing that enhances mass transfer to the vapor phase. Under this regime, the temperature, of the melt can rapidly drop if there is no external energy input, since the latent heat of evaporation is provided by the sensible heat of the DV mass. For example, under adiabatic conditions an MMA-PMMA melt at 250 °C will drop approximately 15 for every 10 wt.%of the melt that vaporizes. As the melt temperature drops, P_1 will drop and the degree of superheat will decrease. On the other hand, melt viscosity will rise, due to both the removal of volatiles and the temperature drop. These effects cause bubble growth and movement to slow down and the free-boiling regime to gradually fade out.

The second regime is termed "bubble growth" and the rate-controlling mechanism is the bubble initiation and growth. The volatile removal rate is slower than in the previous regime, and consequently cool-down is reduced. Melt viscosity increases due to depletion of the volatile.

In the third regime, where the viscosity of the melt is very high and the degree of superheat

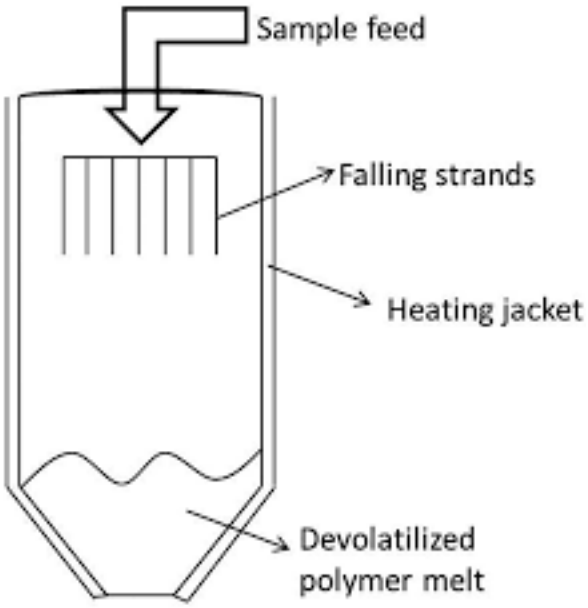

FIGURE 3.1: Falling Strand Devolatilizer

has been reduced due to depletion of volatiles and temperature drop, bubbles are hardly formed and existing bubbles grow very slowly. Under these conditions, the rate of volatile loss is very slow, as it is controlled by the molecular diffusion at the melt/vapor interface. Therefore, for a very low level of volatiles, flash devolatilizers are not efficient.

Nonrotating equipment is efficient for low-viscositiy polymer solutions containing large amounts of volatiles, and particularly useful when dealing with shear-sensitive polymers. However, care must be taken to ensure that they do not have stagnnat areas where the polymer could degrade.

Rotating equipment can be used for DV of highly viscous polymer melts. The rotating parts serve to spread and move the polymer forward along the devolatilizer and also to renew and generate the polymer/vapor phase interface. Typical equipment are wiped-film evaporators and screw struders shown in Figures 3.2 and 3.3, respectively.

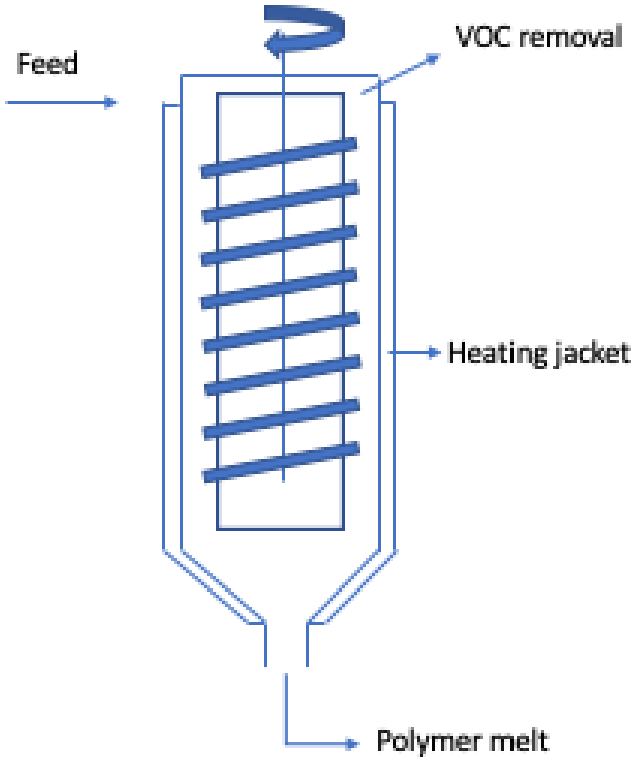

FIGURE 3.2: Wiped-Film Evaporator

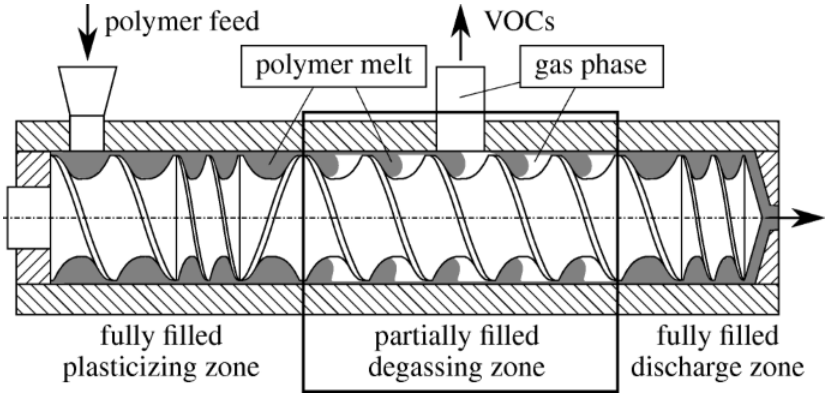

FIGURE 3.3: Single-Screw Extruder [7]

3.3 Mathematical Model of the Continuous DV for the PS Process Using a Lineal Monofunctional Initiator

The DV model proposed herein considers a generic non-rotating or still industrial equipment, where the polymer melt containing volatile species circulates outside a series of tubes forming a falling film in contact with a gas phase. The heating of the mixture is carried out with a heating fluid that circulates inside the tubes. In a simplified way, the equipment can be considered as two phases in contact according to Figure 3.4.

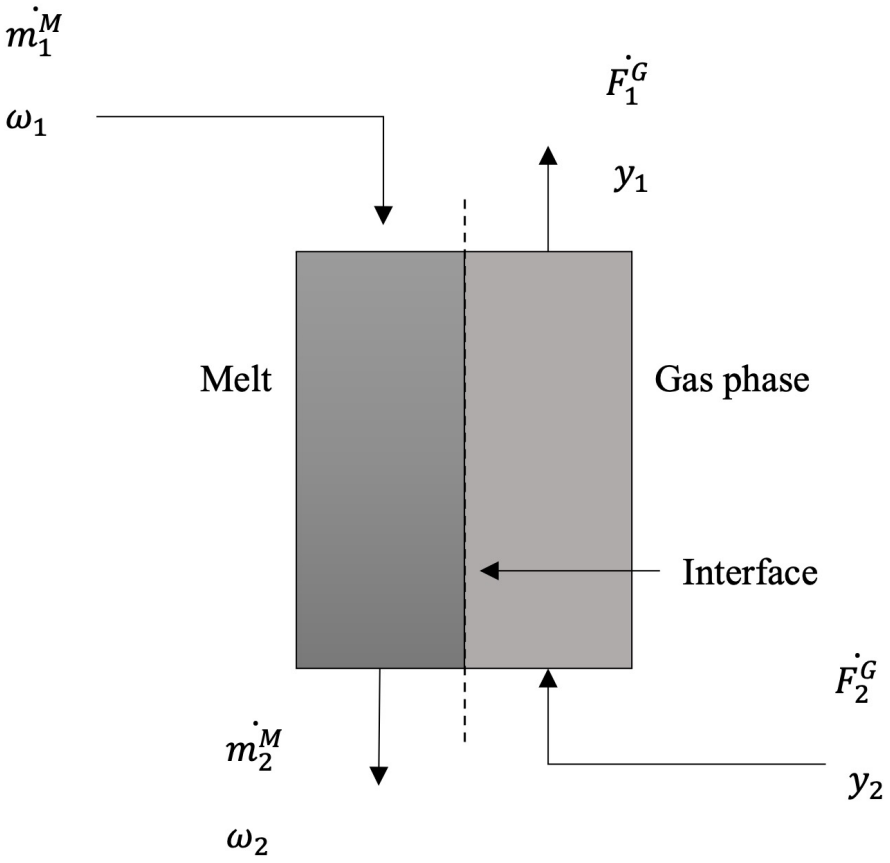

FIGURE 3.4: Two phase simplified scheme for a DV equipment, where $\dot{m}$ is the mass flow rate of melt, ω is the mass fraction of a volatile compound $\dot{F}$ is the molar flow rate of the gas phase and y the molar fraction in the gas phase of the volatile compound.

The equipment is assumed to operate under conditions of constant pressure and temperature. The evaporation of the volatile components causes a cooling that must be compensated by the heat delivered by the heating fluid.

To carry out a balance in the melt (M), a volume element ΔV is considered (see diagram in Fig. 3.5) in which the balance equations were stated. This volume element can be taken as $\Delta V = A\Delta z$, being A the section. The composition of the melt varies as a certain amount ΔW(mass/time) being transferred through an interface area ΔA_{in} . Within the melt volume ΔV, homogeneous chemical reaction takes place, whose reaction rate is given by r. The input

condition is designated by a subscript z and the output condition by $z + \Delta z$.

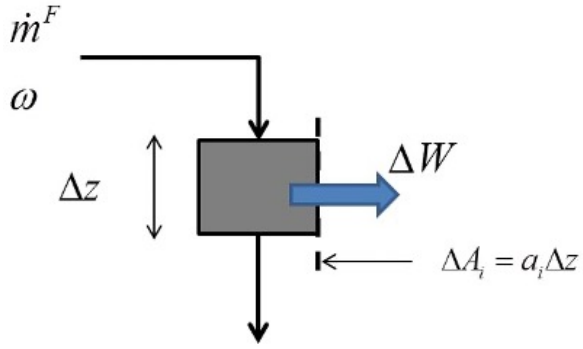

FIGURE 3.5: Scheme of the volume element considered in the mass balance.

Considering that the equipment operates in steady state, the integral material balance for the volatile species in the melt gives:

$$-\omega \dot{m}_M|_z + \omega \dot{m}_M|_{z+\Delta z} = \Delta W + r\Delta V \tag{3.6}$$

The transferred mass of the volatile species can be written in terms of an average total transfer coefficient (which considers the resistance of both phases), a driving force at the interface area and an interface area. Then, a balance by species in the melt gives:

$$W = K^{\omega} \left(\omega_{eq} - \omega(z)\right) A_{in}(z) \tag{3.7}$$

Where, ω_{eq} represents a composition (mass fraction) in the liquid that would be in equilibrium with the gas phase of the corresponding composition at a given point in the equipment. For the analysis in the volume of length Δz it gives:

$$\Delta W = K^{\omega} \left[\left(\omega_{eq} - \omega\left(z + \Delta z\right)\right) A_{in}\left(z + \Delta z\right) - \left(\omega_{eq} - \omega\left(z\right)\right) A_{in}\left(z\right)\right] \tag{3.8}$$

Rearranging,

$$\Delta W = K^{\omega} \left[\omega_{eq}(A_{in}\left(z + \Delta z\right) - A_{in}\left(z\right)) - \left(\omega\left(z + \Delta z\right) A_{in}\left(z + \Delta z\right) - \omega\left(z\right) A_{in}\left(z\right)\right)\right] \tag{3.9}$$

Replacing in the balance and rearranging,

$$\frac{\omega \dot{m}_M|_{z+\Delta z} - \omega \dot{m}_M|_z}{\Delta z} = K^{\omega} \left[\omega_{eq} \frac{A_{in}\left(z + \Delta z\right) - A_{in}\left(z\right)}{\Delta z} - \frac{\omega\left(z + \Delta z\right) A_{in}\left(z + \Delta z\right) - \omega\left(z\right) A_{in}\left(z\right)}{\Delta z}\right] + rA\frac{\Delta z}{\Delta z} \tag{3.10}$$

Taking limit for $\Delta z \to 0$, gives:

$$\frac{d}{dz}(\dot{m}_M \omega_i) = K_i^{\omega} \left[\omega_{eq,i} \frac{dA_{in,i}}{dz} - \frac{d(\omega_i A_{in,i})}{dz}\right] + r_i A \tag{3.11}$$

Developing the product, gives:

$$\dot{m_M}\frac{d\omega_i}{dz}+\omega_i\frac{d\dot{m_M}}{dz}=K_i^{\omega}[\omega_{eq,i}\frac{dA_{in,i}}{dz}-\left(\omega_i\frac{dA_{in,i}}{dz}+A_{in,i}\frac{d\omega_i}{dz}\right)]+r_iA \tag{3.12}$$

Where, r is rate of reaction, A_{in} is interface area and A is the section of the equipment.

The melt mass also changes. Then, with a similar development, a total mass balance for the melt gives:

$$\frac{d\dot{m}_M}{dz}=\sum_{j=1}^{n}K_j^{\omega}\left(\omega_{eq,j}\frac{dA_{in,j}}{dz}-\left(\omega_j\frac{dA_{in,j}}{dz}+A_{in,j}\frac{d\omega_j}{dz}\right)\right) \tag{3.13}$$

Finally, replacing Eq. 3.13 in Eq. 3.12 gives:

$$\dot{m_M}\frac{d\omega_i}{dz}+\omega_i\sum_{j=1}^{n}K_j^{\omega}\left(\omega_j^{eq}\frac{dA_{in,j}}{dz}-\left(\omega_j\frac{dA_{in,j}}{dz}+A_{in,j}\frac{d\omega_j}{dz}\right)\right)= K_i^{\omega}\left(\omega_{eq,i}\frac{dA_{in,i}}{dz}-\left(\omega_i\frac{dA_{in,i}}{dz}+A_{in,i}\frac{d\omega_j}{dz}\right)\right)+r_iA \tag{3.14}$$

A mass balance by species in the equipment gives,

$$\dot{m}_i^G=\omega_i\dot{m}_M|_{in}-\omega_i\dot{m}_M|_{out} \tag{3.15}$$

At equilibrium, the pressure of each volatile component in the vapor phase is equal to the vapor pressure of that species in the solution ($P_{g,k}$) and is calculated with the vapor pressure of the pure component (P_k^0), considering a diluted solution in the DV [12, 90]. Then, the following expression is derived:

$$\omega_{eq,i}=\frac{y_iP\rho_i}{P_i^0\rho_Me^{1+\chi_i}} \tag{3.16}$$

Where,

$\omega_{eq,i}$ is the weight fraction of the volatile species,

y_i is the mole fraction of the volatile species in the vapor phase,

ρ_M is the melt density,

P is the pressure in equilibrium with the melt at the interphase,

P_i^0 is the vapor pressure of the volatile species and

χ_i is the Flory-Huggins binary interaction parameter for the volatile species and the melt.

The composition in the gas phase can be calculated according to:

$$y_i=\frac{\dot{F_i^G}}{\dot{F^G}}=\frac{\dot{m_i^G}}{M_i\left(\sum_{j=1}^{n}\frac{\dot{m_j^G}}{M_j}\right)} \tag{3.17}$$

The mass balance equation for the melt phase can be integrated between 0 and a length L

(length of the equipment) to obtain the composition profile of the melt. Then the DV process can be modeled as a "black box" in which the input variables are: the melt flow, the inlet volatile species content of the melt, the operating temperature, the operating pressure and the equipment length. And the output variables are: the volatile species content of melt outlet, the gas outlet content and the outlet gas flow. The parameter that can be adjusted in the system using experimental data will be the product between the total transport coefficient in the molten phase and the interfacial area per unit length ($K_i^{\omega} a_i$).

This DV model considers monomer thermal initiation, chemical initiation, propagation, transfer to monomer, termination and volatile species generation [154] and it is based on the kinetic mechanism proposed in Table 3.1, where high temperature reactions of formation of dimer (Dm) and trimer (Tm) are included.

TABLE 3.1: PS polymerization using a monofunctional initiator - Proposed kinetic mechanism.

Initiation
Thermal Initiation
$3\mathrm{St} \xrightarrow{k_{i0}} 2S_1\cdot$
Chemical Initiation
$I_2 \xrightarrow{k_d} 2I\cdot$
$I\cdot + St \xrightarrow{k_{i1}} S_1\cdot$
Propagation $(n = 1, 2, 3...)$
$S_n\cdot + \mathrm{St} \xrightarrow{k_p} S_{n+1}\cdot$
Transfer to monomer $(n = 1, 2, 3...)$
$S_n\cdot + \mathrm{St} \xrightarrow{k_{fM}} S_n + S_1\cdot$
Combination termination $(n, m = 1, 2, 3...)$
$S_n\cdot + S_m\cdot \xrightarrow{k_{tc}} S_{n+m}$
High temperature chemical reactions-Oligomer formation
$2\mathrm{St} \xrightarrow{k_D} D_m$
$3\mathrm{St} \xrightarrow{k_T} T_m$

Nomenclature:	
$\bar{I}$	Linear multifunctional initiator
$I\cdot$	Initiator monoradical
$S_1\cdot$	Monomer monoradical
S_n	Polymer with n repetitive units of St
$S_n\cdot$	PS monoradical of chain length n

Then the balance equations by species in the DV for a PS process gives:

Monomer:

$$\frac{d\omega_{St}}{dz} = \frac{1}{\dot{m}_M}\left(-\left(k_p[St][R\cdot] + 2k_{i0}[St]^3\right)A + \left(1-\omega_{St}\right)K^{\omega}_{St}a_i(\omega^{eq}_{St}-\omega_{St}) - \omega_{St}\sum_{j=1,j\neq i}^{n}K^{\omega}_j a_j(\omega^{eq}_j-\omega_j)\right) \tag{3.18}$$

with $[St] = \frac{\rho_M}{M_{St}}\omega_{St}$

Dimer:

$$\frac{d\omega_D}{dz} = \frac{1}{\dot{m}_M}\left(2k_D[St]^2A + \left(1-\omega_D\right)K^{\omega}_D a_i(\omega^{eq}_D-\omega_D) - \omega_D\sum_{j=1,j\neq i}^{n}K^{\omega}_j a_j(\omega^{eq}_j-\omega_j)\right) \tag{3.19}$$

Trimer:

$$\frac{d\omega_T}{dz} = \frac{1}{\dot{m}_M}\left(2k_T[St]^2A + \left(1-\omega_T\right)K^{\omega}_T a_i(\omega^{eq}_T-\omega_T) - \omega_T\sum_{j=1,j\neq i}^{n}K^{\omega}_j a_j(\omega^{eq}_j-\omega_j)\right) \tag{3.20}$$

Nonvolatile species:

$$\frac{d[R\cdot]}{dz} = \frac{\rho_M}{\dot{m}_M}\left(2k_{i0}[St]^3 - k_{tc}[R\cdot]^2\right)A \tag{3.21}$$

Free PS MWD[19]:

$$\frac{dS_{n\cdot}}{dV} = k_{fM}[St][R_{n-1}\cdot] + \frac{1}{2}k_{tc}\sum_{m=1}^{n-1}[R_{n-m}\cdot][R_m\cdot] \tag{3.22}$$

$$\frac{dS_{n\cdot}}{dV} = R_p\left(\tau+\beta\right)\left(\frac{1}{1+\tau+\beta}\right)^n\frac{\tau}{1/2\beta(\tau+\beta)n} \tag{3.23}$$

where,

$$\tau = \frac{k_{fM}}{k_p} \tag{3.24}$$

$$\beta = \frac{k_{tc}R_p}{k_p^2[St]^2} \tag{3.25}$$

It should be noticed that these equations for the calculation of the PS MWD can be used since a lineal monofunctional initiator was considered.

3.3.1 Model Adjustment and Simulations

Experimental data from the literature for a PS industrial process were used to adjust the mass transfer coefficients for volatile species [12]. In this work, the residual content of St, ethylbenzene (EB), Dm, Tm and cumene (C) was studied as a function of the degree of vacuum in a "flash tank" type DV. The feed to the DV comes from a PS reactor and contains approximately 85% polymer and the remainder material St, EB, C, Dm, and Tm. The operating conditions and inlet composition are presented in Tables 3.2 and 3.3. Model parameters for the polymerization reactions were taken from a previous work [84].

Table 3.2: Operating conditions

DV Volume (L)	Operation T (°C)	Operation P (mmHg)	Inlet Flow (kg/s)
1000	230	5-28	1.56

Table 3.3: Feed Composition

Component	Composition (%)
polymer	84.268
St	11.610
EB	2.675
n-propylbenzene	0.504
C	0.626
Dm	0.089
Tm	0.228

Figures 3.6 and 3.7 show the effect of the vacuum applied during the process on the residual content of the volatile species implicated.

An excellent agreement between the experimental values and the predictions can be observed. As expected, the degree of vacuum significantly influences the volatile species content in the devolatilized product. The non-zero origin ordinate indicates that the system is controlled by mass transfer.

The adjustment parameters were the mass transfer coefficients for the volatile species, whose values are shown in Table 3.4

The effect of operating conditions over the residual content of volatile species and the molecular structure of the polymer was studied. Figure 3.8 shows the effect of the operating pressure and temperature on the residual content of the different volatile species involved. Figure 3.9 shows the effect of operating pressure and residence time. In Figure 3.10 the change on the molecular structure during DV is presented.

As expected, the degree of vacuum significantly influences the volatile species content in the devolatilized product.

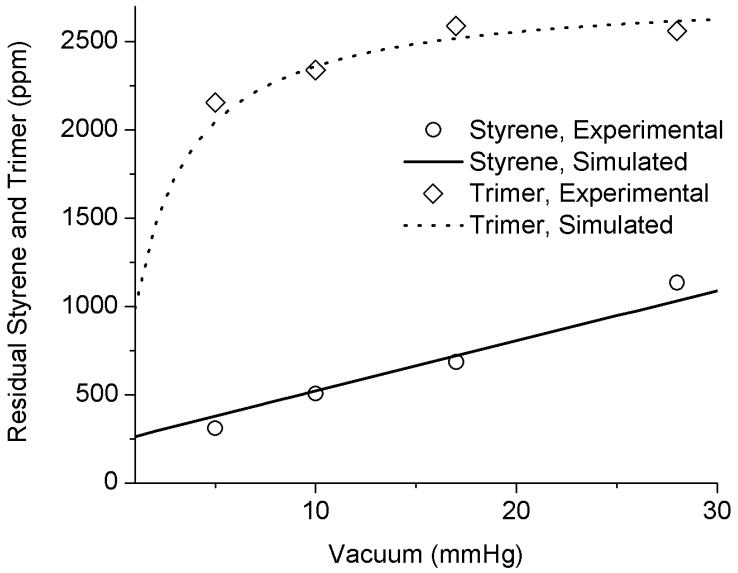

FIGURE 3.6: Effect off vacuum degree on the residual concentration of residual St and trimer

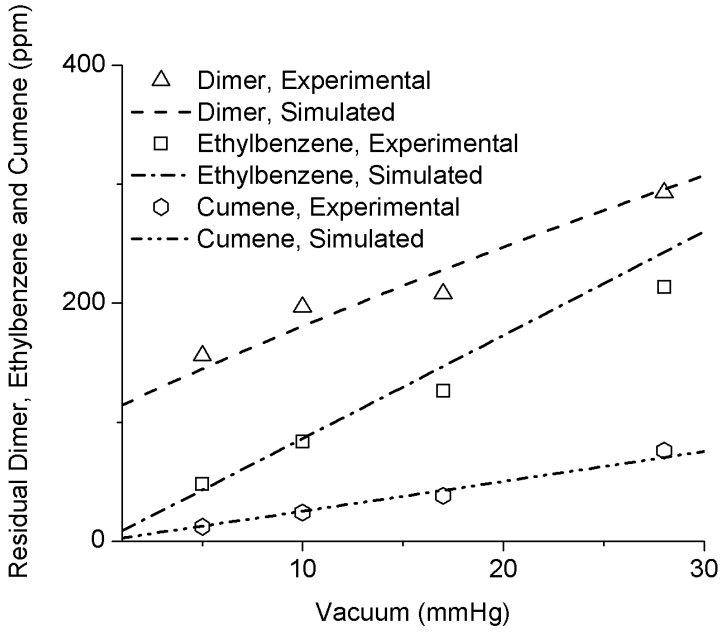

FIGURE 3.7: Effect off vacuum degree on the residual concentration of residual dimer and ethylbenzene

TABLE 3.4: Mass Transfer Coefficients at 230 ° C: adjusted with experimental data for an industrial DV process [12]

Species	$K_i a_i$ (kg/m^{2}s)
Monomer	7.7
Dimer	3.5
Trimer	25.0
Ethylbencene	18.0
Cumene	15.0

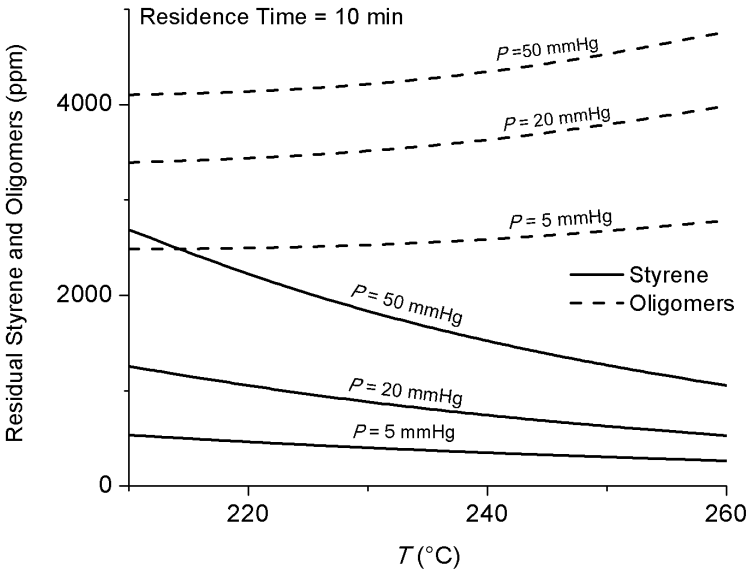

FIGURE 3.8: Effect of pressure and temperature on the residual content of volatile species at a residence time of 10 minutes.

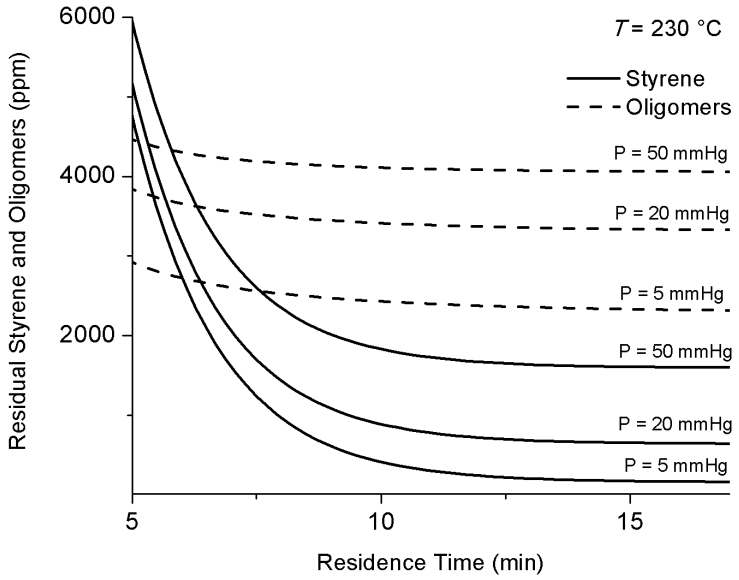

FIGURE 3.9: Effect of pressure and residence time on the residual content of volatile species at 230° C.

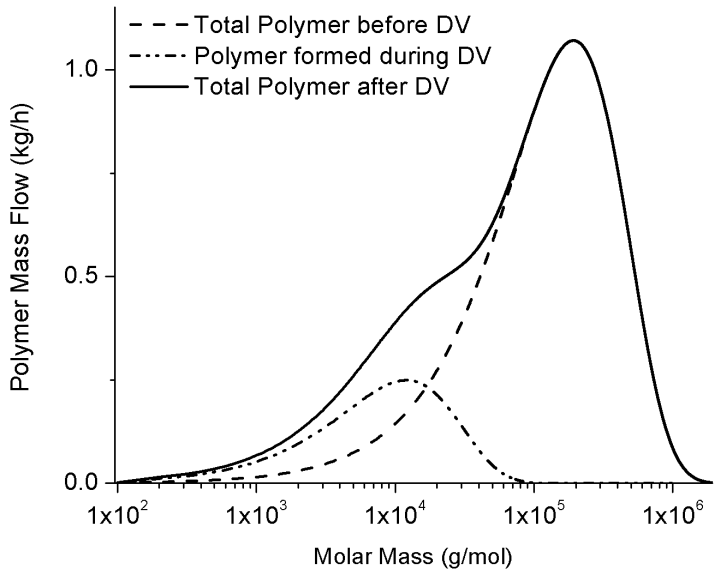

FIGURE 3.10: Changes in the molecular structure of PS during DV at $T = 230$ °C, $P = 5$ mmHg

3.4 Conclusions

On the basis of a deep understanding of the physical and chemical phenomena occurring during DV, a model for the simulation of the DV stage for PS polymerization process was developed, which allowed estimating the chemical composition and molecular structure. The model was adjusted with experimental data from the literature for a continuous process of PS DV, obtaining a very good degree of agreement. The effect of operating conditions over the residual content of volatile species and the molecular structure of the polymer was studied.

This model can also be easily adapted to the continuous processes of HIPS or ABS. The DV model can be then coupled to a model of the reactor train to simulate the complete industrial process. The complete model could be used to simulate, control and optimize industrial processes for HIPS and other PS resins.

Chapter 4
Mathematical Modeling of the Continuous Bulk Process for HIPS Production Using Multifunctional Initiators. Integration to FSD and Structure-Properties Modules.

4.1 Introduction

Mathematical modeling is a necessary and useful tool for the understanding and design of HIPS industrial processes. There is a growing technological interest in improving the quality of the material and increasing the efficiency of the processes by optimizing . Also, there are still many aspects to be elucidated related to the quantitative interrelationships between the process variables, the molecular and/or morphological characteristics, and the final properties. One of the main objectives of the industry is to be able to study the effect on the final properties of possible changes in the recipe and the conditions of synthesis, and thus develop "made to measure" polymers. Furthermore, there is a strong need to systematize grade transition procedures in order to minimize the out-of-specification materials. These processes can be optimized to improve the quality of the final product and / or also the productivity of the system.

The use of multifunctional initiators has been increased in the recent decades, since they allow obtaining high polymerization rates and polymers with high average molecular weights, as a consequence of the sequential decomposition of the initiator [72, 74, 75]. Very few mathematical models are reported in the literature regarding the use of multifunctional initiators, and most of them consider batch reactors [73, 81, 83, 84, 124]. No models have yet been published that consider the use of multifunctional initiators in continuous HIPS production systems.

On the other hand, despite the industrial relevance of the DV stage on the final product properties, it has not yet been included in mathematical models for the synthesis of HIPS. Chemical reactions and transport of low molar mass species during DV have an important effect on the quality of the final product [91]. High-temperature reactions, such as crosslinking, oligomer formation, and degradation occur at this stage. The volatile species content affects the MFI (Melt Flow Index) which is the main processing property. The degree of crosslinking

is measured indirectly through the Swelling Index (SI) and is also clearly affected. There are no references for the study of the modification of molecular structure (degree of crosslinking and MWDs) and the morphology of the material during the DV process, variables that in turn have importance on the final properties such as SI, MFI, and others.

The mathematical model of the industrial HIPS production process presented herin consists of three sub-models: a Polymerization Model for the reactor train, a DV Model for a Falling Strand Devolatilizer (FSD) and a Structure-Properties Model for the calculation of MFI and SI.

The model allows the estimation of all global variables along the process as well as quality variables, such as SI, MFI, oligomer content and residual monomer of the final material. The model can be used to simulate the process with any mono- or multifunctional initiator, either lineal or cyclic. New experimental data for continuous polymerization of St in the presence of PB using different peroxide initiators at a pilot plant scale was obtained to adjust and validate the model. The model is then used to theoretically study the use of multifunctional initiators and the effect of process conditions on the product final properties. The simulation of systems involving multifunctional initiators involve multi-dimensional models, especially in cases where the full molecular structure has to be estimated. Chain length as well as functional group distributions have to be simulated for every reacting species, which may include radicals with several active sites in the same molecule (i.e. multiradicals).

This work is the first attempt to develop a comprehensive mathematical model for the continuous process of HIPS production using multifunctional initiators. The model comprises integrated modules that simulate the polymerization train, DV stage and selected structure-properties relationships. The work presented in this chapter was reported in Laganá et. al [124], "New advances in the mathematical modeling of the continuous bulk process for the production of high-impact polystyrene using multifunctional initiators", Polymer Engineering & Science, 59(s2), E231-E246, 2019.

4.2 Structure-Properties Implications and Relationships

HIPS is a multiphase system consisting of a continuous rigid PS phase and discrete rubber particles 0.5-10 μ in diameter. The incorporated rubber particles are crosslinked and contain a graft copolymer. The inner structure is determined by the manufacturing process and can vary considerably. The toughness of HIPS is caused by flow and energy dissipation processes in the continuous PS phase [8]. In general, the final properties of HIPS and St heterogeneous plastics are determined by composition, molecular structure, and morphological structure. From an industrial point of view, the most important final properties that define the quality of HIPS are MFI and IR (Impact Resistance). The relationship between the structure and properties of HIPS have been ilustrated in Fig. 1.10.

4.2.1 Matrix Molecular Weight

The PS MW affects mechanical, rheological and thermal properties. Relationships between MW of the PS phase and polymer properties are similar to those for the homopolymer. Melt viscosity and the relationship between polymer architecture and processability are controlled predominantly by MW. Increasing the MW of the continuous PS phase increases the melt viscosity. Higher MW will increase toughness properties but decrease processability by lowering the MFI and thus difficult processing. MFI is a measure of the flow (in g/10 min) of molten polymer that passes through a plastometer when it is forced by a piston under constant load (ASTM D1238). MFI is the quality variable mostly used to characterize the material from a rheological point of view [116]. Characteristics of the graft copolymer, the MW and the MWD are optimized during polymer design to provide the desired rheological properties [169].

4.2.2 Elastomer Implications

GPPS is impact modified by the inclusion of an elastomer to yield a product that may exhibit impact properties with an order of magnitude greater than the homopolymer. The most commonly employed rubber is medium-cis PB and high-cis PB. Commercial polymerization processes produce a polymer system that not only has an elastomer incorporated, but also a grafted species where PS side chains attach to the rubber domains. This grafting anchors the discrete elastomer particles in the continuous PS phase, yielding better compatibility and much higher IR [169]. When external forces act on HIPS, the rubber particles have a stress-relaxing action. To do this job, they must be bound sufficiently to the matrix and have a certain elasticity. This means that the rubber used must be capable of grafting and crosslinking. Both properties can be controlled within certain limits via the microstructure. These requirements mean that nowadays use is predominantly made of medium-cis and sometimes also high-cis rubbers, which can be produced using organolithium initiators or coordinate Ziegler catalysts. High-cis PB has relatively high heat resistance, which is advantageous in the processing of HIPS. On the other hand, this type of PB crystallizes at about 0 °C, owing to its stereoregular structure, with the consequence that the low-temperature toughness of polystyrene, produced in this way, is reduced. Apart from pure PB rubbers, St—B block copolymers are also used, enabling products having particle sizes of less than 1 μm to be produced. They have high gloss and high rigidity, but somewhat lower toughness for a comparable PB content. Other rubber systems have been commercially successful. St block copolymers yield a HIPS product with a small particle size and provide high gloss. A mixed rubber system consisting of St—B block rubber and/or ethylene—propylene diene modified (EPDM) rubber can be blended with the PB to form bimodal rubber particle size distribution for acombination of high gloss and high impact. The block rubber generates the typical capsular small particles, and the EPDM, which is incompatible with the block rubber, yields large particles as a separate rubber phase. EPDM, with higher degree of unsaturation and use of a high concentration of crosslinking promoting peroxide (di-tert-butyl peroxide) to stabilize the rubber particles, is required to improve grafting [169].

Different production techniques and formulations allow the rubber phase to be tailored to a wide range of properties. Typically:

1. Increasing the amount of rubber added will increase the toughness.
2. Increasing the rubber particle size increases toughness to a point of diminishing returns.
3. The gel content (fraction not soluble in toluene) of PS in the rubber, indicating the phase volume of crosslinking of the rubber, increases toughness to a point (around 30%) and then is deleterious.
4. The SI (volumetric ratio of a swollen gel to its unswollen state), indicating the strength of the crosslinked domain, follows the same trend as gel content with an optimal toughness achieved typically around 12% swell [169].

Polymer toughness, in the form of IR, is a measure of the ability of a material to withstand the application of a sudden load without "failure". The measured IR of a polymer must be the result of the sum of the contributions of all processes that dissipate any of the energy of the impact blow and is probably the most critical mechanical property of plastics, because it relates to the service life of a part, and involves the increasingly important matters of product safety and liability [170].

Rubber toughening should impart greater ductility, improved crack resistance, and higher IR to the material, accompanied by only a small loss in stiffness and without a detrimental effect on thermal stability. According to Partridge [171] a polymer might be considered to be successfully rubber toughened if its fracture resistance under a particular set of conditions is increased by a factor of 10, while its low-strain stiffness decreases by no more than about 25%. IR is evaluated in terms of the energy absorbed during the impact process. Heterogeneous St polymers are designed for applications where good impact properties are required. The reinforcement of the rubber is considered to be acceptable when it exhibits [115]:

1. a low elastic modulus with respect to the matrix;
2. adequate crosslinking and good adhesion with the matrix;
3. an optimal distribution and average particle size; and
4. a low glass transition temperature.

Almost any engineering plastic can be made tougher by the addition of a small amount of rubbery material. One theory is that the rubber becomes stretched during the fracture process and absorbs a great amount of energy [170]. Another theory proposes that the rubber particles act to introduce a multiplicity of stress concentration points, promoting multiple crazing, which leads to cracks that propagate during the fracture process, requiring greater energy than a single crack, due to the production of further new surfaces [170].

4.2.3 Grafting

The grafting is accomplished in the commercial bulk polymerization process by polymerizing St in the presence of a dissolved rubber. Dissolving the elastomer in the St monomer before polymerization produces HIPS grades. Since the two polymer solutions are incompatible, the St—rubber system phase separates very early in conversion. PS forms the continuous phase, with the rubber phase existing as discrete particles having occlusions of PS [169].

The aim of any grafting is to increase the rubber efficiency, i.e. the ratio between the gel content and the rubber content, and to enable the rubber particles to bond to the PS phase in order to ensure the transmission of external forces from the energy-elastic phase to the entropy-elastic phase. The graft polymer acts as emulsifier and stabilizes the dispersed rubber particles in the two-phase system. Owing to the extremely high importance of grafting for the particle size, the particle structure, the rubber efficiency and the phase adhesion, numerous attempts have been made to increase the graft yiel [169].

4.2.4 Crosslinking

The high hardness and toughness of ABS and HIPS polymers requires controlled crosslinking of the rubber phase. If crosslinking is insufficient, the rubber particles dispersed in the polymer matrix are destroyed by the action of shear forces during processing. Rubber which is not crosslinked has no elasticity. The swelling index (SI) in a good solvent is usually used as a measure of the degree of crosslinking [172]. Quantitative relationships between the degree of swelling and the crosslinking density have also been established [150].

It is considered that the crosslinking and chain propagation reactions are competitive and follow the reaction paths shown in Fig. 4.1 [8]. The rubber radicals produced by reactions b) and c) can cause crosslinking of the rubber by recombination or propagation steps. Since these reactions precede the crosslinking and compete with the propagation reaction a), it is expected that crosslinking of the rubber particles depends on conversion of St monomer.

It has been concluded that crosslinking and formation of crosslink sites increase with monomer conversion and that at St conversions below 95%, the rubber crosslink density is too small for determining the SI [8]. It is also known that crosslinking is influenced by the type and number of double bonds or allylic hydrogen atoms in the rubber. PB microstructure can be controlled easily by suitable anionic polymerization conditions in which parameters like double bond number and MWD remain constant. It was found that crosslinking strongly increases with increasing double bond content of the rubber and that the allylic hydrogen atom of this configuration is primarily responsible for the crosslinking reaction.

Although it also varies with the initiator type, it was found that the ratio of the rate constants from reaction paths a) and b) for an attack by a PS radical on the 1,2-double bond is (at 110 °C) [8]:

$$\frac{k_{12}}{k_{11}} = 1.5 \cdot 10^{-3} \tag{4.1}$$

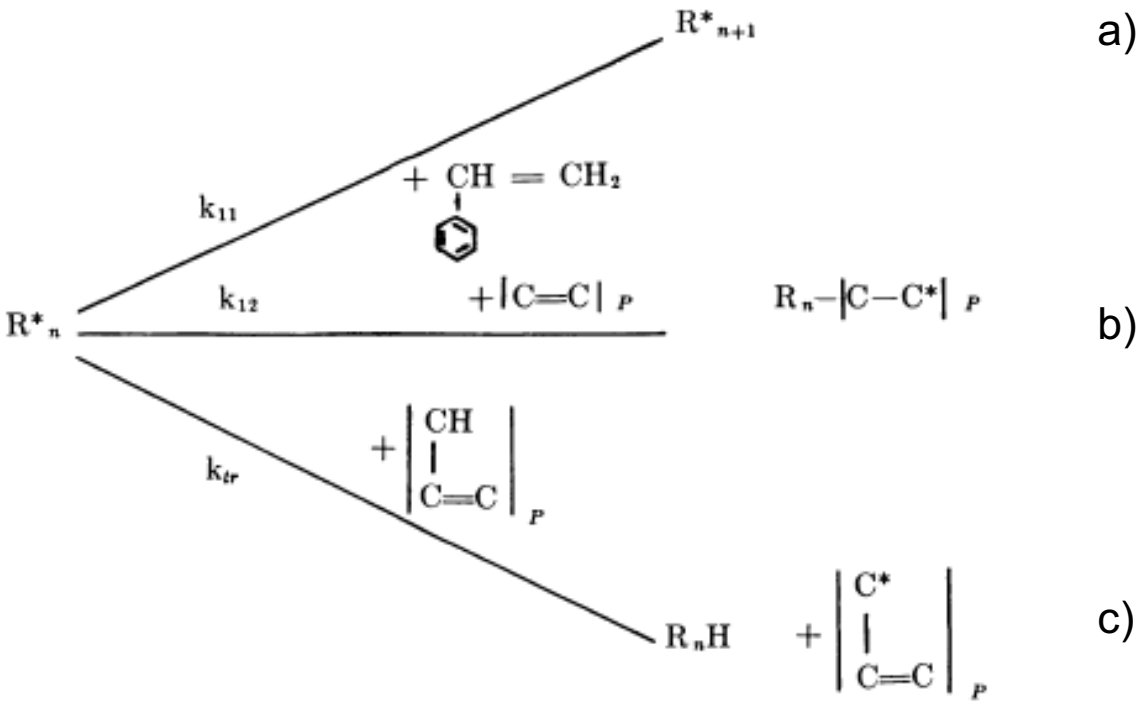

FIGURE 4.1: Illustration of the possible competitive reactions of polystyrene radicals and initiator radicals [8].

In contrast to the grafting reactions, the crosslinking reactions during HIPS process become effective only at very high St conversion (>95%) at which the rubber double bond concentration in the total reaction mixture approaches the monomer concentration [8]. In order to retain the elasticity of the rubber and to avoid increasing the glass transition temperature excessively, the crosslinking density must not be too high.

The rubber gel in HIPS is characterized by the SI. Occlusions, type of rubber, extent of crosslinking, solubility of the rubber, rigid phase and solvent are all factors related to the SI. The absorption of liquids by polymers is an osmotic process. This is closely related to the dissolution process; it involves the diffusion of one species of molecule into a medium composed of a different species. Conventional dissolution consists of the diffusion of a solid into a liquid to form a homogeneous mixture. In the swelling of a polymer, it is the liquid which diffuses into the solid to form a molecular mixture, i.e. a solution. The difference in the case of swelling, from the more familiar type of osmosis in the measurement of the osmotic pressure, is that the mixed phase is a solid and, since molecules cannot detach from solid, there is no need for a semi-permeable membrane.

As the solvent diffuses into the rubber and the material begins to swell, the network structure becomes of importance, since the polymer chains are expanded in much the same way as if they were exposed to an external 3-dimensional force. The two effects, the swelling effect of the solvent and the resisting force of the polymer network, trying to occupy a smaller volume driven by its entropic elasticity, tend to balance out at a precisely defined liquid content or equilibrium degree of swelling. The final extent of swelling depends on the degree to which

the network is crosslinked, which of course affects its elastic modulus. The quantitative theory for this effect is the Flory-Huggins theory [137, 173].

4.2.5 Particle Size and Particle Size Distribution

The rubber particle size range of HIPS is essentially determined by three factors [169]:

1. the shear field of the reacting material during and immediately after phase inversion,
2. the viscosity ratio between the disperse and continouous phases and
3. the degree of grafting, which affects the interfacial tension.

With increasing shear, the particle size decreases, i.e. the particle size distribution peak shifts to lower values, and the relative proportion of smaller particles increases. A decrease in the viscosity of the continuous phase results in an increase in the particle size range and a reduction in the stability of the oil-in-oil emulsion. An increase in grafting initially gives smaller cell particles and ultimately new particle structures.

Commercial rubber-toughened thermoplastics typically have particles smaller than 3 μm in diameter and often smaller than 0.2 μm [171]. For each matrix material there appears to be an optimum range of particle sizes leading to the best toughness improvement. The optimum rubber particle size is related to the nature of the subsequent matrix deformation mechanism. According to Bucknall [174] the rate at which the matrix can respond to stress by forming oriented fibrils (crazing) becomes the limiting factor in determining IR. This is because fibrillation is the most rapid mechanism available for the extension of the damage zone at the crack tip. Fibrils, which can range from 5 to 50 nm in diameter, are the load-bearing members of the craze [175]. In HIPS, where such fibrillation occurs during multiple crazing, particles less than 1 nm are less effective in toughening the system than are larger particles [60].

4.3 Mathematical Model

A mathematical model of the HIPS industrial production process is presented, which consists of three sub-models: a polymerization model for the reactor train, a DV model and a structure-properties model. Fig. 4.2 shows a schematic representation of the inputs and outputs of the integrated sub-models. The complete model allows the estimation of all global variables throughout the process and quality variables, such as SI , MFI, oligomer content and residual monomer. The polymerization train module is based on the model presented in Chapter 2 and allows the simulation of a polymerization train of CSTRs using multifunctional initiators. The module predicts global chemical species (monomer, initiators, total radical species, unreacted butadiene units, undecomposed peroxide groups) and the estimation of all chemical species concentrations, characterized by their chain length and number of undecomposed peroxide groups. The composition and molecular structure calculated in this module are the inputs

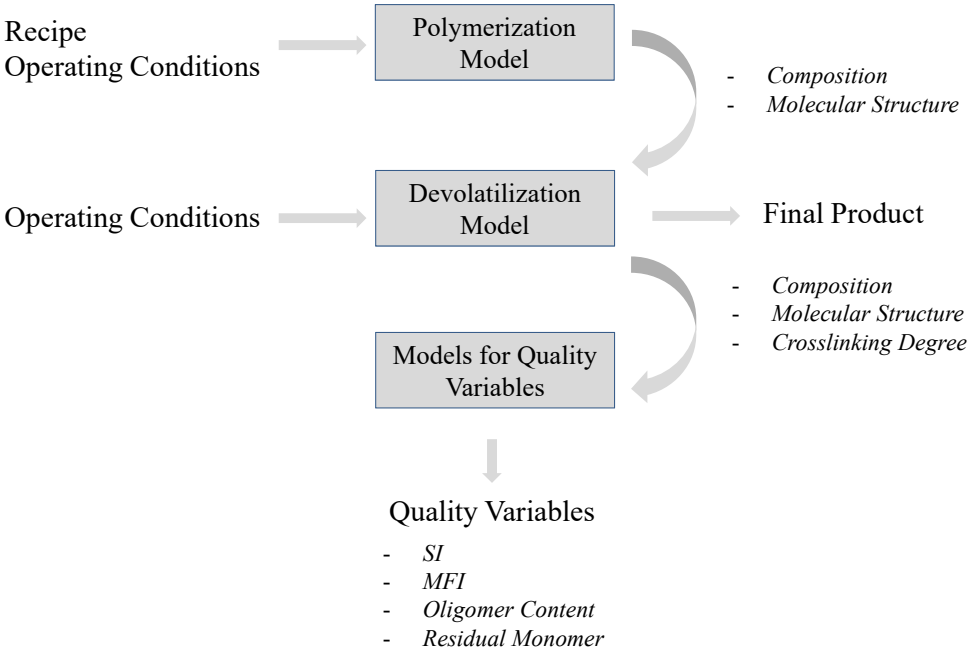

FIGURE 4.2: Inputs and outputs diagram of the continuous HIPS production integrated sub-models. (1) Model for the polymerization reactor train, (2) model for the DV stage, and (3) models for final properties prediction.

to the DV model presented in this Chapter. Finally, the Structure-Properties Model allows the calculation of MFI and SI. The final MW_{PS} and the average molecular weight between crosslinks (Mc) calculated at the DV exit are variables that allow the estimation of the MFI and SI, respectevely.

4.3.1 Mathematical Model of a Falling Strand Devolatilizer for the Continuous HIPS Production Using Multifunctional Initiators

In this section, a DV model for a FSD for the continuous HIPS process is developed. In the configuration of a FSD, the material enters the flash chamber as a multitude of strands, which fall free due to gravity into the accumulated melt pool below. The scheme and geometry of the equipment is shown in Figure 4.3. The free fall of strands, allows easy disengagement of the already grown bubbles. During the free fall, the configuration allows new bubbles to nucleate and grow free of external shear or pressure gradients. A full insight in the description of the equipment operation was presented in the previous chapter (See Section 3.2.1).

The operation is separated into two different stages. In the first stage, the polymer melt falls from a sprinkler forming strands that are in contact with the vapor phase. Bubbles nu-

cleate, grow and rupture releasing the volatile components to the vapor phase, while chemical reactions take place mostly in the melt. This "falling strand stage" in the FSD can be modeled as a Plug Flow Reactor (PFR). The second stage, the "pool stage", involves the boiling polymer melt pool at the bottom of the FSD. As the boiling mechanism produces agitation, a CSTR model is adopted. At this stage, molecular diffusion is very shallow, as most bubbles are likely to be "buried" more rapidly by the falling melt than they can rise through the viscous melt pool. The bubbles therefore contract under the increasing melt head [88, 90].

The input variables to the model are: the equipment geometry, the operating conditions (i.e. temperature, pressure and residence time) and the feed flow inlet (i.e. composition, MWDs of the polymeric species and degree of crosslinking of the rubber), calculated in the polymerization model.

The FSD model is based on the kinetic mechanism proposed in Chapter 2 (see Table 2.4) with the addition of the the high temperature reactions presented in Table 3.1 and also crosslinking reactions.

The following is assumed:

(i) Vapor bubbles are in equilibrium with the melt at the interface [90, 154, 156],

(ii) Mass transfer mechanism: diffusion into bubbles with no interaction effects [8, 155, 156, 156, 163],

(iii) Bubbles expand against surface tension and viscous forces in a Newtonian fluid [8],

(iv) Vapor in bubble behaves as an ideal gas,

(v) No resistance to mass transfer in the vapor phase,

(vi) The melt is considered a continuum,

(vii) DV takes place in the bubble growth regime [88, 156],

(viii) No bubble coalescence,

(ix) Shallow diffusion in melt pool [88, 156, 163] and

(x) Constant pressure and temperature operation: the evaporation of volatile components originates cooling that must be compensated by a heat source (e.g. the heat delivered by a heating fluid).

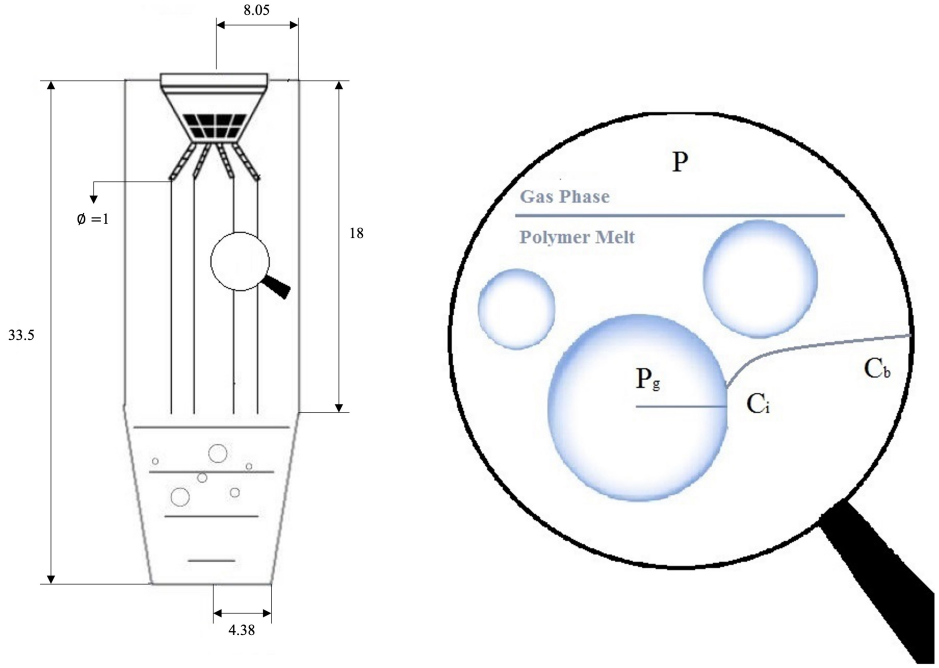

FIGURE 4.3: Geometry of the FSD used in the pilot plant for all experiments (measures in cm) and mass transfer mechanism adopted for the mathematical model: Diffusion of volatiles into isolated bubbles in a continuous melt phase.

PFR Stage

Diffusion Mechanism

In the PFR stage, the molar flux of a volatile species (i.e. solute) into the growing bubble considering equilibrium conditions can be calculated on the base of classical penetration theory, corrected for convective effects due to bubble expansion [156, 163, 167, 168]:

$$N_k = \sqrt{\frac{7}{3}}\left(\sqrt{\frac{D_k}{\pi\theta}} + \frac{D_k}{R}\right)(C_k - C_{in,k}) \tag{4.2}$$

Where,
θ is the contact time of the fluid with the interphase (s),
D_k is the solute mutual-diffusivity, which considers concentration gradients (cm^2/s),
R is the bubble radius (m),
$C_{in,k}$ is the solute concentration at the interphase (mol/l), and
C_k is the solute concentration in the bulk (mol/l).

Where k denotes any of the volatile chemical species (i.e St, Dm and Tm).

For the estimation of St diffusivity, the following expression based on the free volume theory is considered [88].

$$D_k = D_{0,k}(1 - \phi_k^2)(1 - 2\chi\phi_k) \tag{4.3}$$

Where,
$D_{0,k}$ is the solute self-diffusivity (cm^2/s) [154],
ϕ_k is the volume fraction of the solute in the melt, and
χ is the Flory-Huggins interaction parameter
ϕ_k is calculated as

$$\phi_k = \frac{C_k MR_k}{\rho_k} \tag{4.4}$$

Where,
MR_k is the molecular weight of the volatile species (g/mol) and
ρ_k is the solute density (g/l).

Equilibrium Condition

At equilibrium, the pressure of each volatile component in the vapor phase is equal to the vapor pressure of that species in the solution ($P_{g,k}$) and is calculated with the vapor pressure of the pure component (P_k^0), considering a diluted solution in the DV [12, 90]. Then, the following expression is derived:

$$\omega_{in,k} = \frac{y_k P_g \rho_k}{P_k^0 \rho_p e^{1+\chi}} \tag{4.5}$$

Where,
$\omega_{in,k}$ is the weight fraction of the volatile species,
y_k is the mole fraction of the volatile species in the vapor phase,
ρ_p is the polymer density (g/l).
P_g is the pressure inside the bubble, in equilibrium with the melt at the interphase (Pa)

Mass balance in the melt phase

A mass balance in a PFR for the volatile species in the melt phase gives,

$$\frac{dq}{dz} = -\sum_{k=1}^{3} N_k A_{in} \frac{N_r MR_k}{L \rho_k} \tag{4.6}$$

$$q\frac{d[C_k]}{dz} + C_k \frac{dq}{dz} = -N_k A_{in} \frac{N_r}{L} + r_k A_T \tag{4.7}$$

$$r_{St} = -k_p[St][R\cdot] - 2k_{io}[St]^3 - 2k_D[St]^2 - 2k_T[St]^3 \tag{4.8}$$

$$r_{Dm} = 2k_D[St]^2 \tag{4.9}$$

$$r_{Tm} = 2k_T[St]^3 \tag{4.10}$$

Where,

A_{in} is the interfacial area of one bubble (dm^2),

L is the length of the equipment for this stage (m),

N_r is the total number of bubbles in the melt.

For the nonvolatile species and crosslinking points,

$$\frac{d[R\cdot]}{dz} = \frac{A_T}{q}(2k_{i0}[St]^3 + 2f_{i2}k_{dp}[PeP] - k_{tc}[R\cdot][P_0\cdot] - k_{tc}[R\cdot]^2) - [R\cdot]\frac{1}{q}\frac{dq}{dz} \tag{4.11}$$

$$\frac{d[P_0\cdot]}{dz} = \frac{A_T}{q}\left[k_{fG}[R\cdot][B*]\left(k_{i1}[St] + k_{fM}[St] + k_{tc}[P_0\cdot] + k_{tc}[R\cdot]\right)[P_0\cdot]\right] - [P_0\cdot]\frac{1}{q}\frac{dq}{dz} \tag{4.12}$$

$$\frac{d[B*]}{dz} = \frac{A_T}{q}(k_{fM}[St][P_0\cdot] - k_{fG}[R\cdot][B*]) - [B*]\frac{1}{q}\frac{dq}{dz} \tag{4.13}$$

$$\frac{d[PeP]}{dz} = \frac{A_T}{q} - f_{i2}k_{dp}[PeP] - [PeP]\frac{1}{q}\frac{dq}{dz} \tag{4.14}$$

The total number of crosslinking points are estimated as is described in Peng et. al. [94]: and the average molecular weight between crosslinks (Mc) :

$$\frac{d[N_x]}{dz} = k_x[P_0\cdot]^2 A_T \tag{4.15}$$

$$M_C = \frac{M_{n,PB}N_{PB,in}}{N_x} \tag{4.16}$$

Where

A_T is the equipment cross-sectional area (dm^2),

N_x is the number of crosslinks and

M_C is the average molecular weight between crosslinks.

Bubble growth mechanism

Considering the Rayleigh–Plesset Equation for a bubble immersed in an infinite liquid and neglecting inertial and accelerations terms leads to [88]:

$$P_g - P = \frac{2\sigma}{R} + \frac{4\mu}{R}\frac{dR}{dt} \tag{4.17}$$

where

σ is the interfacial tension (N/m),

μ is the viscosity (Pa.s),

P is the equipment operation pressure (Pa) and

P_g is the pressure inside the bubble, in equilibrium with the melt in the interface.

For this derivative to be positive, the following condition for bubble growth shall be considered:

$$P_g - P \geq \frac{2\sigma}{R} \tag{4.18}$$

Mass balance in the gas phase

Assuming that vapor in bubble behaves as an ideal gas and considering spherical bubbles,

$$\frac{P_g^4}{3\pi R^3 N_r} = \dot{n_g} R_g T \tag{4.19}$$

where,

$\dot{n_g}$ is molar gas flow (mol/s) and

R_g is the gas constant (8.314 J/mol K)

A total mass balance in the gas phase is attained, assuming that no chemical reactions occur,

$$\frac{d\dot{n_g}}{dz} = \sum_{k=1}^{3} N_k A_{in} \frac{N_r}{L} \tag{4.20}$$

Now, deriving Eq. 4.19 and combining with Eq. 4.20,

$$\frac{dP_g}{dz} = \sum_{k=1}^{3} N_k 3 \frac{R_g T}{RL} - \frac{3}{R} P_g \frac{dR}{dz} \tag{4.21}$$

$$P_{g,k} = P_g \frac{\dot{n_{g,k}}}{\dot{n_g}} \tag{4.22}$$

$$\frac{dn_{g,k}}{dz} = N_k A_{in} \frac{N_r}{L} \tag{4.23}$$

Where k denotes any of the volatile chemical species (i.e St, Dm and Tm).

Then, Eqs. 4.6 to 4.14, 4.17, 4.21 and 4.23 are simultaneously solved to find the composition at the reactor outlet.

Free PS MWD

$$\frac{d\left([S_n{\cdot}^{(i)}]q\right)}{dz} = (k_p([S_{n-1}{\cdot}^{(i)}] - [S_n{\cdot}^{(i)}]) + 2k_{fM}[{\cdot}S_n{\cdot}^{(i)}])[St]A_T$$
$$-\left(k_{fM}[St] + k_{tc}([R{\cdot}] + 2[{\cdot}R{\cdot}])\right)[S_n{\cdot}^{(i)}]A_T + 2k_{tc}\sum_{j=0}^{i}\sum_{m=1}^{n-1}[{\cdot}S_{n-m}{\cdot}^{(i-j)}][S_m{\cdot}^{(j)}]A_T \quad (4.24)$$

$$\frac{d\left([{\cdot}S_n{\cdot}^{(i)}]q\right)}{dz} = (2k_p[St]([{\cdot}S_{n-1}{\cdot}^{(i)}] - [{\cdot}S_n{\cdot}^{(i)}])A_T$$
$$-\left(2k_{fM}[St] + k_{tc}([R{\cdot}]2[{\cdot}R{\cdot}])\right)[{\cdot}S_n{\cdot}^{(i)}]A_T + 2k_{tc}\sum_{j=0}^{i}\sum_{m=1}^{n-1}[{\cdot}S_{n-m}{\cdot}^{(i-j)}][{\cdot}S_m{\cdot}^{(j)}]A_T \quad (4.25)$$

$$\frac{d\left([S_n^{(i)}]q\right)}{dz} = k_{fM}[St][S_n{\cdot}^{(i)}]A_T + \frac{k_{tc}}{2}\sum_{j=0}^{i}\sum_{m=1}^{n-1}[S_{n-m}{\cdot}^{(i-j)}][S_m{\cdot}^{(j)}]A_T - ik_{d2}[S_n^{(i)}]A_T \quad (4.26)$$

$$\frac{d\left([S_n{\cdot}^{(i)}]q\right)}{dz} = (k_p([S_{n-1}{\cdot}^{(i)}] - [S_n{\cdot}^{(i)}]) + 2k_{fM}[{\cdot}S_n{\cdot}^{(i)}])[St]A_T$$
$$+2k_fG[{\cdot}S_n{\cdot}^{(i)}][B^*]A_T$$
$$-\left(k_{fM}[St] + k_{fG}[B^*] + k_{tc}([R{\cdot}] + 2[{\cdot}R{\cdot}]) + k_{tc}[P_0{\cdot}]\right)[S_n{\cdot}^{(i)}]A_T$$
$$+2k_{tc}\sum_{j=0}^{i}\sum_{m=1}^{n-1}[{\cdot}S_{n-m}{\cdot}^{(i-j)}][S_m{\cdot}^{(j)}]A_T \quad (4.27)$$

$$\frac{d\left([{\cdot}S_n{\cdot}^{(i)}]q\right)}{dz} = (2k_p[St]([{\cdot}S_{n-1}{\cdot}^{(i)}] - [{\cdot}S_n{\cdot}^{(i)}])A_T$$
$$-\left(2k_{fM}[St] + k_{fG}[B^*] + k_{tc}([R{\cdot}]2[{\cdot}R{\cdot}]) + k_{tc}[P_0{\cdot}]\right)[{\cdot}S_n{\cdot}^{(i)}]A_T$$
$$+2k_{tc}\sum_{j=0}^{i}\sum_{m=1}^{n-1}[{\cdot}S_{n-m}{\cdot}^{(i-j)}][{\cdot}S_m{\cdot}^{(j)}]A_T \quad (4.28)$$

$$\frac{d\left([S_n^{(i)}]q\right)}{dz} = k_{fM}[St][S_n{}^{\cdot(i)}]A_T + k_fG[S_n{}^{\cdot(i)}][B^*]A_T + \frac{k_{tc}}{2}\sum_{j=0}^{i}\sum_{m=1}^{n-1}[S_{n-m}{}^{\cdot(i-j)}][S_m{}^{\cdot(j)}]A_T - ik_{d2}[S_n^{(i)}]A_T \tag{4.29}$$

The NCLD for the free PS species is obtained as it is described in Chapter 2.

CSTR Stage

In the pool stage, the mass balances performed for the PFR are reformulated for a CSTR and mass transfer equations are solved considering only shallow diffusion in the polymer melt [88, 156, 163]. Thus, it should be noticed that the interface area (A_{in})in this stage is calculated considering the pool surface, not the number of bubbles nor their radius. The molar flux N_{bk} in this case, was assumed equal to the one calculated at the PFR stage outlet.

Mass balance in polymer melt

$$[St] = \frac{[St]_{in}q_{in} - N_{b1}A_{in} + V(-2k_p[St][R\cdot] - 2k_{i0}[St]^3 - 2k_D[St]^2 - 3k_T[St]^2)}{q} \tag{4.30}$$

$$[Dm] = \frac{[Dm]_{in}q_{in} - N_{b2}A_{in} + Vk_D[St]^2}{q} \tag{4.31}$$

$$[Tm] = \frac{[Tm]_{in}q_{in} - N_{b2}A_{in} + Vk_T[St]^3}{q} \tag{4.32}$$

$$[R\cdot] = \frac{[R\cdot]_{in}q_{in} + V(2k_{i0}[St]^3 - k_{tc}[R]^2 - k_{tc}^{''}[R\cdot][P_0\cdot])}{q} \tag{4.33}$$

$$[P_0\cdot] = \frac{[P_0\cdot]_{in}q_{in} + V\left(k_{fG}[R\cdot][B*] - \left(k_{i1}[St] + k_{fM}^{'}[St] + k_{tc}^{'}[P_0\cdot] + k_{tc}[R\cdot]\right)\right)}{q} \tag{4.34}$$

$$[B*] = \frac{[B*]_{in}q_{in} + V(k_{fM}[St][P_0\cdot] - k_{fG}[R\cdot][B*)}{q} \tag{4.35}$$

$$[PeP] = \frac{[PeP]_{in}q_{in} + V(-f_{i2}k_{dp}[PeP])}{q} \tag{4.36}$$

Then the total number of crosslinking points and Mc are estimated,

$$N_x = N_{x,in} + k_x[P_0\cdot]^2 V \tag{4.37}$$

$$M_C = \frac{M_{n,PB} N_{PB,in}}{N_x} \tag{4.38}$$

Mass balance in the gas phase

$$[St] = N_{b1} A_{in} + [St]_{in} \tag{4.39}$$

$$[Dm] = N_{b2} A_{in} + [Dm]_{in} \tag{4.40}$$

$$[Tm] = N_{b3} A_{in} + [Tm]_{in} \tag{4.41}$$

Free PS MWD

For the MWDs, the same equations as in Chapter 2 are used.

4.3.2 Swelling Index Model

The rubber gel in rubber modified styrenic polymers is characterized by the SI. A mathematical model for prediction of the SI is presented, where the equations are developed for an equivalent gel, that is considered as a spherical occlusion of PS [150].

The model considers:

(i) Equivalent spherical gel,

(ii) Flory- Huggins theory for estimation of activity coefficients,

(iii) No external osmotic pressure from diluted PS,

(iv) No contribution from interfacial tension, and

(v) Simple strain energy function for a crosslinked network.

The SI is calculated by:

$$SI = 1 + \frac{\rho_S}{\omega_{gel}} \left[\frac{\omega_R}{\rho_R} \left(\frac{1}{\phi_R} - 1 \right) + \frac{\omega_{gel} + \omega_R}{\rho_P} \left(\frac{1}{\phi_P} - 1 \right) \right] \tag{4.42}$$

With $\omega_{gel} = \omega_R + \omega_P$

Where,

ω_R is the rubber mass fraction (calculated in the DV model),
ω_P is the PS mass fraction occluded in gel (experimental parameter),
ω_{gel} is the gel mass fraction,
ϕ_R is the rubber volume fraction in the swelled membrane,
ϕ_P is the PS volume fraction in the swelled occlusion,
ρ_R is the rubber density,
ρ_P is the PS density and
ρ_S is the solvent density.

ϕ_R and ϕ_P can be calculated considering phase equilibrium conditions written as radial and circumferential tensions balances (Eqs. 4.43 and 4.44) [150]. A spherical equivalent gel is proposed as shown in Fig 4.4.The activity coefficients are estimated by the Flory-Huggins theory (Eqs. 4.45 and 4.46) and molecular weight between crosslinks (M_C) was calculated in the previous section.

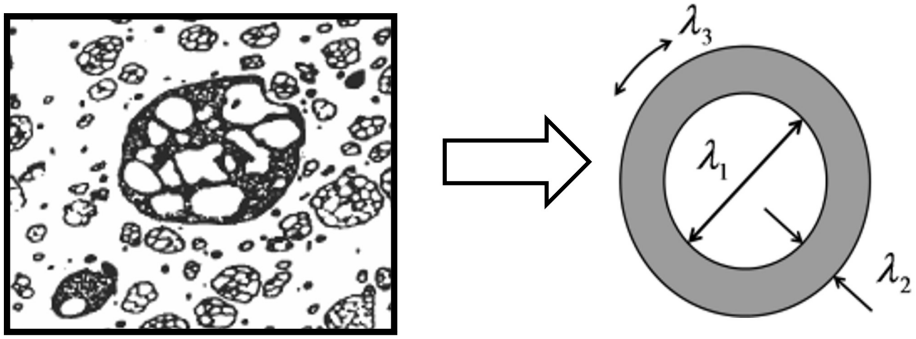

FIGURE 4.4: Equivalent gel model.

$$\ln(1-\phi_R) + \phi_R + \chi_R \phi_R^2 + \frac{\rho_R V_1 \phi_R^{1/3}}{M_C K^{4/3}} = 0 \tag{4.43}$$

With $K = \phi_R/\phi_P$

$$\ln(1-\phi_R)+\phi_R+\chi_R\phi_R^2+\frac{\rho_R V_1 \phi_R^{1/3}(1+2K^2)}{3M_C K^{4/3}}+\frac{(1+K)^2+2K^3}{2[(1+K)^3-K^3]}[ln(1-\phi_P)+\phi_P+\chi_P\phi_P^2]=0 \tag{4.44}$$

Where,
χ_R is the rubber/solvent Flory interaction parameter,
χ_P is the PS/solvent Flory interaction parameter,
V_1 is de solvent molar volume and
M_C is the average molecular weight between crosslinks (calculated in the DV model).

The Flory interaction parameters are calculated as:

$$\chi_R = 0.34 + \frac{\hat{V}_1(\delta_R-\delta_S)^2}{RT} \tag{4.45}$$

$$\chi_R = 0.34 + \frac{\hat{V}_1(\delta_P-\delta_S)^2}{RT} \tag{4.46}$$

Then, solving Eqs. 4.43 and 4.44, ϕ_R and ϕ_P can be calculated, and the SI is estimated with Eq. 4.42.

4.3.3 Melt Flow Index Model

MFI is a measure of the mass flow (in g/10 min) of melted HIPS that passes through the capillary of an extrusion plastometer, while it is forced by a piston loaded with a constant weight. The polymer builds up in the inside of a heated cylindrical ring (barrel or reservoir) before passing through the capillary. Between the reservoir and the capillary there is an abrupt contraction or zone input. The test is carried out between 160-200 °C, similar conditions to those of extrusion of the material. The more viscous the material, the slower it flows. In this way, a lower MFI will result in greater processing difficulty.

For the MFI estimation a model based on mass and momentum balances in a plastomer (Fig. 4.5) was employed [118].

The following is assumed:

(i) steady-state flow,

(ii) zero velocity at the capillary wall, and

(iii) the elongational viscosity can be estimated using Trouton's ratio.

Although assumption (ii) is valid for homogeneous systems, here it is extended to a heterogeneous one. In this model, the Weight Average Molecular Weight for free PS ($M_{w,PS}$) calculated in the Polymerization Module is used for the estimation of Polymer Melt and free PS viscosities.

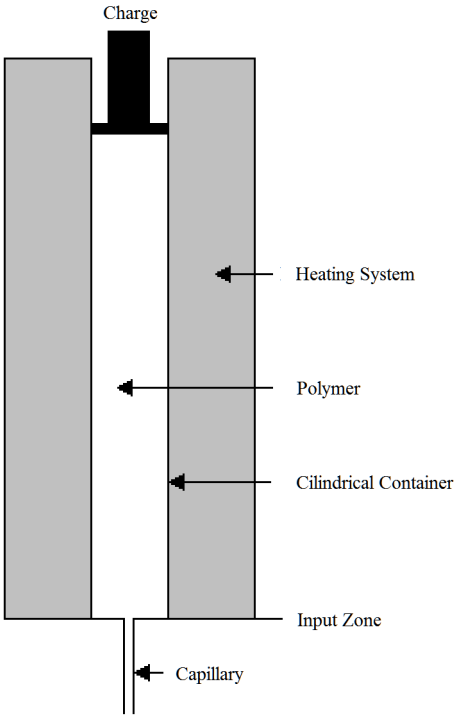

FIGURE 4.5: Extrusion plastometer (ASTM D1238).

First, the estimate of the apparent shear viscosity is considered ($\eta(\dot{\gamma})$) as a function of the strain rate ($\dot{\gamma}$). For this purpose, it is proposed applying the following three-parameter model [176, 177]:

$$\eta(\dot{\gamma}) = \frac{\eta_0}{[1 + (\tau_r \dot{\gamma})^2]^{\frac{n'}{2}}} \tag{4.47}$$

where η_0 is the shear viscosity at low strain rates; τ_r is the relaxation time; and n' the slope of the final asymptote of the curve $\ln \eta$ as a function of $\ln \dot{\gamma}$ (in absolute value). The value of n' is taken directly from the literature [178].

To estimate τ_r, the following equation was used [176, 177].

$$\tau_r = \frac{6\eta_0 M_{w,PS}}{\pi^2 \rho R T} \tag{4.48}$$

To calculate η_0, a logarithmic mixing rule was adopted that allows considering the influence of the mineral oil [179, 180]:

$$\ln \eta_0 = (1 - \phi_{oil}) \ln \eta_{0,P} + \phi_{oil} \ln \eta_{0,oil} \tag{4.49}$$

where $\eta_{0,P}$ is the viscosity at low strain rates of the polymer free of mineral oil, $\eta_{0,oil}$ is the viscosity at low rates of deformation of the mineral oil; and ϕ_{oil} is the volume fraction of mineral oil. The viscosity at low strain rates of the oil-free polymer is estimated through Money's expression [181]:

$$\eta_{0,P} = \eta_{0,PS} e^{\frac{A\phi_D}{1-B\phi_D}} \tag{4.50}$$

where $\eta_{0,PS}$ is the viscosity at low strain rates of free PS; A and B are constant; and ϕ_D is the volume fraction of the dispersed phase in the polymer (free of mineral oil). The constant B was adopted from literature [181], while A is an adjustment parameter. To estimate ϕ_D, it was assumed $\phi_D = \phi_{Rubb}$. This procedure provides ϕ_D values for by default, because ϕ_{Rubb} does not include the free PS occluded in the rubber particles.

Finally, $\eta_{0,PS}$ is estimated as [181]:

$$\eta_{0,PS} = -20.95 + 3.4 \ln(M_{w,PS}/33000) + 11000/T \tag{4.51}$$

Where $M_{w,PS}$ was calculated in the DV model.

With the knowledge of $\eta(\dot{\gamma})$, the model of Seavey et al. (2003) [121] was employed.

To describe the plastometer, the following nomenclature is used: R_b and L_b are the radius and the length of the reservoir; R_c and L_c are the radius and length of the capillary; R_p is the radius of the piston; ΔP_b , ΔP_e, and ΔP_c are the pressure drops in the reservoir, the inlet zone, and the capillary, respectively; m is the weight on the piston; g is the acceleration of gravity; $(\eta_{R_b}, \dot{\gamma_{R_b}})$ is the shear viscosity-strain rate couple evaluated on the wall of the reservoir; $(\eta_{R_c}, \dot{\gamma_{R_c}})$ is the shear viscosity-strain rate couple evaluated in the capillary wall; $(\eta_{a,c}, \dot{\gamma}_a)$ is the apparent shear viscosity -apparent strain rate couple evaluated in the capillary; and $(\eta_{e,c}, \epsilon_a)$ is the apparent elongational viscosity-apparent elongational strain rate couple evaluated in the capillary.

The MFI is given by the following relationship:

$$MFI = \rho Q \tag{4.52}$$

where Q is the volumetric flow rate; and ρ is the density of molten HIPS. Q is related to the viscosity function in the reservoir and capillary through the following balances [121, 182].

$$Q = \frac{\pi R_c^3 \dot{\gamma}_{R_c}}{3} - \frac{\pi}{3}\left(\frac{2L_c}{\Delta P_b}\right)^3 \int_0^{\gamma_{\dot{R}_c}} [\eta(\dot{\gamma})\dot{\gamma}]^3 d\dot{\gamma} \tag{4.53}$$

$$Q = \frac{\pi R_b^3 \dot{\gamma}_{R_b}}{3} - \frac{\pi}{3}\left(\frac{2L_b}{\Delta P_b}\right)^3 \int_0^{\gamma_{\dot{R}_b}} [\eta(\dot{\gamma})\dot{\gamma}]^3 d\dot{\gamma} \tag{4.54}$$

$$\gamma_{\dot{R}_c}\eta_{R_c} = \frac{\Delta P_c R_c}{2L_c} \tag{4.55}$$

$$\gamma_{\dot{R}_b}\eta_{R_b} = \frac{\Delta P_b R_b}{2L_b} \tag{4.56}$$

where η_{R_c} and η_{R_b} are calculated throwgh $\eta(\dot{\gamma})$ with the values of $\gamma_{\dot{R}_c}$ and $\gamma_{\dot{R}_b}$, respectively.

The total pressure drop is:

$$\Delta P_b + \Delta P_e + \Delta P_c = \frac{mg}{\pi R_p^2} \tag{4.57}$$

To estimate ΔP_e, Rohlfing y Janzen (1997) proposed the following expresion [182]:

$$\Delta P_e = \frac{4\sqrt{2}\dot{\gamma}}{3(2-n')}\frac{4-4n'}{4-3n'}^{(1-n'/2)}\sqrt{\eta_{a,c}\eta_{e,c}} \tag{4.58}$$

The same authors also proposed the following expressions for $\dot{\gamma}_a$ and $\dot{\epsilon}_a$.

$$\dot{\gamma}_a = \frac{4}{3+1/(1-n')}\gamma_{\dot{R}_c} \tag{4.59}$$

$$\dot{\epsilon}_a = \frac{4\eta_{a,c}\dot{\gamma}}{3(2-n')\Delta P_e}\left(\frac{4-4n'}{4-3n'}\right)^{(2-n')} \tag{4.60}$$

Finally, Seavey et al. (2003) [121] employed the following relationship between elongational viscosity and share viscosity (Trouton):

$$\eta_e(\dot{\epsilon}) = 3\eta(\dot{\gamma}) \tag{4.61}$$

where $\dot{\epsilon}$ represents the elongational strain rate.

The pair $(\eta_{a,c}, \dot{\gamma}_a)$ is related with Eq. 4.47. In a similar way, the pair $(\eta_{e,c}, \dot{\epsilon}_a)$ is related through Eqs. 4.47 and 4.61 with $\dot{\gamma} = \dot{\epsilon}_a$ [121].

The unknowns of the presented equations are: MFI, Q, ΔP_b, ΔP_e, ΔP_c, $\gamma\dot{}_{R_b}$, $\gamma\dot{}_{R_c}$, $\dot{\gamma}_a$, ϵ_a, η_{R_b}, η_{R_c}, $\eta_{a,c}$, and $\eta_{e,c}$.

The values for the numerical parameters related to plastometer geometry are: $R_b = 4.78$ mm, $R_c = 1.05$ mm, $R_p = 4.74$ mm, $L_b = 46$ mm, $L_c = 8$ mm, $m = 5$ kg and $g = 9,81$ m/s^2 with an essay temperature of $T = 200$ °C. Equations 4.53 to 4.60 are simultaneously solved in order to evaluate the MFI with Equation 4.52.

4.4 Experimental Work

The experimental work consisted of a series of continuous bulk St polymerizations in the presence of dissolved PB, using the multifunctional initiators DEKTP, PDP and L331 (Fig. 2.4) at 0.016% in weight. A 6% in weight of an alkyl lithium polymerized polybutadiene of medium cis –Diene 40AC10- was dissolved into the monomer. The rubber was analyzed by size exclusion chromatography (SEC), and the average molecular weights resulted in $M_{n,PB} = 208,600$ g/mol and $M_{w,PB} = 464,238$ g/mol. The polymerization recipe also included mineral oil to lower the viscosity of the solution and antioxidant to prevent rubber degradation. In addition to the experiments carried out in Chapter 2, some other variations in the operating conditions were considered. In order to obtain different average molecular weights at the DV inlet, different temperatures in the Finishing Reactor were studied and in the FSD, both temperature and vacuum degree were varied. Conditions in the Prepolymerization Reactor were not altered and selected to achieve a proper steadying of the system and to ensure that phase inversion is achieved at this stage. Same reagents, equipment and characterization methods as those described in Chapter 2 were used in these experiments.

4.4.1 Polymerization Process Conditions

The operating conditions selected for each experiment are presented in Table 4.1. In experiments 1-a and 2-a, two different temperatures were considered for R2 to study the DV stage with two different average molecular weights inputs. In the FSD, both different temperatures and vacuum degrees were analyzed for reactions with L331 (i.e. experiments 2-a/b/c/d). Additionally, a further experiment was carried out under the same reaction conditions as in experiment 2-a, but varying the melt pool level in the Devolatilizer (i.e. experiment 2-e). Samples were taken at points S1-S4 as is shown in Fig. 2.7.

TABLE 4.1: Equipment operating conditions adopted in the experiments for the study of HIPS production with three different multifunctional initiators

Experiment	Initiator	TR1 (°C)	TR2 (°C)	TDV (°C)	PDV(mmHg) [1]	Pool Level in DV (mm)
1-a	L-331	115	125	220	14-18	90
2-a	L-331	115	135	220	14-18	90
2-b	L-331	115	135	220	10-12	90
2-c	L-331	115	135	200	14-18	90
2-d	L-331	115	135	200	10-12	90
2-e	L-331	115	135	220	14-18	141
3	PDP	115	135	220	14-18	90
4	DEKTP	115	120/130	220	14-18	90

4.4.2 Experimental Results

Fig. 4.6 shows the evolution of X, $M_{n,PS}$, $M_{w,PS}$ and GE along the pilot plant for experiments 1-a and 2-a and 3, and the main characteristics for experiments carried out at the same DV conditions are presented in Table 4.2. The analysis of these experimental results has been presented in Section 2.3.2.

The characterizations of final products obtained using L331 as the initiator for the five different DV conditions studied are presented in Table 4.3. As expected, an increase in DV temperature reduces the residual monomer content of HIPS, which also results in a decreased IR, because of the monomer plasticizing function. As it can be observed in Experiments 2-c and 2-d, an increase in the vacuum degree enables reducing the residual monomer content, which also results in a decreased IR. The expected behavior with an increased vacuum degree was not obtained in Experiment 2-b, which suggests experimental errors associated to the poor stabilization of the applied vacuum, as was previously noted. Changes in DV temperature did not evidence a significant effect on the $M_{n,PS}$ and $M_{w,PS}$, while the SI was lower at higher DV temperatures, indicating that crosslinking reactions are more important at this stage. Comparing Experiments 2-a and 2-e, the difference in the pool level does not result in significant changes in monomer content, indicating that all DV occurs in the very first portion of the "falling strand" stage, as it has been reported in several works [88, 156, 163]. All the important changes observed in the materials final properties for different conditions at the DV stage suggest that a strict control of this stage is essential to achieve the required product specifications.

[1] A pressure range is reported since vacumm in Devolatilizer resulted difficult to maintain stable.

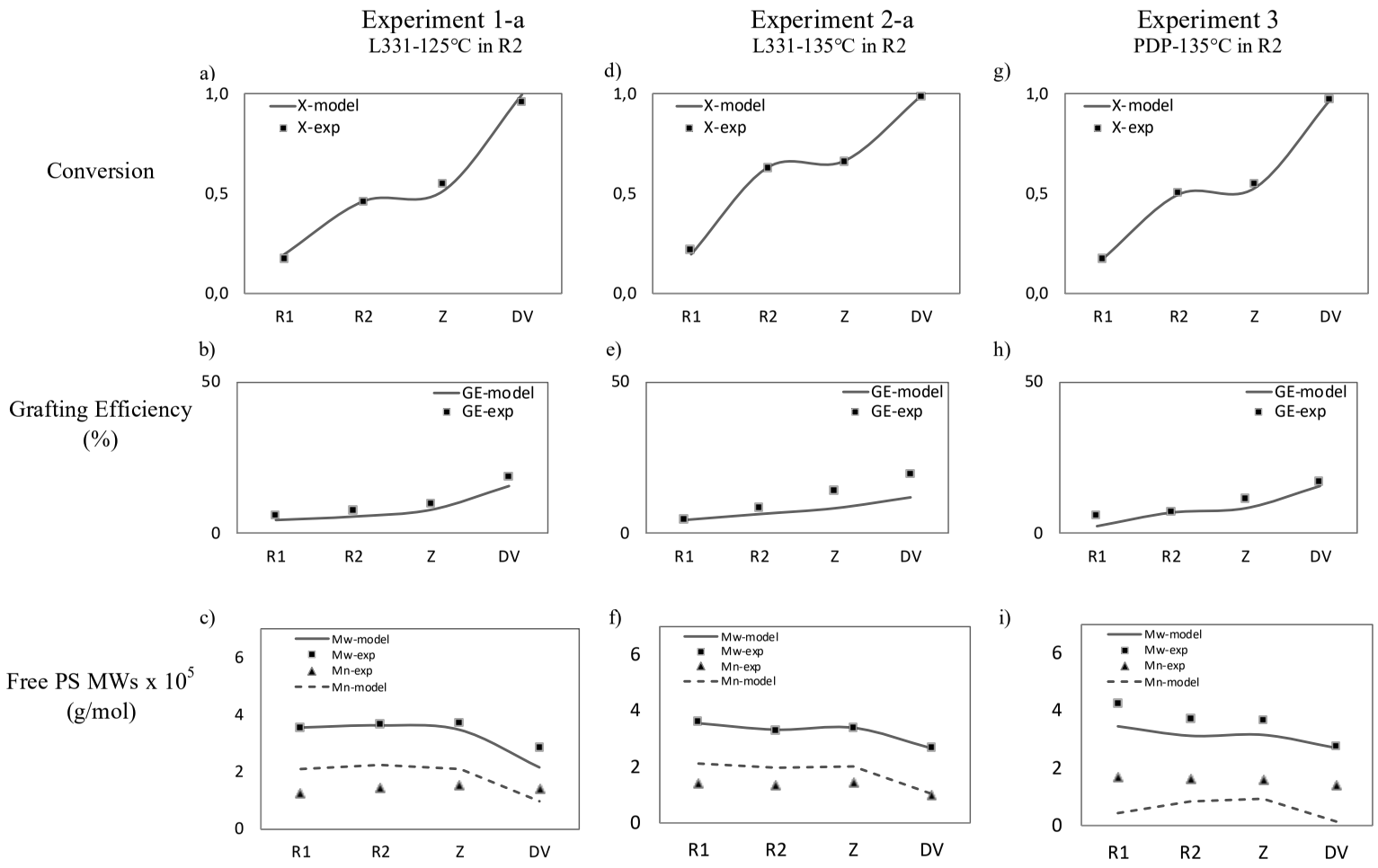

FIGURE 4.6: Experimental results for polymerizations with PDP and L331 at different temperatures in R2.

TABLE 4.2: Final product quality variables for experiments with constant DV conditions (T=220 °C and P=16 mmHg).

Exp.	$M_{w,PS}$ (g/mol)	GE (%)	Residual St (%)	Oligomer content (%)	SI	MFI (g/10min)	IR (J/m)	E (%)	PD (mm)
1-a	288358 (213060)	19.71 (14.74)	3.97 (1.29)	1.38 (0.64)	15.85 (12.32)	6.5 (6.75)	264	13.7	1056
2-a	268338 (264420)	19.47 (13.00)	2.04 (1.97)	1.43 (1.02)	10.53 (12.36)	4.1 (4.32)	191	32.0	955
3	274163 (269880)	17.15 (8.25)	2.95 (2.97)	1.70 (2.71)	12.42 (12.36)	5.5 (4.16)	196	33.2	1123
4	263464 (240590)	16.35 (9.05)	1.10 (3.42)	1.44 (3.47)	9.21 (12.31)	5.5 (5.22)	149	26.9	1196

TABLE 4.3: Final product properties at different DV conditions using L331 as initiator.

Exp.	$M_{n,PS}$ (g/mol)	$M_{w,PS}$ (g/mol)	GE (%)	SI	MFI (g/10min)	IR (J/m)	E (%)	Residual St (%)	Oligomer content (%)
2-a	98617 (103640)	268338 (264420)	19.5 (13.00)	10.5 (12.36)	4.1 (4.32)	191 (202)	32.0 (44.2)	2.04 (1.97)	1.43 (1.02)
2-b	96824 (104620)	265350 (264380)	18.0 (13.10)	9.3 (12.36)	5.6 (4.32)	156 (202)	27.1 (43.13)	2.11 (1.94)	1.65 (0.98)
2-c	107493 (98980)	265825 (264970)	18.8 (9.30)	12.5 (12.36)	7.9 (4.31)	250 (203)	25.5 (49.7)	2.76 (3.47)	1.02 (1.13)
2-d	112754 (100190)	268055 (264930)	17.6 (9.41)	10.1 (12.36)	5.4 (4.31)	157 (203)	32.8 (48.3)	2.26 (3.40)	1.41 (1.08)
2-e	112409 (103650)	280697 (265950)	18.7 (11.85)	10.6 (12.31)	4.4 (4.27)	177 (202)	39.0 (44.8)	2.02 (1.33)	1.67 (0.82)

4.5 Model Adjustment and Validation - Simulation Results

Parameters for the DV Model are presented in Table 4.4. Model parameters for the polymerization reactions were presented in Table 2.5. All other parameters for the DV model were taken from the literature. As regards the diffusion coefficients for volatile species, the obtained values after adjustment are in accordance with those reported [156, 163]. Simulation results are compared to experimental ones in Fig. 4.6, Table 4.5 and Table 4.3 and a very good agreement between experimental and predicted values is observed. Comparing Fig. 2.8 and Fig. 4.6, it can be noticed how the incorporation of FSD model represents a sight better adjustment at this stage of the process.

Other simulation results using the model are presented in Fig. 4.7. The model can be used to obtain smooth surfaces with predicted values of the final properties as function of any selected conditions at any stage of the process (Figures 4.7.a)-c)). In addition, variations in the molecular structure after the DV stage can be observed because of the generation of low molecular weight polymer, due to the high temperature, which promotes thermal initiation of the residual monomer (Figure 4.7.d)). Moreover, Figure 4.7.e) shows that, under these temperature and pressure conditions, when the length of the falling strand stage is increased by reducing the melt volume, opposing effects of mass transfer to the vapor phase and generation by chemical reaction related to the oligomer content in the final product are evidenced. These opposing effects are revealed by observing a minimum concentration in the curve.

TABLE 4.4: DV model parameters.

Parameter	Units	Expression or value	Reference
$D_{0,1}$	cm^2/s	$5.0x10^{-3}$	Adjusted in this work
$D_{0,2}$	cm^2/s	$2.5x10^{-3}$	Adjusted in this work
$D_{0,3}$	cm^2/s	$1.7x10^{-3}$	Adjusted in this work
N_r	$1/cm^3$	600	[163]
χ	-	$0.28 - 0.33$	[24, 151]
k_D	L/mol s	$3.12x10^7 e^{-25097.1/RT}$	Adjusted in this work
k_T	L/mol s	$1.35x10^6 e^{-21907.6/RT}$	Adjusted in this work

TABLE 4.5: Final product quality variables for experiments with constant DV conditions (T=220 °C and P=16 mmHg). Simulation results are presented between parentheses.

Exp.	$M_{w,PS}$ (g/mol)	GE (%)	Residual St (%)	Oligomer content (%)	SI	MFI (g/10min)	IR (J/m)	E (%)	Dp (nm)
1-a	288358 (213060)	19.71 (14.74)	3.97 (1.29)	1.38 (0.64)	15.85 (12.32)	6.5 (6.75)	264	13.7	1056
2-a	268338 (264420)	19.47 (13.00)	2.04 (1.97)	1.43 (1.02)	10.53 (12.36)	4.1 (4.32)	191	32.0	955
3	274163 (269880)	17.15 (8.25)	2.95 (2.97)	1.70 (2.71)	12.42 (12.36)	5.5 (4.16)	196	33.2	1123
4	263464 (240590)	16.35 (9.05)	1.10 (3.42)	1.44 (3.47)	9.21 (12.31)	5.5 (5.22)	149	26.9	1196

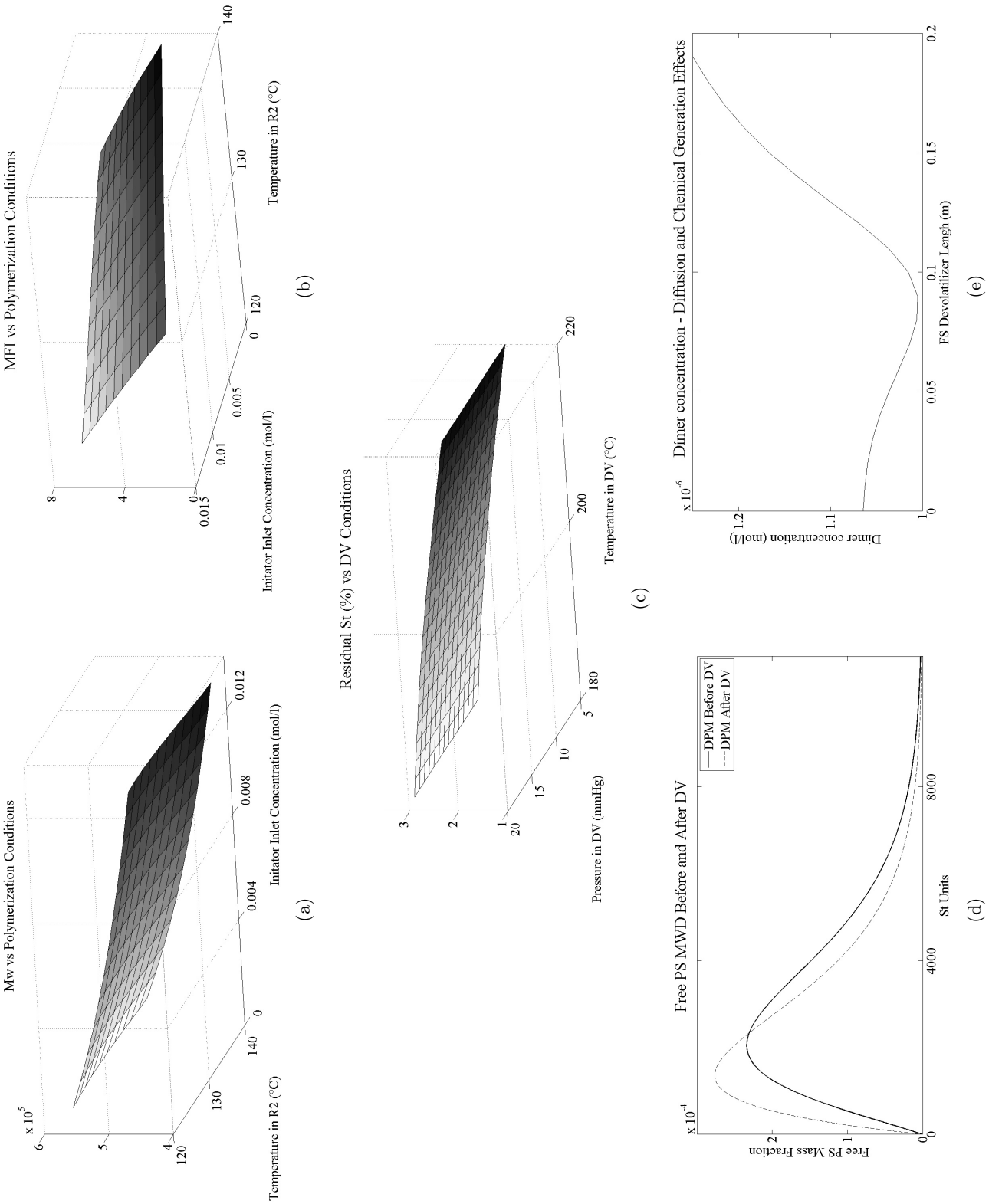

FIGURE 4.7: Theoretical simulations for HIPS polymerization using multifunctional initiators in a continuous plant.

4.6 Conclusions

An integrated mathematical model for the complete HIPS continuous polymerization process using multifunctional initiators was developed. A experimental work was carried out in a continuous pilot plant to study the effects of operating conditions on final properties and structure-properties relationships. Each module of the model was adjusted and validated using these new experimental data. The integrated model can be used to simulate all stages of the continuous HIPS process including the DV stage. Furthermore, it is a comprehensive model, which it can be used with any mono- or multifunctional initiator, either linear or cyclic. The model provides a full insight into the molecular structure of the different polymer species (free PS, residual PB and graft copolymer) and selected main quality variables, such as SI, MFI, oligomer content and residual monomer. The model was then used to theoretically study the effect of the recipe and operating conditions on the molecular structure and final properties of the obtained product. The outcome of this work is a complete mathematical model structured by integrated modules that were developed from a deep understanding of the physical and chemical phenomena in each of the process stages. This model allows systematizing the interrelationships between operating conditions and final product quality for control and optimization of the overall production process. The main long-term objective of this research line is to “invert" the model in order to predict the optimum recipe and operating conditions to obtain tailor made products in an industrial continuous process. The presented models could also be extended to other St polymers, such as SAN and ABS, or polymers from other monomers such as PMMA.

Chapter 5
Mathematical Modeling of the Continuous Bulk Process for the Production of ABS Using Multifunctional Initiators

5.1 Introduction

The bulk process for the production of ABS has been extensively investigated [17, 56, 64, 65, 183–187]. Nevertheless, there are still aspects not elucidated related to interrelationships between process variables, molecular characteristics and/or morphology, and final properties.

In several articles, Locatelli and Riess [56, 183–186] studied different moderately-concentrated solution copolymerizations of St and AN in the presence of PB. They also investigated the equilibrium distributions of co-monomers and benzoyl peroxide (BPO) initiator from blends that emulate the polymerization. Measurements indicated that SAN chains grafted onto PB exhibited a relatively lower AN content than the non-grafted chains [183]. The authors suggested that this was a consequence of a slightly preferential accumulation of St in the PB-rich phase [183]. The molecular weights of the grafted SAN were noticeable higher than those of the non-grafted SAN [56]. This was explained in terms of the different compositions and nature of the phases where grafted and non-grafted SAN are generated. Measurements from blends containing benzene/SAN/PB/BPO and benzene/AN/SAN/PB/BPO showed that initiator concentration was about three times higher in the PB-rich phase than the corresponding concentration of the SAN-rich phase [184]. Locatelli and Riess [185, 186] modeled the copolymerization of St and AN in the presence of PB. To this purpose, a simple kinetic mechanism involving initiation, propagation, and termination was proposed, and rather empirical correlations were employed for estimating initiator efficiencies, initiator concentrations, and termination rate constants in each phase [186].

Hayes et al [64, 65] carried out kinetic studies at low conversions in dilute solution copolymerizations of S and AN in the presence of PB. When a poor promoter of grafting such as 2,20-azoisobutyronitrile (AIBN) was used as initiator, the kinetics could be described as a copolymerization between an average (St+AN) monomer and butadiene repeating units. However, the model was not useful for describing reactions with other initiators that promote

the rubber grafting.

Bouquet et al [187] measured the mass of non-grafted rubber as a function of the reaction time along several bulk copolymerizations of St and AN in the presence of PB and AIBN, bis(2-methylbenzoyl) peroxide, dibenzoyl peroxide, and 1,1-bis(tert-butyl peroxide) cyclohexane. They found that the mass of non-grafted SAN was related with the decomposition rate of the initiator.

There have been relatively few studies of ABS polymerization and most have focused on research of batch systems [17]. In addition, some stages such as DV and its effect on the properties of the final product, has not been included in the developed mathematical models [124]. In Elizarraras et. al. [17] a mathematical model for the discontinuous bulk copolymerization of St and AN in presence of SBR copolymers using BPO as initiator was developed. The model was adjusted and validated with experimental data obtained in a batch reactor and was able to predict conversion, molecular weights and un-grafted SAN composition. No models have been reported for the prediction of quality variables of ABS from molecular and morphological structures.

In this Chapter, the bulk copolymerization of St and AN in the presence of a rubber using the bifunctional initiator luperox-331 M80 (L331) was theoretical and experimentally investigated. A mathematical model for the continuous bulk production of ABS is presented. The model was adjusted and validated with experimental data. The model was developed on the basis of our previous publications [124, 148] and considers: i) the use of multifunctional initiators, ii) the modeling of the DV stage, and iii) the influence of the rubber composition in the industrial quality variables. The model allows the prediction of i) conversion and other global chemical species, ii) grafting efficiency, iii) molecular weights along the train reactor and it also calculates final product properties such as iv) MWDs, v) MFI, vi) SI and vii) residual monomer content. Six different reactions for ABS production were carried out in a pilot plant varying the rubber composition and structure. Samples were taken in order to determine: i) conversion by gravimetry along the reactor train, and final product characterizations such as: ii) residual monomer content by RMN, iii) MFI in an extrusion plastomer, iv) MWDs by Size Exclusion Chromatography, v) morphology by Transmission Electron Microscopy and vi) IR by Izod Impact Testing. Final Mw in the range of 2.1-2.3 10^5 g/mol were measured and a considerable improvement in the IR was observed when using SBR with a 90% content of St.

The pilot plant comprised the main stages of an industrial ABS process: dissolution, pre-polymerization, finishing and DV (see Fig. 2.7). A mathematical model of every stage of the pilot plant was developed and the experimental data was used to adjust model parameters. Theoretical predictions were performed to show that this model can be a useful tool for control and optimization of the industrial production process.

5.2 ABS Production Process

ABS is a graft terpolymer of great commercial importance, produced by the polymerization of a mixture of AN and St in the presence of a rubber. Generally, an azeotropic composition

(76/24) St/AN is used, which allows to obtain a random copolymer of St an AN (SAN) of uniform chemical composition along the reaction. Bulk polymerization leads to a similar morphology to that of HIPS: occlusions and matrix composed of SAN. Bulk production of ABS is carried out under practically the same conditions as HIPS [11, 188, 189] (see Chapter 2).

The final material exhibits high impact strength with little compromise of its elastic modulus with respect to SAN. Processing properties are determined not only by the MWD of the non-grafted SAN matrix but also by the rubber particles characteristics [190, 191]. In turn, these properties are determined during its synthesis, which can be either by successive steps of emulsion polymerization or by bulk (or bulk/suspension) copolymerization of St and AN in the presence of a rubber. The former process usually yields rubber particles with core/shell morphologies, where the core is comprised of rubber and the shell is made of a graft terpolymer produced by the radicals attack onto the rubber. The latter process also yields heterogeneous rubber particles, but, in this case, the rubber particles contain numerous SAN occlusions (salami morphology). Moreover, the bulk process allows the production of well-reinforced polymers using lower amounts of the (expensive) rubber reagent and is friendlier to the environment.

Several analogies can be found when comparing ABS to HIPS. The mechanical properties of both materials are mainly determined by the size, morphology, and volume fraction of the rubber particles [37, 42, 192–201].Typically, HIPS is produced by polymerizing St in the presence of PB, and a St-B graft copolymer is generated from the early stages of the reaction. The generation o graft copolymer compatibilizes the phases, stabilizes the particles, and promotes the formation of particle occlusions [6, 135, 202–204]. When using SBR as precursor rubber, the initial polystyrene (PS) block is compatible with the PS matrix, acts as a surfactant, reduces the interfacial tension, and promotes the formation of smaller particles [205, 206]. It has been proven that a variety of rubber particle morphologies can be produced in HIPS by employing SBR instead of PB, but a rather low reinforcement is obtained [197, 205, 206]. Some differences appear when using SBR to produce ABS. Because of the PS block is no longer being thermodynamically compatible with the SAN generated along the reaction, the rubber particles are relatively bigger and the morphology is of the salami type. Therefore, a better reinforcement is generally obtained [207].

5.3 Experimental Work

The experimental work consisted on a series of continuous bulk polymerizations of a mixture of AN and St in the presence of a dissolved SBR with ethylbence as solvent, using the bifunctional initiator Luperox L331M80 at 0.016% in weight and tert-dodecyl mercaptan as CTA. In all reactions the equipment operating conditions were held constant and with a feed flow of 15 g/min. In order to avoid copolymer compositional drift along the reaction, the comonomer feed ratio was chosen close to the theoretical azeotropic point of the SAN copolymerization (i.e., 23 wt.% of AN).

The first series of experiments consisted on four different reactions using a partially grafted cis medium polybutadiene with 30% St (i.e. SBR 30/70), varying the rubber content, the solvent content and the mass ratio of the CTA and initiator (i.e.CTA/I). Then, another experiment was carried out using a similar rubber but with 10% of St (i.e. SBR 10/90). Finally, the last reaction was carried out using middle cis PB.

The pilot plant used for all experiments is the same as that described in Chapter 2 (see Fig. 2.7). The operating conditions selected for all experiment are presented in Table 5.1. Table 5.2 shows the recipe used for each experiment.

TABLE 5.1: Equipment operating conditions

Equipment	Mass (g)	Operation T (° C)	Operation P (mmHg)
R1	1500	100	760
R2	800	125	760
Zapper Unit	-	140	760
Devolatilizer	-	205	12-20

TABLE 5.2: Recipe adopted in the experiments for the study of ABS production

Reaction	Rubber Type	Rubber Content (%)	CTA/I	Solvent Content (%)
1	SBR 30/70	12	6	15
2	SBR 30/70	6	6	15
3	SBR 30/70	10	7	25
4	SBR 30/70	11	16	25
5	SBR 10/90	6	6	15
6	PB	8	6	15

5.3.1 Reagents

St monomer (St, 99.6%) was provided by Plastiformas (Monterrey, Mexico) with constant inhibitor level (10-28 ppm) verified by spectrophotometry according to ASTM D4590 and was used as received. AN monomer, ethylbencene and tert-dodecyl mercaptan were provided by Adrich. PB, SBR 30/70 and SBR 10/90 were donated by a local company. L331M80 is a linear bifunctional initiator supplied by Atofina and was used as received.

5.3.2 Characterization

Samples taken from the reactor were promptly cooled with ice. From each sample, a small amount was weighted (m_s) and then dissolved in a (50:50 v/v) toluene/methyl ethyl ketone

solution containing hydroquinone as inhibitor. The polymer was precipitated with an excess of methanol, filtered, and dried under vacuum at 40 °C until constant weight (m_p) was reached. The comonomer conversion (χ), defined as the ratio between the mass of polymerized comonomers (i.e., grafted and non-grafted SAN) and the initial mass of comonomers, was calculated through Eq. 5.1:

$$\chi = \frac{m_p - m_s\omega^0_{SB}}{m_s(1-\omega^0_{SB})} \tag{5.1}$$

where ω^0_{SB} is the weight fraction of SBR in the reaction recipe.

The non-grafted SAN was separated from the polymer mixture (i.e., non-grafted SAN + unreacted SB + SB-g-SAN) by a solvent extraction technique using acetone as selective solvent for the non-grafted SAN [208] . The extraction involved 5 consecutive cycles of a 24 h under agitation followed by ultracentrifugation at 20 °C and 21 000 rpm. The soluble fraction was first isolated with the help of a syringe, and then concentrated by rotoevaporation, precipitated with methanol, and dried until constant weight at room temperature (m_{ngSAN}). The absence of SBR in the non grafted SAN was confirmed by 300 MHz resolution ^{1}H NMR. The cumulative SAN grafting efficiency (E_{SAN}), defined as the ratio between the mass of grafted SAN and the mass of polymerized co-monomers, was calculated through Eq. 5.2:

$$E_{SAN} = \frac{m_p - m_{ngSAN} - m_s\omega^0_{SB}}{m_p - m_s\omega^0_{SB}} = \frac{m_p - m_{ngSAN} - m_s\omega^0_{SB}}{\chi m_s(1-\omega^0_{SB})} \tag{5.2}$$

The MWD of the non-grafted SAN was measured by size exclusion chromatography (SEC). To such effect, a Hewlett Packard HPLC 1100 chromatograph was fitted with a set of three columns with nominal pore diameters of 10^3, 10^5 and 10^6 A°. The carrier solvent was tetrahydrofuran at 1 mL.min^{-1}. The MWD and its average values were first referred to PS standards, and then corrected by the universal calibration method [209]. The fraction containing the unreacted SB+SB-g-SAN was also analyzed by SEC. Finally, the average AN content in the non-grafted SAN ($\bar{\omega}_{AN;ngSAN}$) was determined by ^{1}H NMR, relating the areas of the aliphatic (1–3 ppm) and aromatic (6.2–7.5 ppm) protons.

The different morphological structures were observed by Transmission Electron Microscopy (TEM). The samples were first cut to a thickness less than 100 nm with a diamond knife in a cryogenic ultra microtome provided by Leica at a chamber temperature of -130 °C, and -180 °C. Then, they were placed in a closed container and osmium tetroxide was added in order to stain and contrast the insoluble phase and left for a period of 2 hours.

Other final properties characterizations (i.e. Dp, MFI and IR) were analyzed in a similar way than for the HIPS experiments. The Average Particle Diameters (Dp) were estimated from the micrographs using a public domain digital image processing program (ImageJ). The MFI of the final product was determined following ASTM D-1238-13. An extrusion plastometer Dynisco Ph 800-332-224 was operated at 200 °C, and weighted with a 5 kg load. IR was determined by Izod Impact Testing. The samples were first processed to obtain test specimens by compression molding. The test specimens were conditioned according to specifications required by standard ASTM D-256 (test specimens dimensions: 64 x 12.7 x 3.2 mm) and were subjected to an IZOD impact strength measurement. All measurements were made using a CSI equipment model 137 according to ASTM D-256 standard.

Table 5.3 indicates the tests to which different materials resulting from the exploratory tests were subjected.

TABLE 5.3: Characterization of ABS samples

Test	Conditions	Equipment	Standard
MFI	220 °C/10Kg	Tinius Olsen Plastometer	ASTDM D1238
Impact Resistance	$1/2 * 1/8$ with groove	CSI model 137	ASTM D256
Residual Monomer	$CDCl_3$ as solvent	RMN, Jeol Eclipse of 300 MHz	-
Molecular Weight	THF as solvent	GPC, Hewlett-Packard series 1100	-
Morphology	Staining with OsO_4	TEM, JEOL JSM-7401F	-

5.3.3 Experimental Results

Table 5.4 shows the results of the characterizations carried out for each experiment. For all experiments a 20-22% conversion was achieved in the first reactor and 50-52% in the second reactor.

In the first series of experiments (i.e. using SBR 30/70, a graft co-polymer), comparing the results of Exp. 1 and 2, a small increase in the IR is observed with the decrease in the rubber content. The slightly increase in IR observed in Exp. 2 is probable due to the higher residual monomers and solvent content acting as plasticizers. Comparing Exp. 2 and 5, a significant improvement in IR is observed. As all other variables were held constant, this can only be attributed to molecular structure of the rubber. A higher IR is expected with the increase of B/St ratio.

Finally, comparing the results of experiment 5 and 6 (i.e. using only PB), an improvement in the IR and also in the Mw is observed when using SBR 10/90, even though with a higher rubber content (experiment 6) . Moreover, the MFI also decreased in experiment 5 because of the higher content of residual monomers and solvent.

Figures 5.1, 5.2 and 5.3 show the morphology obtained for experiments 2, 5 and 6, respec-

tively. In the case of Exp. 5 smaller particles are observed, probably due to the compatibilizer effect of St. The fact of having grafted St does not seem to produce significant change in the morphology (i.e. experiment 2).

Table 5.4: Characterization of the ABS obtained in each experiment

Reaction	**Final Rubber Content (%)**	**Residual St, AN and EB (%)**	**MFI (g/10min)**	**IR (lb·ft/in)**	**Mw (kg/mol)**
1	13.6	1.4, 0.03, 0.4	6	3	293
2	6.4	3.2, 0, 1.1	20.2	4.1	249
3	11.1	7.2, 0, 6.3	12.6	7.3	163
4	11.9	4.8, 0, 5.8	20.3	7.8	159
5	6.4	3.4, 0, 1.9	14	7.9	245
6	9.2	1.1	5.2	6.3	227

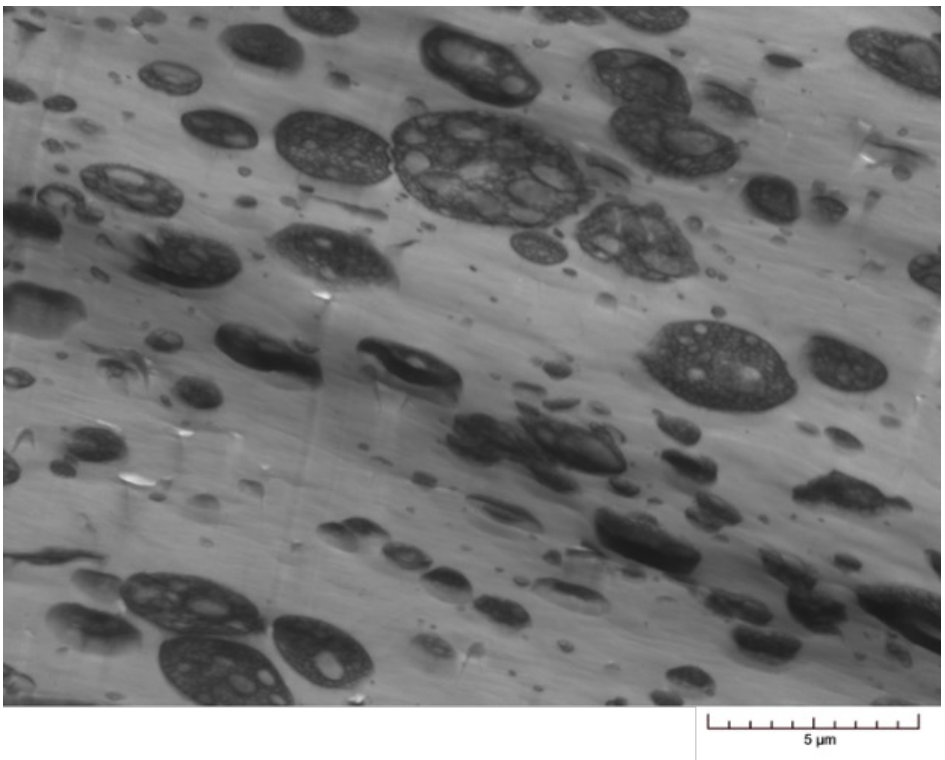

Figure 5.1: ABS morphology using SBR 30/70.

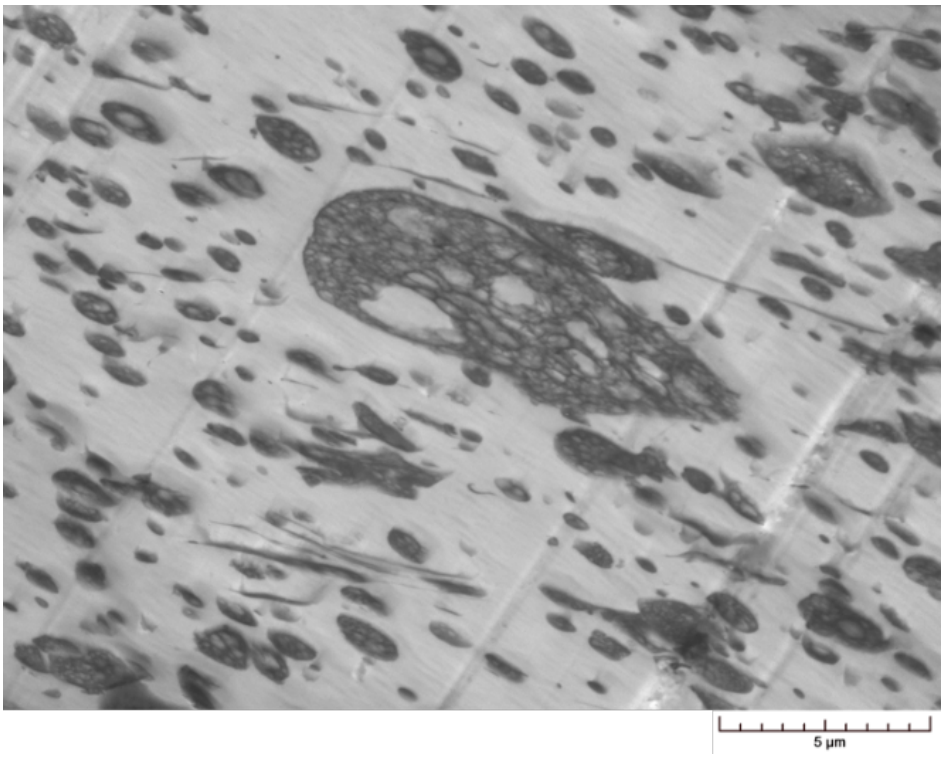

FIGURE 5.2: ABS morphology using SBR 10/90.

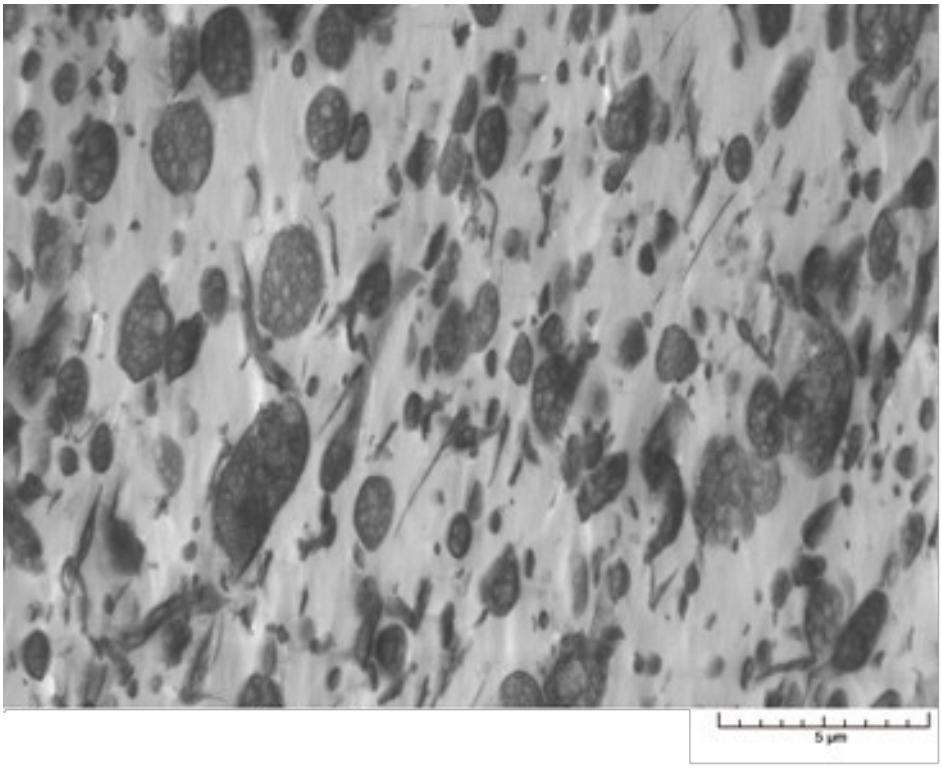

FIGURE 5.3: ABS morphology using PB.

5.4 Mathematical Model

The present model is an extension of the model presented for HIPS in the previous chapters, therefore, equivalent assumptions and resolution methods for each stage of the process were adopted. The kinetic mechanism used for describing the copolymerization of St and AN in the presence of a rubber is presented in Table 5.5. It considers chemical initiation, thermal initiation of St, propagation, chain transfer reactions to co-monomers and to the rubber, and termination by recombination of radicals.

Considering the set of equations of the Basic module developed for the HIPS bulk continuos model, in the case of ABS, a new species (AN) is introduced in the recipe, which derives in a different reaction scheme with generation of new species and with new kinetic parameters due to the copolymerization of the monomers. A Basic module for a generic CSTR was developed allowing the prediction of global chemical species (monomers, initiators, total radical species, unreacted butadiene units, undecomposed peroxide groups).

For the Distributions and DV modules, the St and AN copolymerization is assumed as a pseudo-homopolymerization [17]. This approximation allows the calculation of the cumulative grafting efficiency and the the estimation of all chemical species concentrations, characterized by their chain length and number of undecomposed peroxide groups, based on the mathematical models developed for HIPS (See Section 2.4.2 and Section 4.3.1).

The Basic module is solved using a Newton-Raphson method programmed in Matlab V. 8.3. The Distributions module is then solved using the results from the Basic module. In the Distributions module, a large number of equations (more than 500,000) must be simultaneously solved for the calculation of MWDs. Given the large number of species considered and the re-initiation reactions involved, these mass balances are solved using an iteration algorithm, also programmed in Matlab V. 8.6. To account for the non-ideality of the reactors, each reactor is considered as a series of "n" CSTRs, where "n" is an adjustment parameter [19]. The simulation of the reactor train model involved the sequential resolution of each reactor in the train. Note that the Prepolymerization Reactor (R1), the Termination Reactor (R2), the Zapper Unit (ZU) and the last stage of the Devolatilizer are considered CSTR reactors. Predictions at the ZU outlet are used to feed the DV model.

5.4.1 Basic Module

Balances for non-polymeric reagents and products

Multifunctional initiators ($\phi = 1, 2, 3$)

$$\frac{d}{dt}\left([\bar{I}^{(\phi)}]V\right) = -\phi k_{d1}[\bar{I}^{(\phi)}]V + q_{in}[\bar{I}^{(\phi)}]_{in} - q[\bar{I}^{(\phi)}] \tag{5.3}$$

Secondary initiator species ($\phi > i = 1, 2$)

TABLE 5.5: ABS polymerization using multifunctional initiators - Proposed kinetic mechanism.

Initiation($\phi = 1, 2, 3; i < \phi; j = 0, 1, ...$)

Thermal Initiation

$3\mathrm{St} \xrightarrow{k_{i0}} 2S_1{}^{.(0)}$

Chemical Initiation

$\bar{I}^{(\phi)} \xrightarrow{\phi k_{d1}} I^{.(i)}$

$I^{.(i)} + \mathrm{St} \xrightarrow{k_{i1s}} S_1{}^{.(i)}$

$I^{.(i)} + \mathrm{AN} \xrightarrow{k_{i1a}} S_1{}^{.(i)}$

$I^{.(i)} + T^{(j)} \xrightarrow{k_{i2}} P_0{}^{.(j)} + \bar{I}^{(i)}$

Propagation ($n = 1, 2, 3...; i = 0, 1, 2...$)

$St_n{}^{.(i)} + \mathrm{St} \xrightarrow{k_{pss}} St_{n+1}{}^{.(i)}$

$St_n{}^{.(i)} + \mathrm{AN} \xrightarrow{k_{psa}} St_{n+1}{}^{.(i)}$

$AN_n{}^{.(i)} + \mathrm{St} \xrightarrow{k_{pas}} AN_{n+1}{}^{.(i)}$

$AN_n{}^{.(i)} + \mathrm{AN} \xrightarrow{k_{paa}} AN_{n+1}{}^{.(i)}$

$P_0{}^{.(i)} + \mathrm{St} \xrightarrow{k_{ps}} TS_1{}^{.(i)}$

$P_0{}^{.(i)} + \mathrm{AN} \xrightarrow{k_{pa}} TAN_1{}^{.(i)}$

$TS_n{}^{.(i)} + \mathrm{St} \xrightarrow{k_{pss}} TS_{n+1}{}^{.(i)}$

$TS_n{}^{.(i)} + \mathrm{AN} \xrightarrow{k_{psa}} TAN_{n+1}{}^{.(i)}$

$TAN_n{}^{.(i)} + \mathrm{St} \xrightarrow{k_{pas}} TS_{n+1}{}^{.(i)}$

$TAN_n{}^{.(i)} + \mathrm{AN} \xrightarrow{k_{paa}} TAN_{n+1}{}^{.(i)}$

Transfer to monomer ($n = 1, 2, 3...; i = 0, 1, 2...$)

$St_n{}^{.(i)} + \mathrm{St} \xrightarrow{k_{fss}} C_n{}^{(i)} + S_1{}^{.(0)}$

$St_n{}^{.(i)} + \mathrm{AN} \xrightarrow{k_{fsa}} C_n{}^{(i)} + AN_1{}^{.(0)}$

$AN_n{}^{.(i)} + \mathrm{St} \xrightarrow{k_{fas}} C_n{}^{(i)} + S_1{}^{.(0)}$

$AN_n{}^{.(i)} + \mathrm{AN} \xrightarrow{k_{faa}} C_n{}^{(i)} + AN_1{}^{.(0)}$

$TS_n{}^{.(i)} + \mathrm{St} \xrightarrow{k_{fss}} T_n{}^{(i)} + S_1{}^{.(0)}$

$TS_n{}^{.(i)} + \mathrm{AN} \xrightarrow{k_{fsa}} T_n{}^{(i)} + AN_1{}^{.(0)}$

$TAN_n{}^{.(i)} + \mathrm{St} \xrightarrow{k_{fas}} T_n{}^{(i)} + S_1{}^{.(0)}$

$TAN_n{}^{.(i)} + \mathrm{AN} \xrightarrow{k_{faa}} T_n{}^{(i)} + AN_1{}^{.(0)}$

Transfer to rubber ($n = 1, 2, 3...; i, j = 0, 1, 2...$)

$St_n{}^{.(i)} + P^{(j)} \xrightarrow{k_{fsb}} C_n{}^{(i)} + P_0{}^{.(j)}$

$AN_n{}^{.(i)} + P^{(j)} \xrightarrow{k_{fab}} C_n{}^{(i)} + P_0{}^{.(j)}$

$TS_n{}^{.(i)} + P^{(j)} \xrightarrow{k_{fsb}} T_n{}^{(i)} + P_0{}^{.(j)}$

$TAN_n{}^{.(i)} + P^{(j)} \xrightarrow{k_{fab}} T_n{}^{(i)} + P_0{}^{.(j)}$

Combination termination ($n, m = 1, 2, 3...; i, j = 0, 1, 2...$)

$St_n{}^{.(i)} + St_m{}^{.(j)} \xrightarrow{k_{tss}} C_{n+m}{}^{(i+j)}$

$St_n{}^{.(i)} + AN_m{}^{.(j)} \xrightarrow{k_{tsa}} C_{n+m}{}^{(i+j)}$

$St_n{}^{.(i)} + TS_m{}^{.(j)} \xrightarrow{k_{tss}} T_{n+m}{}^{(i+j)}$

$St_n{}^{.(i)} + TAN_m{}^{.(j)} \xrightarrow{k_{tsa}} T_{n+m}{}^{(i+j)}$

$AN_n{}^{.(i)} + AN_m{}^{.(j)} \xrightarrow{k_{taa}} C_{n+m}{}^{(i+j)}$

$AN_n{}^{.(i)} + TS_m{}^{.(j)} \xrightarrow{k_{tsa}} T_{n+m}{}^{(i+j)}$

$AN_n{}^{.(i)} + TAN_m{}^{.(j)} \xrightarrow{k_{taa}} T_{n+m}{}^{(i+j)}$

$TS_n{}^{.(i)} + TS_m{}^{.(j)} \xrightarrow{k_{tss}} T_{n+m}{}^{(i+j)}$

$TS_n{}^{.(i)} + TAN_m{}^{.(j)} \xrightarrow{k_{tsa}} T_{n+m}{}^{(i+j)}$

$TAN_n{}^{.(i)} + TAN_m{}^{.(j)} \xrightarrow{k_{taa}} T_{n+m}{}^{(i+j)}$

$P_0{}^{.(i)} + St_n{}^{.(j)} \xrightarrow{k_{tbs}} T_n{}^{(i+j)}$

$P_0{}^{.(i)} + AN_n{}^{.(j)} \xrightarrow{k_{tba}} T_n{}^{(i+j)}$

$P_0{}^{.(i)} + TS_n{}^{.(j)} \xrightarrow{k_{tbs}} T_n{}^{(i+j)}$

$P_0{}^{.(i)} + TAN_n{}^{.(j)} \xrightarrow{k_{tba}} T_n{}^{(i+j)}$

Re-initiation ($n = 2, 3, ...; m = 1, 2, ..., n-1; i = 1, 2...; j = 0, 1, ..., i-1$)

$C_n{}^{(i)} \xrightarrow{ik_{d2}} AN_{n-m}{}^{.(i-j)} + AN_m{}^{(j-1)}$.

$C_n{}^{(i)} \xrightarrow{ik_{d2}} St_{n-m}{}^{.(i-j)} + St_m{}^{(j-1)}$.

$C_n{}^{(i)} \xrightarrow{ik_{d2}} St_{n-m}{}^{.(i-j)} + AN_m{}^{(j-1)}$.

$T_n{}^{(i)} \xrightarrow{ik_{d2}} TAN_{n-m}{}^{.(i-j)} + AN_m{}^{(j-1)}$.

$T_n{}^{(i)} \xrightarrow{ik_{d2}} TAN_{n-m}{}^{.(i-j)} + St_m{}^{(j-1)}$.

$T_n{}^{(i)} \xrightarrow{ik_{d2}} TS_{n-m}{}^{.(i-j)} + AN_m{}^{(j-1)}$.

$T_n{}^{(i)} \xrightarrow{ik_{d2}} TS_{n-m}{}^{.(i-j)} + St_m{}^{(j-1)}$.

Nomenclature:

AN	AN monomer
$AN_1{}^{.(i)}$	AN primary radical with i undecomposed peroxide groups
$AN_n{}^{.(i)}$	Copolymer radical with n repetitive units and with radical end group AN and i undecomposed peroxide groups
$St_n{}^{.(i)}$	Copolymer radical with n repetitive units and with radical end group St and i undecomposed peroxide groups
$TAN_1{}^{.(i)}$	Terpolymer primary radical with radical end group AN and i undecomposed peroxide groups
$TAN_n{}^{.(i)}$	Terpolymer radical with n repetitive units and with radical end group AN and i undecomposed peroxide groups
$TS_1{}^{.(i)}$	Terpolymer primary radical with radical end group St and i undecomposed peroxide groups
$TS_n{}^{.(i)}$	Terpolymer radical with n repetitive units and with radical end group St and i undecomposed peroxide groups
$C_n{}^{(i)}$	Non-grafted SAN copolymer with n repetitive units and i undecomposed peroxide groups
$T_n{}^{(i)}$	Terpolymer with n repetitive units and i undecomposed peroxide groups

$$\frac{d}{dt}\left([\bar{I}^{(i)}]V\right) = -ik_{d1}[\bar{I}^{(i)}]V + (1-f_1)\sum_{j=i+1}^{\phi} jk_{d1}[\bar{I}^{(j)}]V + q_{in}[\bar{I}^{(i)}]_{in} - q[\bar{I}^{(i)}] \tag{5.4}$$

Comonomers

Assuming long chain approximation (by which comonomers are only consumed in the propagation reactions), the following balances are derived:

$$\frac{d}{dt}\left([\mathrm{St}]V\right) = -kp_{ss}[\mathrm{St}]\left([St\cdot]+[TS\cdot]\right)V - kp_{as}[\mathrm{St}]\left([AN\cdot]+[TAN\cdot]\right)V + q_{in}[\mathrm{St}]_{\mathrm{in}} - q[\mathrm{St}] \tag{5.5}$$

$$\frac{d}{dt}\left([\mathrm{AN}]V\right) = -kp_{sa}[\mathrm{AN}]\left([St\cdot]+[TS\cdot]\right)V - kp_{aa}[\mathrm{AN}]\left([AN\cdot]+[TAN\cdot]\right)V + q_{in}[\mathrm{AN}]_{\mathrm{in}} - q[\mathrm{AN}] \tag{5.6}$$

where,

$$[St\cdot] = \sum_{i=0}^{\infty}\sum_{n=1}^{\infty}[St_n\cdot^{(i)}] \tag{5.7a}$$

$$[TS\cdot] = \sum_{i=0}^{\infty}\sum_{n=1}^{\infty}[TS_n\cdot^{(i)}] \tag{5.7b}$$

$$[AN\cdot] = \sum_{i=0}^{\infty}\sum_{n=1}^{\infty}[AN_n\cdot^{(i)}] \tag{5.7c}$$

$$[TAN\cdot] = \sum_{i=0}^{\infty}\sum_{n=1}^{\infty}[TAN_n\cdot^{(i)}] \tag{5.7d}$$

(5.7e)

represent the total concentrations of each type of radical present in the mixture.

Unreacted B units

$$\frac{d}{dt}\left([B*]V\right) = -\left\{k_{i2}\sum_{j=0}^{\phi-1}[I\cdot^{(j)}] + k_{fsb}\left([St\cdot]+[TS\cdot]\right) + k_{fab}\left([AN\cdot]+[TAN\cdot]\right)\right\}[B*]V + q_{in}[B*]_{in} - q[B*] \tag{5.8}$$

Radical species

$$\frac{d}{dt}\left([I.^{(i)}]V\right) = \sum_{j=i+1}^{\phi} p_j(i) f_1 j k_{d1}[\bar{I}^{(j)}]V - (k_{is}[\mathrm{St}] + k_{ia}[\mathrm{AN}] + k_{i2}[B*])\,[I.^{(i)}]V + q_{in}[I.^{(i)}]_{in} - q[I.^{(i)}] \tag{5.9}$$

$$\frac{d}{dt}\left([P_0\cdot]V\right) = \left(k_{i2}\sum_{j=0}^{\phi-1}\left([I.^{(j)}]\right) + k_{fsb}\left([St\cdot] + [TS\cdot]\right) + k_{fab}\left([AN\cdot] + [TAN\cdot]\right)\right)[B*]V$$
$$-\left(k_{bs}[\mathrm{St}] + k_{ba}[\mathrm{AN}] + k_{tas}\left([AN\cdot] + [TAN\cdot]\right) + k_{tss}\left([St\cdot] + [TS\cdot]\right)\right)[P_0\cdot]V + q_{in}[P_0\cdot]_{in} - q[P_0\cdot] \tag{5.10}$$

$$\frac{d}{dt}\left([St\cdot]V\right) = \left(k_{is}\sum_{j=0}^{\phi-1}[I.^{(j)}]\right)[\mathrm{St}]V + 2k_{i0}[\mathrm{St}]^3V - kp_{sa}[\mathrm{AN}][St\cdot]V + kp_{as}[\mathrm{St}][AN\cdot]V$$
$$+ kf_{as}[\mathrm{S}][AN\cdot]V - kf_{sa}[\mathrm{AN}][St\cdot]V + kf_{ss}[\mathrm{St}][TS\cdot]V + kf_{as}[\mathrm{St}][TAN\cdot]V$$
$$-\left(kf_{sb}[\mathrm{B}] + kt_{ss}\left([St\cdot] + [TS\cdot]\right) + kt_{sa}\left([TAN\cdot] + [AN\cdot]\right) + kt_{bs}[P_0\cdot]\right)[St\cdot]V + q_{in}[St\cdot]_{in} - q[St\cdot] \tag{5.11}$$

$$\frac{d}{dt}\left([AN\cdot]V\right) = \left(k_{ia}\sum_{j=0}^{\phi-1}[I.^{(j)}]\right)[\mathrm{St}]V + kp_{sa}[\mathrm{AN}][St\cdot]V - kp_{as}[\mathrm{St}][AN\cdot]V$$
$$- kf_{as}[\mathrm{S}][AN\cdot]V + kf_{sa}[\mathrm{AN}][St\cdot]V + kf_{aa}[\mathrm{AN}][TAN\cdot]V + kf_{as}[\mathrm{AN}][TS\cdot]V$$
$$-\left(kf_{sb}[\mathrm{B}] + kt_{aa}\left([AN\cdot] + [TAN\cdot]\right) + kt_{sa}\left([TS\cdot] + [St\cdot]\right) + kt_{ba}[P_0\cdot]\right)[AN\cdot]V + q_{in}[AN\cdot]_{in} - q[AN\cdot] \tag{5.12}$$

$$\frac{d}{dt}\left([TS\cdot]V\right) = k_{bs}[B*][\mathrm{St}]V + kp_{as}[\mathrm{St}][TAN\cdot]V - kp_{as}[\mathrm{AN}][TS\cdot]V$$
$$-\left(kf_{as}[\mathrm{AN}] + kf_{ss}[\mathrm{St}] + kf_{sb}[B*] + kt_{ss}\left([St\cdot] + [TS\cdot]\right) + kt_{sa}\left([AN\cdot] + [TAN\cdot]\right) + kt_{bs}[P_0\cdot]\right)[TS\cdot]V$$
$$+ q_{in}[TS\cdot]_{in} - q[TS\cdot] \tag{5.13}$$

$$\frac{d}{dt}\left([TAN\cdot]V\right) = k_{ba}[B*][\mathrm{AN}]V + kp_{sa}[\mathrm{AN}][TS\cdot]V - kp_{as}[\mathrm{St}][TAN\cdot]V$$
$$-\left(kf_{as}[\mathrm{St}] + kf_{aa}[\mathrm{AN}] + kf_{ab}[B*] + kt_{aa}\left([AN\cdot] + [TAN\cdot]\right) + kt_{as}\left([St\cdot] + [TS\cdot]\right) + kt_{ba}[P_0\cdot]\right)[TAN\cdot]V$$
$$+ q_{in}[TAN\cdot]_{in} - q[TAN\cdot] \tag{5.14}$$

Peroxide groups

$$[\mathrm{Pe}] = \sum_{j=1}^{\phi} j[\bar{\mathrm{I}}^{(j)}] + [\mathrm{Pe_C}] + [\mathrm{Pe_T}] \tag{5.15}$$

with

$$[\mathrm{Pe_C}] = \sum_{i=0}^{\infty}\sum_{n=1}^{\infty} i[{C_n}^{(i)}] \tag{5.16a}$$

$$[\mathrm{Pe_T}] = \sum_{i=0}^{\infty} i[\mathrm{T}^{(i)}] \tag{5.16b}$$

$$\frac{d}{dt}\left([\mathrm{Pe}]V\right) = -\sum_{i=1}^{\phi} jk_{d1}[\bar{\mathrm{I}}^{(i)}]V - k_{d2}\left([\mathrm{Pe_C}] + [\mathrm{Pe_T}]\right)V + q_{in}[\mathrm{Pe}]_{in} - q[\mathrm{Pe}] \tag{5.17}$$

Using this result and Equation 5.15, the molar concentration of peroxide groups accumulated in the SAN copolymer and the terpolymer can be calculated from the following difference

$$\frac{d}{dt}\left(\{[\mathrm{Pe_C}] + [\mathrm{Pe_T}]\}V\right) = \frac{d}{dt}\left([\mathrm{Pe}]V\right) - \sum_{j=1}^{\phi} j\frac{d}{dt}[\bar{\mathrm{I}}^{(j)}]V + q_{in}\left([\mathrm{Pe_C}]_{in} + [\mathrm{Pe_T}]_{in}\right) - q\left([\mathrm{Pe_C}] + [\mathrm{Pe_T}]\right) \tag{5.18}$$

Conversion and volumetric flow rate

The monomer conversion can be calculated from

$$\chi = \frac{\left([\mathrm{St}]_{in} + [\mathrm{AN}]_{in}\right)q_{in} - \left([\mathrm{St}] + [\mathrm{AN}]\right)q}{\left([\mathrm{St}]_{in} + [\mathrm{AN}]_{in}\right)q_{in}} \tag{5.19}$$

where the subscript "in" indicates inlet conditions. The reaction volumetric flow rate q is obtained from:

$$q = q_{in}^{\mathrm{St+AN}}\,(1 - \varepsilon X) + q_{in}^{\mathrm{PB}} \tag{5.20}$$

with

$$\varepsilon = \frac{q_{in}^{\mathrm{St+AN}} - q_f^{SAN}}{q_{in}^{\mathrm{St+AN}}} \tag{5.21}$$

Where ε is the volume contraction factor, $q_{in}^{\mathrm{St+AN}}$ and q_{in}^{PB} are the inlet monomers and PB volumetric flow rates respectively and q_f^{SAN} is the final volumetric flow rate of free and grafted copolymer at full conversion.

With derivatives equal to zero, equations eqs. (5.3) to (5.6) and (5.8) to (5.20) are solved to find the concentration at the reactor outlet of species $[\bar{I}^{(i)}]$, [St], [AN], $[B*]$, $[I.^{(i)}]$, $[P_0\cdot]$, $[St\cdot]$, $[AN\cdot]$, $[TS\cdot]$, $[TAN\cdot]$, $([\mathrm{Pe_C}] + [\mathrm{T_C}])$, x and q.

5.4.2 Distributions Module

For the Distributions module, the St and AN copolymerization is assumed as a pseudo-homopolymerization [17]. This approximation allows the calculation of the cumulative grafting efficiency and the the estimation of all chemical species concentrations, characterized by their chain length and number of undecomposed peroxide groups, with analogue equations that were presented in Section 2.4.2. In this way, some definitions are first considered. From the global concentrations of species that are calculated in the Basic Module, the total comonomers concentration $[M]$, total non-grafted macroradicals concentration [C·], and total grafted radicals concentration [T·] can be calculated, as follows:

$$[\mathrm{M}] = [\mathrm{St}] + [\mathrm{AN}] \tag{5.22}$$

$$[\mathrm{C}\cdot] = [\mathrm{St}\cdot] + [\mathrm{AN}\cdot] \tag{5.23}$$

$$[\mathrm{T}\cdot] = [\mathrm{TAN}\cdot] + [\mathrm{TS}\cdot] \tag{5.24}$$

Also, the following global rate constants of propagation (k_p), chain transfer to the comonomers (k_{fm}), chain transfer to the rubber (k_{fb}), termination by recombination of copolymer radicals (k_t), and termination by recombination between butadienyl and copolymer radicals (k_{tb}) are defined.

$$k_p = k_{paa}zw + k_{psa}(1-w)z + k_{pas}(1-z)w + k_{pss}(1-w)(1-z) \tag{5.25}$$

$$k_{fm} = k_{faa}zw + k_{fsa}(1-w)z + k_{fas}(1-z)w + k_{fss}(1-w)(1-z) \tag{5.26}$$

$$k_{fb} = k_{fsb}(1-w) + k_{fab}w \tag{5.27}$$

$$k_t = k_{taa}w^2 + 2k_{tsa}(1-w)w + k_{tss}(1-w)^2 \tag{5.28}$$

where w and z are the radical and comonomer concentration ratios, given by:

$$w = \frac{[AN\cdot]}{[C\cdot]} = \frac{[TAN\cdot]}{[T\cdot]} \tag{5.29}$$

$$z = \frac{[AN]}{[M]} \tag{5.30}$$

5.4.3 DV and Final Properties Module

Also using the pseudo-homopolymerization approximation, the equations presented in Sections 4.3.1, 4.3.3 and 4.3.2 were adapted to simulate the DV stage and to estimate the MFI and SI.

5.5 Model adjustment and Simulations

Model parameters are presented for the complete model of the process in Table 5.6. Notice that the kinetic constants for initiator decomposition, transfer to St monomer, transfer to the rubber and termination, and also DV parameters were all taken from the HIPS model. The kinetic constants for AN propagation were adjusted using the above presented experimental data for conversion and molecular weights, respectively.

The model is then used to study the effect of the rubber content in the polymerization

[1] $C_1 = 2.75 - 0.00505T, C_2 = -9.56 - 0.0176T, C_3 = 3.03 + 0.00785T$

TABLE 5.6: Polymerization and DV models parameters for ABS.

Parameter	Units	Expression or value	Reference
k_{d1}, k_{dp} (L331)	s^-1	$8.06x10^{11}e^{-30800.9/RT}$	[124]
f_1, f_2 (L331)	-	1	[124]
k_{i0}	L^2/mol^2s	$1.1x10^5e^{-13810/RT}$	[93]
k_{i1s}, k_{pss}	L/mol s	$1.051x10^7e^{-7067/RT}$	[124]
k_{i1a}, k_{paa}	L/mol s	$6.28x10^9e^{-3663/RT}$	[210]
k_{pas}	L/mol s	$2.1x10^6e^{-7067/RT}$	Adjusted in this work
k_{psa}	L/mol s	$2.1x10^6e^{-7067/RT}$	Adjusted in this work
k_{i2} (L331)	L/mol s	$2.13x10^3e^{-5867.6/RT}$	[124]
k_{fss}	L/mol s	$7.28x10^4e^{-10080.3/RT}$	[124]
k_{fsb}, k_{fab}	L/mol s	$6.03x10^8e^{-17311/RT}$	[124]
k_{faa}	L/mol s	$2.77x10^6e^{-5837/RT}$	[210]
k_{fsa}	L/mol s	$4.15x10^9e^{-12670/RT}$	[210]
k_{fas}	L/mol s	$1.38x10^7e^{-5837/RT}$	[210]
k_{tss}, k_{tsa}, k_{taa}, k_{tbs}, k_{tba}	L/mol s	$1.686x10^9e^{-844/T-2(C_1X+C_2X^2-C_3X^3)}$1	[93]
$D_{0,1}$	cm^2/s	$5.0x10^{-3}$	[124]
$D_{0,2}$	cm^2/s	$2.5x10^{-3}$	[124]
$D_{0,3}$	cm^2/s	$1.7x10^{-3}$	[124]
N_r	$1/cm^3$	600	[163]
χ	-	$0.28 - 0.33$	[24, 151]
k_D	L/mol s	$3.12x10^7e^{-25097.1/RT}$	[124]
k_T	L/mol s	$1.35x10^6e^{-21907.6/RT}$	[124]

process. Some model simulations are presented in Figure 5.4 showing how the rubber content affects conversion, copolymer Mw and GE at the exit of the polymerization reactors train.

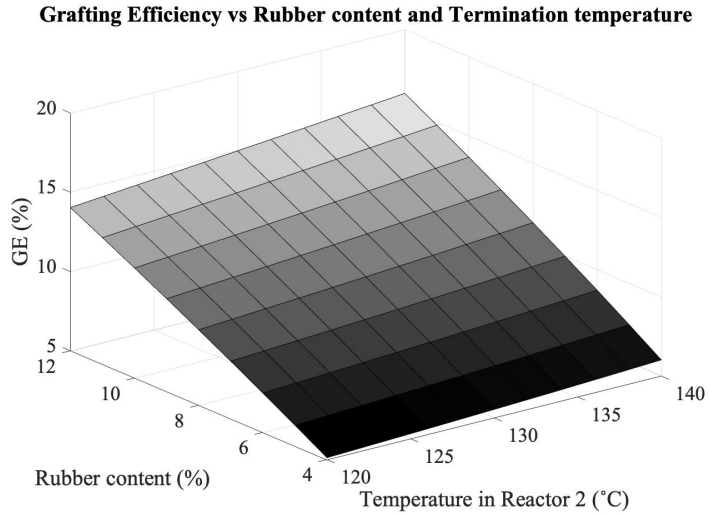

(a)

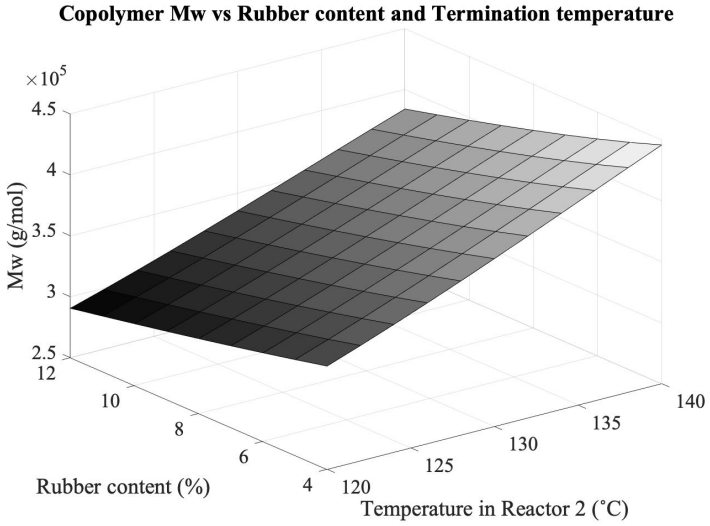

(b)

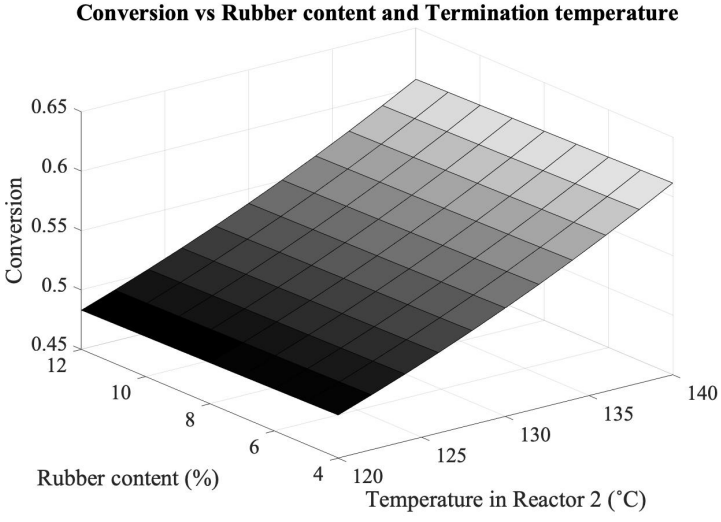

(c)

FIGURE 5.4: Theoretical simulations for ABS polymerization using multifunctional initiators in a continuous plant.

5.6 Conclusions

A mathematical model for the complete ABS continuous polymerization process using multifunctional initiators was developed. The integrated model can be used to simulate all stages of the continuous ABS process including the DV stage. Furthermore, it is a comprehensive model, meaning it can be used with any mono- or multifunctional initiator, either linear or cyclic. The model provides a full insight into the molecular structure of the different polymer species and the main quality variables, such as SI and MFI.

An experimental work was carried out in a continuous pilot plant to study the effects of the rubber composition and structure on the final properties and morphology.

The model was adjusted using new experimental data and can be used to simulate the polymerizaton of ABS in a CSTR train.

This model allows systematizing the interrelationships between operating conditions and final product quality for control and optimization of the overall production process, with the final objective of developing the “inversion" of the model in order to find the optimum recipe and operating conditions to obtain tailor made products in an industrial continuous process. In addition, the presented model could be extended to polymers from other monomers such as PMMA.

Bibliography

[1] Spyra, "Global styrene/market outlook on size, trends and 2020 key player analysis report," tech. rep., The Business Research Company, London, 2020.

[2] D. B. Priddy and U. by Staff, *Styrene Plastics*. 2006.

[3] J. Maul, B. G. Frushour, J. R. Kontoff, H. Eichenauer, K.-H. Ott, and C. Schade, *Polystyrene and Styrene Copolymers*. 2007.

[4] N. Niessner and H. Gausepohl, "Polystyrene and styrene copolymers–an overview," *Modern styrenic polymers: poly styrenes and styrenic copolymers. Wiltshire: John Wiley & Sons*, 2003.

[5] G. R. Meira, C. V. Luciani, and D. A. Estenoz, "Continuous Bulk Process for the Production of High-Impact Polystyrene: Recent Developments in Modeling and Control," *Macromolecular Reaction Engineering*, vol. 1, pp. 25–39, Jan. 2007.

[6] G. Soto, E. Nava, M. Rosas, M. Fuenmayor, I. M. Gonza, G. R. Meira, and H. M. Oliva, "Bulk Polymerization of Styrene in the Presence of Polybutadiene : Effect of Initiator Type and Prepolymerization Conditions on Particle Morphology," *Journal of Applied Polymer Science*, vol. 91, pp. 1397–1412, 2004.

[7] S. Hirschfeld and O. Wünsch, "Mass transfer during bubble-free polymer devolatilization: A systematic study of surface renewal and mixing effects," *Heat and Mass Transfer*, vol. 56, no. 1, pp. 25–36, 2020.

[8] J. D. Stein, G. Fahrbach, and H. Adler, "Crosslinking Reactions in High Impact Polystyrene Rubber Particles," *Advances in Chemistry Series*, 1975.

[9] R. Kirk and D. Othmer, *Kirk-Othmer Encyclopedia of Chemical Technology, Styrene.* Encyclopedia of Chemical Technology, Wiley and Sons, 2001.

[10] L. E. Ball and B. S. Curatolo, *Acrylonitrile Polymers, Survey and SAN*. 2000.

[11] K. D., *ABS Resins. Kirk-Othmer Encyclopedia of Chemical Technology.* Encyclopedia of Chemical Technology, John Wiley & Sons, 1998.

[12] B. J. Meister and A. E. Platt, "Evaluation of the performance of a commercial polystyrene devolatilizer," *Industrial & Engineering Chemistry Research*, vol. 28, pp. 1659–1664, Nov. 1989.

[13] T. B. R. Company, "Polystyrene-plastic material and resins global market report 2021," tech. rep., The Business Research Company, London, 2021.

[14] R. Acumen and Consulting, "Styrene market size – global industry analysis, market size, opportunities and forecast 2021 – 2028," tech. rep., Acumen, Research and Consulting, 2022.

[15] T. B. R. Company, "Styrene-petrochemicals global market report 2021," tech. rep., The Business Research Company, London, 2021.

[16] R. Acumen and Consulting, "Global polystyrene market; regional analysis; historical market and forecast (2017-2027); market dynamics: Swot analysis; competitive landscape; industry events and developments," tech. rep., Expert Market Research, 2021.

[17] D. Elizarrarás, G. Morales, R. Díaz De León, C. Luciani, and D. Estenoz, "A mathematical model of the bulk copolymerization of styrene and acrylonitrile in the presence of polystyrene-block-polybutadiene," *Macromolecular Theory and Simulations*, vol. 17, no. 4-5, pp. 180–197, 2008.

[18] L. Mascia and M. Xanthos, "An overview of additives and modifiers for polymer blends: Facts, deductions, and uncertainties," *Advances in Polymer Technology*, vol. 11, no. 4, pp. 237–248, 1992.

[19] D. A. Estenoz and G. R. Meira, "Mathematical model of a continuous industrial high-impact polystyrene process," *AIChE Journal*, vol. 44, pp. 427–441, Feb. 1998.

[20] J. SCHEIRS and D. B. PRIDDY, "Modern styrenic polymers: Polystyrenes and styrenic copolymers," 2003.

[21] J. R. Wünsch, *Polystyrene: Synthesis, production and applications*, vol. 112. iSmithers Rapra Publishing, 2000.

[22] J. Maul, B. G. Frushour, J. R. Kontoff, H. E., K. Ott, and C. Schade, "Polystyrene and Styrene Copolymers," in *Ullmann's Encyclopedia of Industrial Chemistry*, pp. 475–522, Weinheim, Germany: Wiley-VCH Verlag GmbH & Co. KGaA, July 2007.

[23] G. Odian, *Principles of Polymerization*. 2004.

[24] A. W. Hui and A. E. Hamielec, "Thermal Polymerization of Styrene at High Conversion and Temperatures. An Experimental Study," *Journal of Applied Polymer Science*, vol. 16, no. 3, pp. 749–769, 1972.

[25] W. A. Pryor and L. D. Lasswell, "An excellent review on the subject of spontaneous polymerization of styrene," *Advanced Free Radical Chemistry*, vol. 5, pp. 27–99, 1975.

[26] K. S. Khuong, W. H. Jones, W. A. Pryor, and K. N. Houk, "The mechanism of the self-initiated thermal polymerization of styrene. Theoretical solution of a classic problem.," *Journal of the American Chemical Society*, vol. 127, pp. 1265–77, Feb. 2005.

[27] G. Moad and D. Solomon, *The Chemistry of Radical Polymerization*. Elsevier Science, 2 ed., 2006.

[28] S. Zhu and A. E. Hamielec, "Polymerization Kinetic Modeling and Macromolecular Reaction Engineering," in *Polymer Science: A Comprehensive Reference*, vol. 4, pp. 779–831, Elsevier B.V., 2012.

[29] J. R. Cerna Cortez, *Uso de peróxidos cíclicos multifuncionales como iniciadores de la polimerización*. Tesis de doctorado, Centro de Investigación en Química Aplicada, 2002.

[30] A. Alfarraj and E. B. Nauman, "Super hips: improved high impact polystyrene with two sources of rubber particles," *Polymer*, vol. 45, no. 25, pp. 8435–8442, 2004.

[31] C. de Anda, G. Morales, P. Acuna, J. Sosa, D. Knoeppel, and J. Mays, "Synthesis of hips using an a2b2 star-type graft copolymer (pb-g-ps)," *Macromolecular Reaction Engineering*, vol. 4, no. 6-7, pp. 381–386, 2010.

[32] R. D. de Leon and G. Morales, "Evaluation of the interfacial state in high impact polystyrene through dynamic mechanical analysis as a function of the synthesis conditions," *Polymer Engineering & Science*, vol. 47, no. 11, pp. 1827–1838, 2007.

[33] F. J. Enríquez-Medrano, P. Acuña, and G. Morales, "Synthesis strategies in the preparation of high impact polystyrene with different type of particles as the dispersed phase, towards a balance between impact strength and gloss," *Brazilian Journal of Chemical Engineering*, vol. 37, no. 4, pp. 715–727, 2020.

[34] D. M. Kulich, S. K. Gaggar, V. Lowry, and R. Stepien, *Acrylonitrile–Butadiene–Styrene (ABS) Polymers*. 2003.

[35] J. M. Maffi, G. R. Meira, and D. A. Estenoz, "Mechanisms and conditions that affect phase inversion processes. a review.," *The Canadian Journal of Chemical Engineering*.

[36] J. M. Maffi, N. Casis, P. Acuña, G. Morales, and D. A. Estenoz, "Mechanisms and conditions that affect phase inversion processes. the case of high-impact polystyrene," *Polymer Engineering & Science*, vol. 60, no. 3, pp. 491–502, 2020.

[37] J. Moore, "An electron microscope study of the microstructure of some rubber-reinforced polystyrenes," *Polymer*, vol. 12, no. 8, pp. 478–486, 1971.

[38] A. Echte, *Rubber-Toughened Styrene Polymers*, ch. 3, pp. 15–64. 1989.

[39] L. Bohn, "Angew. effect of acrylonitrile content on the toughness of abs materials," *Makromol Chem*, vol. 20, pp. 129–133, 1971.

[40] H. Kim, H. Keskkula, and D. Paul, "Effect of acrylonitrile content on the toughness of abs materials," *Polymer*, vol. 32, no. 8, pp. 1447–1455, 1991.

[41] V. G. Kämpf and H. Schuster, "Struktur und eigenschaften von abs-polymeren. ix. quantitative untersuchungen zur morphologie von abs-polymerisaten," *Die Angewandte Makromolekulare Chemie: Applied Macromolecular Chemistry and Physics*, vol. 27, no. 1, pp. 81–98, 1972.

[42] E. Wagner and L. Robeson, "Impact polystyrene: factors controlling the rubber efficiency," *Rubber Chemistry and Technology*, vol. 43, no. 5, pp. 1129–1137, 1970.

[43] H. F. Mark, *Encyclopedia of polymer science and technology, concise.* John Wiley & Sons, 2013.

[44] L. Morbitzer, D. Kranz, G. Humme, and K. Ott, "Structure and properties of abs polymers. x. influence of particle size and graft structure on loss modulus temperature dependence and deformation behavior," *Journal of Applied Polymer Science*, vol. 20, no. 10, pp. 2691–2704, 1976.

[45] A. Ghosh and J. Lindt, "Processing of abs latex in a single screw extruder," *International Polymer Processing*, vol. 5, no. 3, pp. 195–200, 1990.

[46] A. K. Ghosh and J. T. Lindt, "Processing of polymer latex emulsion: Batch coagulation," *Journal of applied polymer science*, vol. 39, no. 7, pp. 1553–1568, 1990.

[47] G. E. Molau, "Heterogeneous polymer systems. ii. mechanism of stabilization of polymeric oil-in-oil emulsions," *Journal of Polymer Science Part A: General Papers*, vol. 3, no. 12, pp. 4235–4242, 1965.

[48] S. Zhiqiang, Y. Huigen, and P. Zuren, "Studies on the rheological behavior of high-impact polystyrene prepolymerizing systems," *Journal of applied polymer science*, vol. 32, no. 2, pp. 3349–3369, 1986.

[49] G. Freeguard and M. Karmarkar, "The production of rubber-modified polystyrene. ii. the significance of shear in the phase inversion," *Journal of Applied Polymer Science*, vol. 15, no. 7, pp. 1657–1663, 1971.

[50] G. E. Molau and H. Keskkula, "Heterogeneous polymer systems. iv. mechanism of rubber particle formation in rubber-modified vinyl polymers," *Journal of Polymer Science Part A-1: Polymer Chemistry*, vol. 4, no. 6, pp. 1595–1607, 1966.

[51] B. Bender, "Dispersion of microgel in impact polystyrene," *Journal of Applied Polymer Science*, vol. 9, no. 8, pp. 2887–2894, 1965.

[52] J. L. Amos, "The spe international award address—1973 the development of impact polystyrene–a review," *Polymer Engineering & Science*, vol. 14, no. 1, pp. 1–11, 1974.

[53] F.-D. Rumscheidt and S. Mason, "Particle motions in sheared suspensions xii. deformation and burst of fluid drops in shear and hyperbolic flow," *Journal of Colloid Science*, vol. 16, no. 3, pp. 238–261, 1961.

[54] R. W. Flumerfelt, "Drop breakup in simple shear fields of viscoleastic fluids," *Industrial & Engineering Chemistry Fundamentals*, vol. 11, no. 3, pp. 312–318, 1972.

[55] M. Baer, "Studies on heterogeneous polymeric systems. i. influence of morphology on mechanical properties," *Journal of Applied Polymer Science*, vol. 16, no. 5, pp. 1109–1123, 1972.

[56] J.-L. Locatelli and G. Riess, "Étude de copolymčres greffés abs (acrylonitrile-butadične-styrčne). ii. comparaison des masses moléculaires des greffons et du copolymčre san libre," *Die Angewandte Makromolekulare Chemie: Applied Macromolecular Chemistry and Physics*, vol. 28, no. 1, pp. 161–175, 1973.

[57] N. Platzer, "Design of continuous and batch polymerization processes," *Industrial & Engineering Chemistry*, vol. 62, no. 1, pp. 6–20, 1970.

[58] H. G. Pohlemann and A. Echte, "Fifty years of polystyrene," ACS Publications, 1981.

[59] A. M. Donald and E. J. Kramer, "Craze initiation and growth in high-impact polystyrene," *Journal of Applied Polymer Science*, vol. 27, no. 10, pp. 3729–3741, 1982.

[60] C. B. Bucknall, P. Davies, and I. K. Partridge, "Rubber toughening of plastics," *Journal of Materials Science*, vol. 22, no. 4, pp. 1341–1346, 1987.

[61] D. Gilbert and A. Donald, "Toughening mechanisms in high impact polystyrene," *Journal of materials science*, vol. 21, no. 5, pp. 1819–1823, 1986.

[62] A. Brydon, G. Burnett, and G. Cameron, "Free-radical grafting of monomers to polydienes. ii. kinetics and mechanism of styrene grafting to polybutadiene," *Journal of Polymer Science: Polymer Chemistry Edition*, vol. 12, no. 5, pp. 1011–1021, 1974.

[63] V. Gupta, G. Bhargava, and K. Bhattacharyya, "Studies on mechanism of grafting of polystyrene on elastomer backbone," *Journal of Macromolecular Science—Chemistry*, vol. 16, no. 6, pp. 1107–1116, 1981.

[64] R. A. Hayes and S. Futamura, "Kinetics and mechanism of the polymerization of styrene–acrylonitrile in the presence of polybutadiene," *Journal of Polymer Science: Polymer Chemistry Edition*, vol. 19, no. 4, pp. 985–991, 1981.

[65] R. A. Hayes, "Determination of reactivity ratios for the copolymerization of styrene and styrene–acrylonitrile with polybutadienes," *Journal of Polymer Science: Polymer Chemistry Edition*, vol. 19, no. 4, pp. 993–997, 1981.

[66] A. E. Hamielec and H. Tobita, "Polymerization Processes, 1. Fundamentals," in *Ullmann's Encyclopedia of Industrial Chemistry*, pp. 317–388, Weinheim, Germany: Wiley-VCH Verlag GmbH & Co. KGaA, Oct. 2011.

[67] T. Meyer and J. Keurentjes, eds., *Handbook of Polymer Reaction Engineering*. Wiley, 2005.

[68] "Carbon-carbon bond-type macromolecular radical initiator and preparation method thereof," July 8 2015. CN Patent 103,342,765.

[69] C. Sheppard and R. MacLeay, "Peroxide free radical initiators containing ultraviolet light stabilizing groups," Dec. 12 1978. US Patent 4,129,586.

[70] R. Kirk, D. Othmer, J. Kroschwitz, and M. Howe-Grant, *Kirk-Othmer Encyclopedia of Chemical Technology, Pigments to Powders, Handling*. Encyclopedia of Chemical Technology, Wiley, 1996.

[71] "Organic Peroxide Market by Type, Applications & Geography - Global Industry Trends & Forecasts to 2020," tech. rep., Markets and Markets, 2015.

[72] M. A. Villalobos, A. E. Hamielec, and P. E. Wood, "Kinetic Model for Short-Cycle Bulk Styrene Polymerization through Bifunctional Initiators," *Journal of Applied Polymer Science*, vol. 42, pp. 629–641, 1991.

[73] Ceresana, "Market Study: Engineering Plastics," 2013.

[74] J. R. Cerna, G. Morales, G. N. Eyler, and A. I. Cañizo, "Bulk polymerization of styrene catalyzed by bi- and trifunctional cyclic initiators," *Journal of Applied Polymer Science*, vol. 83, pp. 1–11, Jan. 2002.

[75] K. Shanmugananda Murthy, K. Kishore, and V. Krishna Mohan, "Vinyl Monomer Based Polyperoxides as Potential Initiators for Radical Polymerization: An Exploratory Investigation with Poly(.alpha.-methylstyrene peroxide)," *Macromolecules*, vol. 27, pp. 7109–7114, Nov. 1994.

[76] A. V. Castañeda Facio, *Estudio de la Descomposición Térmica del Diperóxido de Pinacolona: Formación de Oligómeros y Polímeros a base de Estireno con estructura definida*. PhD thesis, Instituto Teconlógico de la Laguna, 2007.

[77] W. Sheng, J. Wu, G. Shan, Z. Huang, and Z. Weng, "Free-radical bulk polymerization of styrene with a new trifunctional cyclic peroxide initiator," *Journal of Applied Polymer Science*, vol. 94, pp. 1035–1042, Nov. 2004.

[78] L. Cavin, A. Rouge, T. Meyer, and A. Renken, "Kinetic modeling of free radical polymerization of styrene initiated by the bifunctional initiator 2,5-dimethyl-2,5-bis (2-ethyl hexanoyl peroxy)hexane," *Polymer*, vol. 41, pp. 3925–3935, 2000.

[79] I. M. Gonzalez, G. R. Meira, and H. M. Oliva, "Synthesis of Polystyrene with Mixtures of Mono- and Bifunctional Initiators," *Journal of Applied Polymer Science*, vol. 59, no. 3000, pp. 1015–1026, 1996.

[80] R. López-Negrete de la Fuente, J. Lopez-Rubio, A. Flores-Tlacuahuac, and E. Saldívar-Guerra, "Steady-State Multiplicity Behavior Analysis of a High-Impact Polystyrene Continuous Stirred Tank Reactor Using a Bifunctional Initiator," *Industrial & Engineering Chemistry Research*, vol. 45, pp. 1689–1707, Mar. 2006.

[81] D. A. Estenoz, G. R. Leal, Y. R. Lopez, H. M. Oliva, and G. R. Meira, "Bulk polymerization of styrene in the presence of polybutadiene. The use of bifunctional initiators," *Journal of Applied Polymer Science*, vol. 62, pp. 917–939, Nov. 1996.

[82] A. Rudin, *The Elements of Polymer Science and Engineering.* 3 ed., 2012.

[83] H. Weber, I. De Grave, and E. Röhrl, "Foamed Plastics," in *Ullmann's Encyclopedia of Industrial Chemistry*, pp. 73–198, Weinheim, Germany: Wiley-VCH Verlag GmbH & Co. KGaA, June 2000.

[84] E. Berkenwald, L. Laganá, P. Acuña, G. Morales, and D. Estenoz, "Bulk Polymerization of Styrene using Multifunctional Initiators in a Batch Reactor : A Comprehensive Mathematical Model," *International Journal of Chemical Reactor Engineering*, vol. 14, no. 1, pp. 315–329, 2016.

[85] C. V. Luciani, *Poliestireno de Alto Impacto. Modelado matemático del proceso productivo, predicción de la estructura molecular, la morfología, y las propiedades finales.* PhD thesis, Universidad Nacional del Litoral, 2006.

[86] P. Acuña, G. Morales, and R. Díaz de León, "Synthesis and Characterization of High-Impact Polystyrene Using a Multifunctional Cyclic Peroxide as the Initiator," *Journal of Applied Polymer Science*, vol. 114, pp. 3198–3210, 2009.

[87] M. J. Scorah, *Experimental and modeling investigation of a novel tetrafunctional initiator in free radical polymerization.* Doctoral thesis, University of Waterloo, 2005.

[88] R. Albalak, ed., *Polymer Devolatilization.* New York: Routledge, 1 ed., 1996.

[89] D. J. Stein and H. Mosthaf, "Formation of Oligomers During the Thermal Polymerization of Styrene," *Die Angewandte Makromolekulare Chemie 2*, no. 22, pp. 39–50, 1968.

[90] M. Wäckerlin and P. Nising, "Recent Advances in Modern Static Devolatilization," *Macromolecular Symposia*, vol. 259, pp. 17–25, Dec. 2007.

[91] K. Kirchner and K. Riederle, "Thermal Polymerization of Styrene - The Formation of Oligomers and Intermediates, I," *Die Angewandte Makromolekulare Chemie*, vol. 111, no. 1703, pp. 1–16, 1983.

[92] D. A. Estenoz, I. M. González, H. M. Oliva, and G. R. Meira, "Polymerization of styrene in the presence of polybutadiene: determination of the molecular structure," *Journal of Applied Polymer Science*, vol. 74, pp. 1950–1961, 1999.

[93] N. Casis, D. A. Estenoz, L. M. Gugliotta, H. M. Oliva, and G. R. Meira, "Heterogeneous bulk polymerization of styrene in the presence of polybutadiene: Calculation of the macromolecular structure," *Journal of Applied Polymer Science*, vol. 99, pp. 3023–3039, Mar. 2006.

[94] F. M. Peng, "Polybutadiene Grafting and Crosslinking in High-Impact Polystyrene Bulk Thermal Process," *Journal of Applied Polymer Science*, vol. 40, pp. 1289–1302, 1990.

[95] N.-J. Huang and D. C. Sundberg, "A gel permeation chromatography method to determine grafting efficiency during graft copolymerization," *Polymer*, vol. 35, no. 26, pp. 5693 – 5698, 1994.

[96] R. A. Hall and P. Jacoby, "The effect of grafting on rubber-phase oxidative etch resistance in high-impact polystyrene," *Journal of Applied Polymer Science*, vol. 23, no. 5, pp. 1453–1460, 1979.

[97] G. Meira, *Data reduction in size exclusion chromatography of polymers.* J. Wiley & Sons, Inc.: New York, 1991.

[98] G. Meira and J. Vega, "Characterization of copolymers by size exclusion chromatography," *Handbook of Size Exclusion Chromatography and Related Techniques*, pp. 139–156, 2003.

[99] Y. M. Meira G., Vega J., *Gel Permeation and Size Exclusion Chromatography.* CRC Press, 2004.

[100] J. Runyon, D. Barnes, J. Rudd, and L. Tung, "Multiple detectors for molecular weight and composition analysis of copolymers by gel permeation chromatography," *Journal of Applied Polymer Science*, vol. 13, no. 11, pp. 2359–2369, 1969.

[101] R. Bielsa and G. Meira, "Linear copolymer analysis with dual-detection size exclusion chromatography: Correction for instrumental broadening," *Journal of applied polymer science*, vol. 46, no. 5, pp. 835–845, 1992.

[102] W. Keqiang and H. Honghong, "A method for determining molecular weight of copolymers by gpc," 2000.

[103] D. Estenoz, J. Vega, H. Oliva, and G. Meira, "Analysis of a styrene—butadiene graft copolymer by size exclusion chromatography i. computer simulation study for estimating the biases induced by branching under ideal fractionation and detection," *International Journal of Polymer Analysis and Characterization*, vol. 6, no. 3-4, pp. 315–337, 2001.

[104] J. Vega, D. Estenoz, H. Oliva, and G. Meirra, "Analysis of a styrene-butadiene graft copolymer by size exclusion chromatography ii. determination of the branching exponent with the help of a polymerization model," *International Journal of Polymer Analysis and Characterization*, vol. 6, no. 3-4, pp. 339–348, 2001.

[105] L. Mrkvičková, "Characterization of chemical heterogeneity of graft copolymer by conventional sec," *Journal of liquid chromatography & related technologies*, vol. 22, no. 2, pp. 205–214, 1999.

[106] C. Maestrini, M. Merlotti, M. Vighi, and E. Malaguti, "Second phase volume fraction and rubber particle size determinations in rubber-toughened polymers: A simple stereological approach and its application to the case of high impact polystyrene," *Journal of materials science*, vol. 27, no. 22, pp. 5994–6016, 1992.

[107] G. Cigna, "Dynamic mechanical properties, structure, and composition of impact polystyrene," *Journal of Applied Polymer Science*, vol. 14, no. 7, pp. 1781–1793, 1970.

[108] T. Craig, R. Quick, and T. Jenkins, "Measurement of particle size distribution in the discrete phase of high-impact polystyrene. i. errors in direct coulter counter techniques," *Journal of Polymer Science: Polymer Chemistry Edition*, vol. 15, no. 2, pp. 433–439, 1977.

[109] T. Craig, R. Quick, and T. Jenkins, "Measurement of particle size distribution in the discrete phase of high-impact polystyrene. ii. an improved coulter counter procedure," *Journal of Polymer Science: Polymer Chemistry Edition*, vol. 15, no. 2, pp. 441–444, 1977.

[110] R. A. Hall, R. D. Hites, and P. Plantz, "Characterization of rubber particle size distribution of high-impact polystyrene using low-angle laser light scattering," *Journal of Applied Polymer Science*, vol. 27, no. 8, pp. 2885–2890, 1982.

[111] G. E. Molau and H. Keskkula, "Heterogeneous polymer systems. iv. mechanism of rubber particle formation in rubber-modified vinyl polymers," *Journal of Polymer Science Part A-1: Polymer Chemistry*, vol. 4, no. 6, pp. 1595–1607, 1966.

[112] M. Baer, "Studies on heterogeneous polymeric systems. i. influence of morphology on mechanical properties," *Journal of Applied Polymer Science*, vol. 16, no. 5, pp. 1109–1123, 1972.

[113] C. Bucknall, "Relation between the structure and mechanical properties of rubber-modified thermoplastics. ii," *British Plastics*, vol. 40, no. 12, pp. 84–86, 1967.

[114] J. Silberberg and C. Han, "The effect of rubber particle size on the mechanical properties of high-impact polystyrene," *Journal of Applied Polymer Science*, vol. 22, no. 3, pp. 599–609, 1978.

[115] A. Savadori, "Methods of measurement and interpretation of results," in *Rubber Toughened Engineering Plastics*, pp. 90–135, Springer, 1994.

[116] M. D. Dalal and R. C. Armstrong, "Relationship between rheological properties and impact strength in high impact polystyrene," *Polymer Engineering & Science*, vol. 22, no. 11, pp. 684–691, 1982.

[117] G. Dagli, A. Argon, and R. Cohen, "Particle-size effect in craze plasticity of high-impact polystyrene," *Polymer*, vol. 36, no. 11, pp. 2173–2180, 1995.

[118] V. Luciani, C, D. A. Estenoz, R. Meira, G, and H. M. Oliva, "Reduction of Transients between Steady States in the Continuous Production of High-Impact Polystyrene," *Industrial & Engineering Chemistry Research*, vol. 44, pp. 8354–8367, Oct. 2005.

[119] A. Flores-Tlacuahuac, L. T. Biegler, and E. Saldívar-Guerra, "Dynamic Optimization of HIPS Open-Loop Unstable Polymerization Reactors," *Industrial & Engineering Chemistry Research*, vol. 44, pp. 2659–2674, Apr. 2005.

[120] A. Flores-Tlacuahuac, V. Zavala-Tejeda, and E. Saldívar-Guerra, "Complex nonlinear behavior in the full-scale high-impact polystyrene process," *Industrial & engineering chemistry research*, vol. 44, no. 8, pp. 2802–2814, 2005.

[121] K. C. Seavey, Y. A. Liu, N. P. Khare, T. Bremner, and C. Chen, "Quantifying Relationships among the Molecular Weight Distribution, Non-Newtonian Shear Viscosity, and Melt Index for Linear Polymers," *Industrial & Engineering Chemistry Research*, vol. 42, pp. 5354–5362, Oct. 2003.

[122] D. Bertin, F. Coutand, M. Duc, C. Galindo, D. Gigmès, S. Marque, P. Tordo, and B. Vuillemin, "Evolution of the partition coefficients of peroxide initiators during the synthesis of high-impact polystyrene," *e-Polymers*, vol. 4, no. 1, 2004.

[123] W. A. Ludwico and S. L. Rosen, "The kinetics of two-phase bulk polymerization. I. Monomer and initiator distribution," *Journal of Applied Polymer Science*, vol. 19, no. 3, pp. 757–768, 1975.

[124] M. L. Laganá, E. Berkenwald, P. Acuña, J. Enríquez Medrano, G. Morales, and D. Estenoz, "New advances in the mathematical modeling of the continuous bulk process for the production of high-impact polystyrene using multifunctional initiators," *Polymer Engineering & Science*, vol. 59, no. s2, pp. E231–E246, 2019.

[125] A. Hamielec, J. MacGregor, S. Webb, and T. Spychaj, "Thermal and chemical–initiated copolymerization of styrene/acrylic acid at high temperatures and conversions in a continuous stirred tank reactor," *Huthig & Wepf Verlag Basel, Polymer Reaction Engineering,*, pp. 185–199, 1986.

[126] J. D. Campbell, F. Teymour, and M. Morbidelli, "High Temperature Free Radical Polymerization. 1. Investigation of Continuous Styrene Polymerization," *Macromolecules*, vol. 36, pp. 5491–5501, July 2003.

[127] J. D. Campbell, F. Teymour, and M. Morbidelli, "High temperature free radical polymerization. 2. Modeling continuous styrene polymerization," *Macromolecules*, vol. 36, no. 15, pp. 5502–5515, 2003.

[128] D. Moscatelli, C. Cavallotti, and M. Morbidelli, "Prediction of Molecular Weight Distributions Based on ab Initio Calculations: Application to the High Temperature Styrene Polymerization," *Macromolecules*, vol. 39, pp. 9641–9653, Dec. 2006.

[129] M. L. Poutsma, "Mechanistic analysis and thermochemical kinetic simulation of the products from pyrolysis of poly (α-methylstyrene), especially the unrecognized role of phenyl shift," *Journal of Analytical and Applied Pyrolysis*, vol. 80, no. 2, pp. 439–452, 2007.

[130] R. J. Albalak, Z. Tadmor, and Y. Talmon, "Polymer Melt Devolatilization Mechanisms," *AIChE Journal*, vol. 36, no. 9, pp. 1313–1320, 1990.

[131] G. Astarita and P. L. Maffettone, "Polymer Devolatilization: State of the Art," *Makromolecular Chemie Symposia*, vol. 68, no. 1, pp. 1–12, 1993.

[132] R. Salazar, P. Ilundain, D. Alvarez, L. Da Cunha, J. Barandiaran, and M. Asua, "Reduction of the Residual Monomer and Volatile Organic Compounds by Devolatilization," *Industrial & Engineering Chemistry Research*, vol. 44, pp. 4042–4050, May 2005.

[133] H. Tobita, "Simultaneous Long-Chain Branching and Random Scission :," *Journal of Polymer Science Part B: Polymer Physics*, vol. 39, no. November 2000, p. 391, 2001.

[134] I. M. Maafa, J. B. P. Soares, and A. Elkamel, "Prediction of Chain Length Distribution of Polystyrene Made in Batch Reactors with Bifunctional Free-Radical Initiators Using Dynamic Monte Carlo Simulation," *Macromolecular Reaction Engineering*, vol. 1, pp. 364–383, May 2007.

[135] M. Fischer and G. Hellmann, "On the evolution of phase patterns during the high-impact-modified polystyrene process," *Macromolecules*, vol. 29, no. 7, pp. 2498–2509, 1996.

[136] A. Brydon, G. M. Burnett, and G. G. Cameron, "Free-Radical Grafting of Monomers to Polydienes . I . Effect of Reaction Conditions on Grafting of Styrene to Polybutadiene," vol. 11, no. 1, pp. 3255–3269, 1973.

[137] P. J. Flory, *Principles of polymer chemistry*. Cornell University Press, 1953.

[138] T. Inoue, T. Soen, T. Hashimoto, and H. Kawai, "Studies on domain formation of the ab-type block copolymer from its solutions. ternary polymer blend of the styrene-isoprene block colopymer with polystyrene and polyisoprene," *Macromolecules*, vol. 3, no. 1, pp. 87–92, 1970.

[139] R.-J. Roe and W.-C. Zin, "Determination of the polymer-polymer interaction parameter for the polystyrene-polybutadiene pair," *Macromolecules*, vol. 13, no. 5, pp. 1221–1228, 1980.

[140] G. F. Freeguard, "Structural control of rubber modified thermoplastic as produced by the mass process," *British Polymer Journal*, vol. 6, no. 4, pp. 205–228, 1974.

[141] G. F. Freeguard and M. Karmarkar, "The production of rubber-modified polystyrene. II. The significance of shear in the phase inversion," *Journal of Applied Polymer Science*, vol. 15, pp. 1657–1663, July 1971.

[142] B. J. Meister and C. J. Cummings, "Commercial processes for the manufacture of polystyrene," in *Modern Styrenic Polymers: Polystyrenes and Styrenic Copolymers*, pp. 45–69, Wiley Online Library, 2003.

[143] K. Y. Choi, W. R. Liang, and G. D. Lei, "Kinetics of bulk styrene polymerization catalyzed by symmetrical bifunctional initiators," *Journal of Applied Polymer Science*, vol. 35, pp. 1547–1562, May 1988.

[144] K. J. Kim, W. Liang, and K. Y. Choi, "Bulk free radical polymerization of styrene with unsymmetrical bifunctional initiators," *Industrial & engineering chemistry ...*, vol. 0, no. I, pp. 131–138, 1989.

[145] K. J. Kim and K. Y. Choi, "Modeling of free radical polymerization of styrene catalyzed by unsymmetrical bifunctional initiators," *Chemical engineering science*, vol. 44, no. 2, pp. 297–312, 1989.

[146] E. Berkenwald, C. Spies, G. Morales, and D. A. Estenoz, "Mathematical model for the bulk polymerization of styrene chemically initiated by sequential and total decomposition of the trifunctional initiator diethyl ketone," *Polymer Engineering and Science*, pp. 1–11, 2014.

[147] R. D. de León, G. Morales, P. Acuña, and F. Soriano, "Phenomenon of phase inversion in high impact polystyrene: Physico-chemical, rheological and morphological study in the presence of chain transfer agent and using different tapered block copolymers as the precursor rubber," *Polymer Engineering & Science*, vol. 50, no. 2, pp. 373–383, 2010.

[148] E. Berkenwald, M. L. Laganá, J. Maffi, P. Acuña, G. Morales, and D. Estenoz, "Experimental and theoretical study of the use of multifunctional initiators in the high impact polystyrene bulk process," *Polymer Engineering & Science*, vol. 58, no. 2, pp. 198–212, 2018.

[149] S. J. Lee, H. G. Jeoung, and K. H. Ahn, "Influence of solvent contents on the rubber-phase particle size distribution of high-impact polystyrene," *Journal of Applied Polymer Science*, vol. 89, no. 13, pp. 3672–3679, 2003.

[150] H. J. Karam and L. Tien, "Analysis of Swelling of Crosslinked Rubber Gel with Occlusions," *Journal of Applied Polymer Science*, vol. 30, pp. 1969–1988, 1985.

[151] J. H. Duerksen and A. E. Hamielec, "Polymer reactors and molecular weight distribution. IV. Free-radical polymerization in a steady-state stirred-tank reactor train," *Journal of Polymer Science Part C: Polymer Symposia*, vol. 25, pp. 155–166, Mar. 2007.

[152] J. D. Campbell, F. Teymour, and M. Morbidelli, "High Temperature Free Radical Polymerization. 2. Modeling Continuous Styrene Polymerization," *Macromolecules*, vol. 36, pp. 5502–5515, July 2003.

[153] M. Poutsma, "Mechanistic analysis and thermochemical kinetic simulation of the pathways for volatile product formation from pyrolysis of polystyrene, especially for the dimer," *Polymer Degradation and Stability*, vol. 91, pp. 2979–3009, Dec. 2006.

[154] D. S. Achilias and C. Kiparissides, "Development of a general mathematical framework for modeling diffusion-controlled free-radical polymerization reactions," *Macromolecules*, pp. 3739–3750, 1992.

[155] J. S. Vrentas, J. L. Duda, and H. C. Ling, "Self-Diffusion in Polymer-Solvent-Solvent Systems.," *Journal of polymer science. Part A-2, Polymer physics*, vol. 22, no. 3, pp. 459–469, 1984.

[156] J. A. Biesenberger, *Devolatilization of Polymers, Fundamentals - Equipment - Applications*. Hanser Publishers, New York, 1983.

[157] J. H. Han and C. Dae Han, "Bubble nucleation in polymeric liquids. ii. theoretical considerations," *Journal of Polymer Science Part B: Polymer Physics*, vol. 28, no. 5, pp. 743–761, 1990.

[158] S. Lee and J. A. Biesenberger, "A Fundamental Study of Polymer Melt Devolatilization IV: Some Theories and Models for Foam-Enhanced Devolatilization," *Polymer Engineering and Science*, vol. 29, no. 12, pp. 782–790, 1989.

[159] R. Foster and J. Lindt, "Bubble growth controlled devolatilization in twin-screw extruders," *Polymer Engineering & Science*, vol. 29, no. 3, pp. 178–185, 1989.

[160] N. Ramesh, D. H. Rasmussen, and G. A. Campbell, "The heterogeneous nucleation of microcellular foams assisted by the survival of microvoids in polymers containing low glass transition particles. part i: Mathematical modeling and numerical simulation," *Polymer Engineering & Science*, vol. 34, no. 22, pp. 1685–1697, 1994.

[161] A. L. Yarin, D. Lastochkin, Y. Talmon, and Z. Tadmor, "Bubble nucleation during devolatilization of polymer melts," *AIChE Journal*, vol. 45, pp. 2590–2605, Dec. 1999.

[162] J. Colton and N. Suh, "The nucleation of microcellular thermoplastic foam with additives: Part i: Theoretical considerations," *Polymer Engineering & Science*, vol. 27, no. 7, pp. 485–492, 1987.

[163] R. E. Newman and R. H. M. Simon, "A mathematical model of devolatilization promoted by bubble formation," 1980.

[164] M. Amon and C. D. Denson, "A study of the dynamics of foam growth: Analysis of the growth of closely spaced spherical bubbles," *Polymer Engineering & Science*, vol. 24, no. 13, pp. 1026–1034, 1984.

[165] J. Vrentas, J. Duda, and H.-C. Ling, "Enhancement of impurity removal from polymer films," *Journal of applied polymer science*, vol. 30, no. 12, pp. 4499–4516, 1985.

[166] J. Barwich, O. Aydin, U. Erhardt, and W. Holtrup, "Elimination of volatile residues from polyacrylate melts," June 30 1998. US Patent 5,772,851.

[167] J. A. Biesenberger, "Polymer Devolatilization: Theory of Equipment," *Polymer Engineering and Science*, vol. 20, no. 15, pp. 1015–1022, 1980.

[168] J. A. Biesenberger, "Polymer Melt Devolatilization: On Equipment Design Equations," *Advances in Polymer Technology*, vol. 7, no. 3, pp. 267–278, 1987.

[169] J. Scheirs and D. Priddy, *Modern styrenic polymers: Polystyrenes and Styrenic Copolymers*. 2003.

[170] W. G. Perkins, "Polymer toughness and impact resistance," *Polymer Engineering & Science*, vol. 39, no. 12, pp. 2445–2460, 1999.

[171] I. Partridge, "Rubber-toughened polymers," *Multicomponent Polymer Systems, Longman Scientific Technical*, 1992.

[172] K. McCreedy and H. Keskkula, "Effect of thermal crosslinking on decomposition of polybutadiene," *Polymer*, vol. 20, no. 9, pp. 1155–1159, 1979.

[173] L. Treolar, *The physics of rubber elasticity. Clarendon*. Oxford, 1975.

[174] C. B. Bucknall, "Brittle-tough transition temperatures in impact tests on rubber-toughened plastics," in *Makromolekulare Chemie. Macromolecular Symposia*, vol. 16, pp. 209–224, Wiley Online Library, 1988.

[175] E. J. Kramer, "Craze fibril formation and breakdown," *Polymer Engineering & Science*, vol. 24, no. 10, pp. 761–769, 1984.

[176] B. Elbirli and M. T. Shaw, "Time Constants from Shear Viscosity Data," *Journal of Rheology*, vol. 22, no. 5, p. 561, 1978.

[177] C. Carreau, De Kee, "Rheology of polymeric systems, principles and applications," *AIChE Journal*, vol. 45, no. 8, pp. 1836–1837, 1999.

[178] J. Z. Liang and J. N. Ness, "Effect of die angle on flow behaviour for high impact polystyrene melt," *Polymer Testing*, vol. 16, no. 4, pp. 403–412, 1997.

[179] R. Kruse and J. Southern, "Viscosities and normal stress coefficients of high impact polystyrene-mineral oil mixtures," *Polymer Engineering & Science*, vol. 19, no. 11, pp. 815–817, 1979.

[180] T. Bremner, A. Rudin, and D. Cook, "Melt flow index values and molecular weight distributions of commercial thermoplastics," *Journal of Applied Polymer Science*, vol. 41, no. 7-8, pp. 1617–1627, 1990.

[181] R. L. Kruse, "Viscosities and Normal Stress Coefficients of High Impact Polystyrene Fluids," *Journal of Rheology*, vol. 24, no. 6, p. 755, 1980.

[182] J. Rohlfing, C. D.; Janzen, "What's happening in the melt-flow plastometer: The role of elongational viscosity," *Society of Plastics Engineers, Inc. (SPE)*, 1997.

[183] P. J.-L. Locatelli and G. Riess, "Étude de copolymères greffés abs (acrylonitrile-butadiène-styrène). i. influence de la solvatation préférentielle du polybutadiène sur la composition des greffons," *Die Angewandte Makromolekulare Chemie: Applied Macromolecular Chemistry and Physics*, vol. 27, no. 1, pp. 201–214, 1972.

[184] J. Locatelli and G. Riess, "Etude de copolymères abs (acrylonitrile–butadiène–styrène): Solvatation préférentielle du polybutadiène par les promoteurs," *Journal of Polymer Science: Polymer Chemistry Edition*, vol. 11, no. 12, pp. 3309–3320, 1973.

[185] P. J.-L. Locatelli and e. G. Riess, "Étude de copolymères greffés abs (acrylonitrile-butadiène-styrène). iv. évolution de la fraction greffée dans la réaction de greffage," *Die Angewandte Makromolekulare Chemie: Applied Macromolecular Chemistry and Physics*, vol. 32, no. 1, pp. 117–129, 1973.

[186] P. J.-L. Locatelli and G. Riess, "Etude de copolymères greffés abs (acrylonitrile-butadiène-styrène) v. mécanisme et cinétique de la réaction de greffage," *Die Angewandte Makromolekulare Chemie: Applied Macromolecular Chemistry and Physics*, vol. 35, no. 1, pp. 57–74, 1974.

[187] G. Bouquet, W. Kentie, P. DeTheije, and F. VanDamme, "Grafting on polybutadiene during the free radical polymerisation of styrene and acrylonitrile. effect of different initiators.," in *Abstracts of Papers of the American Chemical Society*, vol. 212, pp. 224–POLY, Amer. Chemical Soc. 1155 16TH ST, NW, Washington, DC 20036, 1996.

[188] J. Maul, B. G. Frushour, J. R. Kontoff, H. Eichenauer, K.-H. Ott, and C. Schade, "Polystyrene and styrene copolymers," *Ullmann's encyclopedia of industrial chemistry*, 2000.

[189] G. Bouquet, "Rubber particle formation in mass abs," *Modern Styrenic Polymers: Polystyrenes and Styrenic Copolymers*, pp. 305–319, 2003.

[190] H. Münstedt, "Rheology of rubber-modified polymer melts," *Polymer Engineering & Science*, vol. 21, no. 5, pp. 259–270, 1981.

[191] H. Kubota, "Curing of highly reactive polyester resin under pressure: kinetic studies by differential scanning calorimetry," *Journal of Applied Polymer Science*, vol. 19, no. 8, pp. 2279–2297, 1975.

[192] F. Ramsteiner, G. McKee, W. Heckmann, W. Fischer, and M. Fischer, "Rubber toughening of polystyrene–acrylonitrile copolymers," *Acta polymerica*, vol. 48, no. 12, pp. 553–561, 1997.

[193] G. Cigna, P. Lomellini, and M. Merlotti, "Impact thermoplastics: combined role of rubbery phase volume and particle size on toughening efficiency," *Journal of applied polymer science*, vol. 37, no. 6, pp. 1527–1540, 1989.

[194] G. Giaconi, L. Castellani, C. Maestrini, and T. Ricco, "Development of toughness in abs resins," *Polymer*, vol. 39, no. 25, pp. 6315–6324, 1998.

[195] L. Castellani, R. Frassine, A. Pavan, and M. Rink, "Rate and temperature dependence of fracture toughness in abs resins in relation to dispersed-phase structure," *Polymer*, vol. 37, no. 8, pp. 1329–1338, 1996.

[196] Y. Han, R. Lach, and W. Grellmann, "Effects of rubber content and temperature on unstable fracture behavior in abs materials with different particle sizes," *Journal of applied polymer science*, vol. 79, no. 1, pp. 9–20, 2001.

[197] K. Sardelis, H. Michels, and G. Allen, "Toughened polystyrene containing block, graded block and randomized copolymers of butadiene-styrene," *Polymer*, vol. 28, no. 2, pp. 244–250, 1987.

[198] Y. Okamoto, H. Miyagi, M. Kakugo, and K. Takahashi, "Impact improvement mechanism of hips with bimodal distribution of rubber particle size," *Macromolecules*, vol. 24, no. 20, pp. 5639–5644, 1991.

[199] E. T. C. Mui, V. B. Boateng, J. F. Fellers, and J. L. White, "Interaction of polymerization conditions, structural variables, and mechanical properties of rubber-modified plastics produced from bulk polymerized styrene/poly (butadiene-co-styrene)," *Journal of Applied Polymer Science*, vol. 27, no. 4, pp. 1395–1407, 1982.

[200] V. Yenalyev, N. Noskova, and B. Kravchenko, "Modification of polystyrene with polybutadiene and method of studying morphology of obtained multiphase high impact systems," in *Abstracts of Papers of the American Chemical Society*, no. 169, pp. 83–83, Amer Chemical Soc 1155 16TH ST, NW, Washington, DC 20036, 1975.

[201] C. Bucknall, F. P. Cote, and I. Partridge, "Rubber toughening of plastics. ix: Effects of rubber particle volume fraction on deformation and fracture in hips," *Journal of materials science*, vol. 21, no. 1, pp. 301–306, 1986.

[202] M. Demirors, R. Veraert, and C. Hermans, "New particle morhologies with controlled grafting," *Polymer Preprints-America*, vol. 40, pp. 71–72, 1999.

[203] F. Peng, "Polybutadiene hydroperoxide by singlet oxygen: Its grafting and morphology in polystyrene matrix," *Journal of applied polymer science*, vol. 31, no. 6, pp. 1827–1842, 1986.

[204] D. Kekhaiov and B. Mikhnev, "Correlation of conditions of polymerisation of high-impact polystyrene(hips) with the parameters of the two disperse phases and the properties," *Int. Polym. Sci. Technol.*, vol. 12, no. 11, 1985.

[205] R. Díaz de León. PhD thesis, Centro de Investigación en Química Aplicada, México, 2003.

[206] A. Diaz de Leon, Morales, "Mechanical behavior of high impact polystyrene based on sbr copolymers: Part i," *Polymer Engineering & Science*, vol. 45, no. 9, pp. 1288–1296, 2005.

[207] D. A. Elizarrarás. PhD thesis, Centro de Investigación en Química Aplicada, México, 2003.

[208] V. H. Schuster, M. Hoffmann, and K. Dinges, "Struktur und eigenschaften von abspolymeren. iii.. charakterisierung der pfropfcopolymerisate von styrol-acrylnitril auf polybutadien durch oxydativen abbau," *Die Angewandte Makromolekulare Chemie: Applied Macromolecular Chemistry and Physics*, vol. 9, no. 1, pp. 35–46, 1969.

[209] L. H. Garcia Rubio, J. MacGregor, and A. Hamielec, "Size exclusion chromatography of copolymers," 1983.

[210] A. Keramopoulos and C. Kiparissides, "Development of a comprehensive model for diffusion-controlled free-radical copolymerization reactions," *Macromolecules*, vol. 35, no. 10, pp. 4155–4166, 2002.